6-2001

Impedance and Photo-Electrochemical Properties of Oxide Films on Stainless Steel Formed by Different Polarization Techniques

Mona Salim Saleh AI Kaabi

Impedance and Photo-Electrochemical Properties of Oxide Films on Stainless Steel Formed by Different Polarization Techniques

A Thesis Submitted to
The Deanship of Graduate Studies
of The United Arab Emirates University

By

Mona Salim Saleh Al Kaabi

In Partial Fulfillment of The Degree of M.Sc in
Materials Science and Engineering

June 2001

To my daughter Bushra…..

Supervision Committee Members

Prof. Dr. Rashid Abdel Rahman Al Saeed
Professor of Physical Chemistry
Department of Chemistry,
College of Science, UAEU.

Dr. Ahmed Galal Helmy
Assistant Professor of Physical & Materials Chemistry
Department of Chemistry,
College of Science, UAEU.

Examination Committee Members

Dr. Ahmed Al Shamsi
Assistant Professor of Physical Chemistry & Corrosion Science
Department of Chemistry,
College of Science, UAEU.

Dr. Ali N. Moosawi
Senior Corrosion Engineer
Abu Dhabi Company for Onshore Oil Operations (ADCO), UAE.

Acknowledgement

Thanks for Allah who gave me help, strength and patience until I finished this master degree research. One may meet many kinds of people as he goes on through his life, but those, are few who can stay in mind because of what they gave you from their time, effort and knowledge without expecting anything back from you. Those are my supervisors: Prof. Dr. Rashid Al Saeed and Dr. Ahmed Galal Helmy. Many thanks go to the Deanship of Graduate Studies Dr. Hadif Al Owais, for his support and help. I also want to thank the Deanship of the College of Science for the help I had been given from all Science Departments, especially Chemistry, Physics and Geology in providing my research with materials, equipment and advisement. They facilitate for me the use of their valuable equipment such as: the electrochemical unit, the X-ray diffraction unit and the photo-electrochemical unit. Special thanks should be extended to the Council of Master Degree of Materials Science and Engineering for their kind supervision and advisement especially Dr. Nabil Kenawy and Dr. Abdulla Al Khanbashi. For all the work in the central laboratory unit (CLU), I have to say thank you for the time and effort you spent on my surface measurements. XPS measurements were conducted by courtesy of Prof. J. F. Boreo of the University of Cincinnati. Finally, I thank the United Arab Emirates University, which offered me this chance to enroll in the Master Program.

To my friends who gave me a hand and helped me until I finished my study; every one with her owns way especially Sadia Sediq; I am grateful. I am also grateful to my family, mother and father, sisters and my dear brothers Abdulla and Ali. To my husband Saeed and my little daughter Bushra, I must say thank you for your help and patience for the last three years.

Acknowledgement

Thanks for Allah who gave me help, strength and patience until I finished this master degree research. One may meet many kinds of people as he goes on through his life, but those, are few who can stay in mind because of what they gave you from their time, effort and knowledge without expecting anything back from you. Those are my supervisors: Prof. Dr. Rashid Al Saeed and Dr. Ahmed Galal Helmy. Many thanks go to the Deanship of Graduate Studies Dr. Hadif Al Owais, for his support and help. I also want to thank the Deanship of the College of Science for the help I had been given from all Science Departments, especially Chemistry, Physics and Geology in providing my research with materials, equipment and advisement. They facilitate for me the use of their valuable equipment such as: the electrochemical unit, the X-ray diffraction unit and the photo-electrochemical unit. Special thanks should be extended to the Council of Master Degree of Materials Science and Engineering for their kind supervision and advisement especially Dr. Nabil Kenawy and Dr. Abdulla Al Khanbashi. For all the work in the central laboratory unit (CLU), I have to say thank you for the time and effort you spent on my surface measurements. XPS measurements were conducted by courtesy of Prof. J. F. Boreo of the University of Cincinnati. Finally, I thank the United Arab Emirates University, which offered me this chance to enroll in the Master Program.

To my friends who gave me a hand and helped me until I finished my study; every one with her owns way especially Sadia Sediq; I am grateful. I am also grateful to my family, mother and father, sisters and my dear brothers Abdulla and Ali. To my husband Saeed and my little daughter Bushra, I must say thank you for your help and patience for the last three years.

TABLE OF CONTENT

Abbreviations & Symbols

Symbol	Abbreviation
AISI	American Institute of Steel and Iron
PFZ	Precipitate Free Zone
XPS	X-Ray Photoelectron Spectroscopy
SS	Stainless Steel
SSRT	Slow Strain-Rate Test
AES	Auger Electron Spectroscopy
OMCVD	Organ-metallic Chemical Vapor Deposition
PC	Propylene Carbonate
DME	Dimethoxyethane
AFM	Atomic Force Microscopy
NWC	Normal Water Chemistry
HWC	Hydrogen Water Chemistry
SEM	Scanning Electron Microscopy
TEM	Transmission Electron Microscopy
SCE	Saturated Calomel Electrode
EDXA	Energy Dispersive X-ray Analysis
EIS	Electrochemical Impedance Spectroscopy
BF	the Break point Frequency method
MPI	the Most Probable Impedance equivalent circuit method
TML	Transmission Line Model
PSP	Power Spectral Density
ODA	Octadecyclamine
SERS	Surface Enhanced Raman Spectroscopy
P/M	Powder Metallurgy
SIMS	Secondary Ion Mass Spectrometry
UV	Ultra Violet
GIXS	Grazing Incidence X-ray Scattering
GDS	Glow Discharge optical emission spectroscopy
XRD	X-Ray Diffraction
TGA	Thermal Gravimetric Analysis
POSAP	built Position Sensitive Atom Probe
ESCA	Electron Surface Chemical Analysis
EDS	Electron Diffraction Spectroscopy
FTIR	Fourier Transmission Infra-Red spectroscopy
SRFTIR	Surface Reflectance Fourier Transform Infra –Red Spectroscopy
MPY	Mills Per Year

List of Figures

List of Tables

ABSTRACT

ABSTRACT

Stainless steel alloys have a very active and important role in industry. Because many of these industries have to work in aggressive media; stainless steels are threatened by corrosion which may affect their performance and cost the manufacturers millions of dollars yearly. Several treatments have been taken part to solve this problem, one is by forming a protective oxide layer on the stainless steel (SS) surface to prevent it from corrosion. In this thesis, this way of protecting SS surface is applied to two different types of Stainless Steel, those are AISI 316 and AISI 310; respectively. The oxide film was formed using a potential step programming at different thicknesses, varying the programs and bath compositions in a three-electrode electrochemical cell. The electrochemical behavior of the oxide film has been studied using several techniques : potentiodynamic polarization , Tafel experiments, polarization resistance, and electrochemical impedance spectroscopic techniques. Then, surface analysis was applied to the oxide film in order to investigate its elemental composition, morphology and thickness. Surface techniques used in this study were: electron spectroscopy for chemical analysis (ESCA), scanning electron microscopy, surface reflectance FT-IR, energy dispersive x-ray analysis and x-ray diffraction. It was found that the polarization behavior of the different types of stainless steels studied is strongly dependent on the steel structure. Also, the ability of stainless steels type 316 and type 310 to passivate in 5.0 M sulfuric acid is realized and stabilized within a relatively wide range of potential. However, oxide film formed over stainless steel

type 316 is relatively more stable than that formed over stainless steel type 310 surfaces under similar experimental conditions. From the EIS data, it was found that -for SS 316- the resistance of the oxide film to pore formation and charge transfer through the oxide film increased as the film thickness increased. On the other hand, the coating capacitance and the double layer capacitance of the oxide film decreased gradually as the oxide thickness increased. It was concluded that the presence of chromate and molybdate in the film-forming bath enhances the structure of the passive film due to the presence of chromium as hydroxide and molybdenum as the oxide. It has been shown that the film deposited at the stainless steel type 316 has a bilayer (hydroxide/oxide) structure. The graphs depicted from the scanning electron microscope (SEM) gave a good idea about the morphology of the oxide at SS surface. The important result of the SEM experiments is the identification of the systematic growth of the oxide layer that consists of oval, pentagonal and pyramidal aggregates with a high micro-roughness.

I.INTRODUCTION

Stainless steels represent about 4% of the total amount of steel production in the world. However, because of their need to the construction materials, and corrosion-resistant equipments in chemical, and petroleum industries, they acquired technological and economic importance. Due to the chromium content that is at least 11%, stainless steels are relatively corrosion resistant than many other metals and alloys. The origin of this corrosion resistance emerged from the thin passive film that is, self-healing in most environments. This passive film depends to a great extent on the structure of the stainless steel and the environment is which the film is deposited. More than 180 alloys belong to the stainless steel family. Diagram 1 shows the compositional-property linkages in the stainless steels.[1]

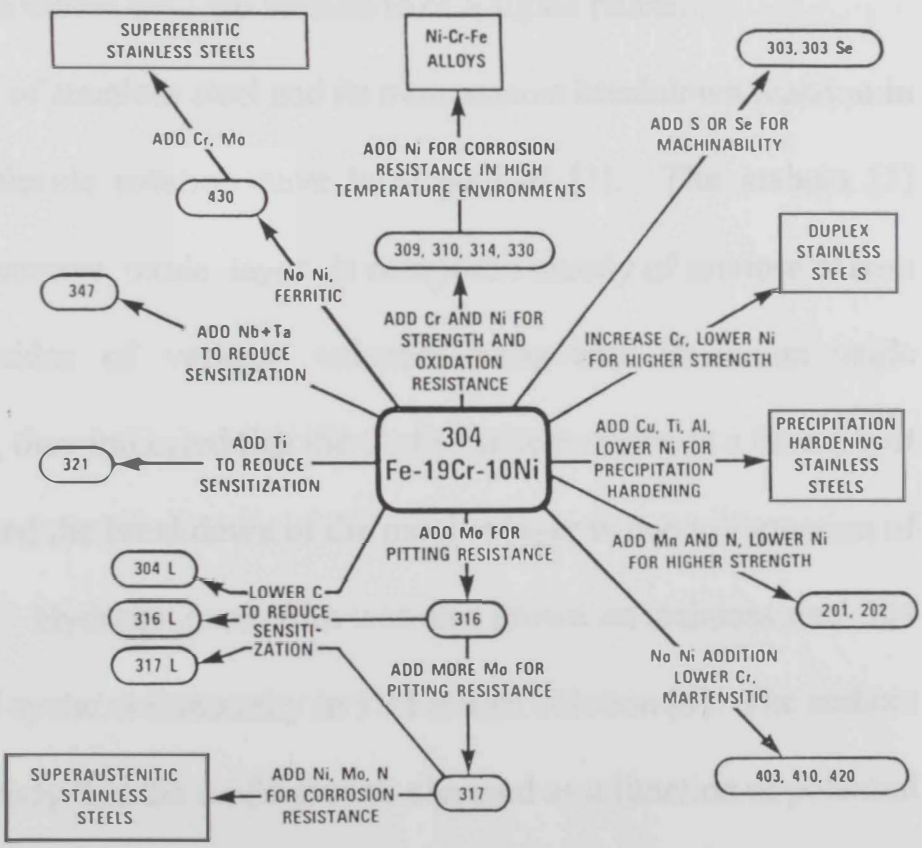

[1] From: "Corrosion of Stainless Steels," by A. John Sedriks, Wiley-Interscience Publication, New York, 1996.

1.1 Oxide film formation at stainless steel surfaces

The oxidation of AISI 316 steel was achieved at 550 °C for different time periods ranging from 24 – 3000 hours [1]. In this study [1], the vanadium content increased on the behalf of molybdenum and showed a considerable increase in the thickness of the oxide formed that is richer in iron at the outermost layer. In another study, Strutt and Vecchio [2] investigated the oxidation of 347 austenitic stainless steel and the simultaneous formation of a sigma phase. The authors [2] found that the oxidation rate followed a parabolic kinetic behavior in the temperature range from 650 °C to 816 °C used for oxide formation. However, the oxidation rate accelerated above 816 °C and the precipitate-free zone (PFZ) near the metal surface was found not to be limited by a Cr depletion associated with the formation of a sigma phase.

The passivation of stainless steel and its transpassive breakdown reaction in neutral sodium chloride solution have been studied [3]. The authors [3] indicated that the passive oxide layer is composed mainly of mixture of iron oxides and hydroxides of various valences along with chromium oxide (Cr_2O_3). Moreover, they indicated that the Cr_2O_3 content varies as a function of applied potential and the breakdown of the passive layer is due to formation of the soluble CrO^{2-}_4. Hydrous oxide film was also grown on stainless steel 304 under conditions of cyclic voltammetry in 1 M NaOH solution [4]. The authors [4] found in their study that the oxide growth changed as a function of potential limits, sweep rates and number of potential cycles. It was found that the oxide placed in an acid solution remains enriched in chromium due to selective

dissolution of nickel and iron, this oxide being formed previously by potential cycling in an alkaline solution. This model was confirmed by the data obtained from voltammetric, rotating ring-disc electrode and x-ray photoelectron spectroscopy (XPS) measurements [4]. Saeki et al. of type 430 stainless steels with 0.09 and 0.9 mass % Mn, at the temperature range 1013- 1273 K [5]. In their study, the authors found that - in case of stainless steels (SS) with 0.09 mass % Mn - the Cr concentration increased at the oxide surface and the Mn content. On the other hand, a protective layer forms on type - 304 stainless steels that are oxidized in annealed atmospheres corresponding to air/CH_4 greater than or equal to 11 at 1373 K [6]. This layer breaks down due to formation of an iron oxide layer on the surface that is mainly composed of small crystals of spinal (Cr_2O_3/FeO). The layer was found to be non-protective as the ratio of air/ CH_4 decreases. The structure of oxide formed by repetitive cycling of stainless steel type 302 in 1 M NaOH was also studied [7]. In this work, the structure of the oxide layer was investigated by cyclic voltammetric technique that revealed two pairs of hydrous oxide peaks that belonged to $Fe(OH)_2$/FeOOH and $Ni(OH)_2$/NiOOH transitions. Ohmi et al. [8]developed a new technology using electrochemical buffed 316L austenitic stainless steel to form an oxide scale as a passivation film, which consists of an outer surface that is a perfect chromium oxide (Cr_2O_3) layer of several tens of nanometers thickness. An inner part that contains iron and nickel oxides was also found. The authors [8] found that the corrosion resistance of this film

showed an excellent characteristic compared with the conventional electropolished surface.

On the other hand through Devanathan hydrogen permeation tests, slow strain-rate tests (SSRT), Auger-electron spectroscopy (AES) depth profiles of component and a mathematical analysis, the retarding effect of thermally grown oxide films on the hydrogen embrittlement and entry of AISI 430 stainless steel has been investigated [9]. The author found that the AISI 430 SS specimen oxidized at 1073 K for 40 min could form not only a uniform, but also a chromium-rich oxide film[9]. In addition to that, an organ-metallic chemical vapor deposition (OMCVD) process was developed [10] for the preparation of protective erbium oxide coatings resistant to corrosion by liquid plutonium. The substrates used for process developed were 304 stainless steel flats. This study [10] revealed that coatings deposited on SS that are resistant to corrosion by liquid plutonium, although an erbium-thickness threshold is observed. The failure mechanism for samples with thicknesses below the threshold value is most likely related to flaws in the film morphology, for example large pinholes, rather than grain boundary attack. On the other hand, the beneficial effect of the addition of yttrium and erbium by ion implantation on the oxidation behavior of AISI 304 stainless steel at 1173 k has been investigated [11]. It was concluded in this study [11] that both reactive elements inhibit the growth of the poorly protective and adherent oxides rich in iron and chromium, which helps the spalled behavior, together with a smaller oxide gain size.

1.2 The structure and properties of oxide films formed at stainless steel surfaces

Stainless steel 304 was modified electrochemically by potentiostatic and potentiodynamic methods in 1 M NaOH solution, hydrothermally in 1 M NaOH at 200 °C, and chemically in 0.5 M $K_2Cr_2O_7$ solution[12]. In this study [12], it was found that the hydrothermally grown oxide film was most stable, whereas the most efficient oxide growth was achieved by the use of potentiodynamic method of modification. On the other hand, the passivation and breakdown behavior of 304 stainless steel in propylene carbonate(PC) or dimethoxyethane (DME) mixtures with water and containing 0.5 M $LiAsF_6$ were studied[13]. This study[13] revealed that no pitting was observed in either PC-H_2O-0.5 M $LiAsF_6$ mixture or mixed DME-H_2O-0.5 M $LiAsF_6$ solutions if the polarizations were conducted below the oxidation potential of the $LiAsF_6$. In another study, corrosion-resistant chromium oxide films over stainless steel (Fe-27 Cr alloy) were obtained by chemical conversion and thermal treatment[14]. It was found that as converted films are amorphous and thermal treatment promotes crystallization and the passivating efficiency of the film is strongly dependent on the dominant phase structure[14]. Moreover, direct observation by oxygen-induced structural changes in stainless steel surfaces was obtained [15]. In this study [15], oxidation of stainless steel was performed at 450 °C and oxygen partial pressure of 10^{-9} –10^{-4} torr. Atomic force microscopy (AFM) images and surface-sensitive photo emission spectroscopy spectra clearly showed that at 450 °C oxygen pressure lower than the

critical pressure (1×10^{-8} torr) favor the formation of a smooth Cr_2O_3 oxide film whereas at higher pressures, the oxide film formation exhibits a rough surface with distinct grains that contain a significant amount of iron and manganese[15]. In addition to that, characterization of the microstructure and chemistry of the oxide film of an air-oxidized type 316L stainless steel was carried out by an energy filtering transmission electron microscope equipped with an electron energy loss spectroscopy detector[16]. It is demonstrated [16] that the corrosion resistance of the steel in a 105 °C, 30 % sulfuric acid solution can be improved by an oxidation pretreatment of the steel in air at 500 ° C for 5 min, which produced an oxide film 70 nm thick. The oxide has a multi layered microstructure in which the topmost layer is composed of nanoscale gamma Fe_2O_3 grains of size similar to 4 nm, followed by a mixture of alpha- Fe_2O_3 and Fe_3O_4 phases of grain size ranging from 20 to 75 nm. In addition[16] it is observed that an alloying depletion of Cr and Mn exists in the steel. However, characteristics of the oxide film formed on type 316 stainless steel in 288 °C water under a cycle of normal water chemistry (NWC) and hydrogen water chemistry (HWC) conditions were examined by scanning electron microscopy (SEM), transmission electron microscopy (TEM), and auger electron microscopy (AES)[17]. It was found that [17] the oxide film mainly consists of two oxide layers: an outer oxide layer with a large particle (nickel-enriched magnetite) and an intermediate or small particle (hermatite structure) and a very fine-grain inner layer with a chromium-enriched Fe_3O_4 type structure. Under cyclic water chemistry, the inner oxide layer composition was shown to be dependent upon the water chemistry, while the inner oxide layer remained

unaffected [17]. In another study, passivation and its transpassive breakdown reactions of stainless steel in neutral sodium chloride solutions have been studied using cyclic voltammetric and spectrochemical experiments[18]. It was found that the composition of the passive film [18] formed from the iron oxidation mixture of iron oxides and hydroxides of various valences along with Cr_2O_3 already present on the applied potential. The breakdown of the passive layer at an iron, nickel and chromium alloy has been investigated in aqueous concentrated and anhydrous organic solutions of sulfuric acid[19]. The results of electrochemical and X-Ray spectroscopy (XPS) investigations[19] showed that in a hydrous solutions an oxide-hydroxide passive film could be formed on metal surfaces. In this study [19], the mechanism of passivation proposed is one in which undissociated acid molecules take part in the anodic oxidation of metal surfaces by acting as a source of oxygen . On the other hand, temperature dependence of out gassing was measured for differently surface treated type 316L stainless steel chambers in the temperature range of 25-330 °C [20]. The following are the important findings[20]: (1) at temperatures below 250 °C, the contribution from water and carbon monoxide outgassing becomes significant. (2) The surface oxide layer formed by the oxidation in air is predominantly iron oxide layer appears to serve as a more effective diffusion barrier for hydrogen outgassing compared with the mixed iron and chromium oxide layer formed on the fully degassed surface [20]. Looking to another study, the effects of solid NaCl, which deposits on the oxide scales of the technical steels, on the oxidation were investigated at 700 °C [21]. It was found that [21], the presence of NaCl (s), independent of the alloy composition, initiated

a markedly accelerated F_2O_3 growth on the surface of preoxidized samples, under formation of voluminous, non protective layers. Also, below these scales on the metallic matrix in all cases chloride was detected which reduces the adhesion of the oxide scale and leads to spalling upon cooling to room temperature[21]. Wengar et al. studied the evolution of the impedance of an AISI 340 steel electrode affected by pitting corrosion[22]. Open pits were obtained in sulfuric acid solution[22]. The results obtained with open pits, some changes affecting the shape of the impedance diagram, are explained by the increase in the roughness induced by their development. With closed pits, the electrode impedance behave like the impedance of a porous electrode [22]. Chemical characterization of passive films formed on AISI 304 austenitic stainless steel, in a borate/ boric acid solution at pH 9.2, under various conditions of potential, temperature and polarization time, was accomplished by Auger electron spectroscopy (AES) combined with ion sputtering and XPS [23]. The authors [23] determined the depth chemical composition, thickness and duplex character of the passive layers using AES by a quantitative approach based on the sequential layer-sputtering model. Moreover, detailed resolution of microscopic depassivation events on stainless steel in chloride solution leading to pitting was done by Mattin et al.[24]. They found that the nucleation of corrosion pits is fast , showing a rise time less than 1 ms, and is ascribed to rupture of the passivating oxide film, caused by the formation of microscopic patches of metal chloride at the metal-oxide film interface.[24].

Effects of MoO^-_4 in the acidic electrolytes on the corrosion behavior of sensitized 304 stainless steel in the acidic electrolytes were studied [25]. The

composition of the passive film formed in the passive region was analyzed using XPS. It is observed [25] that the addition of molybdate to various electrolytes such as H_2SO_4, KSCN and HCl solutions increased the corrosion potential, pitting potential and repassivation potential of the sensitized 304 stainless steel, and decreased the active current density, passive current density and reactivation current density. However, the passive current density in H_2SO_4 solution increased with the molybdate addition [25]. A comparative study of the oxidation behavior of AISI 316 steel was published, where the molybdenum has been substituted by increasing amount of vanadium [1]. The samples were oxidized at 550 °C for time periods ranging from 24-3000 hours, in static air. The results [1] showed similar oxidation characteristics in all the samples, being the variations attributed to the presence of vanadium and the oxide layer presented two clearly defined zones, separated by a rock. The outer section, rich in iron, the inner rich in chromium [1]. In another study, electrochemical behavior of surface alloys rich in Ni-Mo produced by laser surface alloying was studied in a mixture of de-aerated aqueous solutions of 0.5M H_2SO_4 and0.5 M NaCl [26]. Grover et al. [26] found that pitting potential of laser processed and polished alloys ranged between 460 and 560 mV, i.e. much higher than that for stainless steel 304 substrate (200 mV). The results suggested the efficiency of laser alloying technique for producing surface alloy with improved localized corrosion resistance [26]. Moreover, the effect of Mo addition as an alloying element to stainless steel alloys is investigated by capacitance (Mott Schottky approach), and photoelectrochemistry measurements [27]. These two approaches showed that the presence of Mo as an alloying element

affects the semiconductive properties of the oxide film. On the other hand, complementary studies [27] were made using AES and XPS and their results have shown that the oxide films formed on stainless steel are composed of an external Fe rich region and an inner Cr rich region. It was concluded that [27], the presence of Mo leads to an increase of the chromium content in the inner layers of the film thickness. However, indication of chromium oxide-hydroxide evaporation during oxidation of 304 L at 873 k; in the presence of 10% water vapor were demonstrated by Asteman et al. [28]. The oxidation was investigated at 873K in the presence of O_2 and O_2+10% H_2O with oxidation time varied between 1-672 hours. Oxidation in dry oxygen results [28] in the formation of corundum-type oxide which contained mainly chromium, with smaller amounts of Fe and Mn. Whereas, oxidation in the presence of water vapor results in an oxide that contains more Fe and less Cr, also a mass loss is detected after prolonged exposure caused by chromium evaporation as $CrO_2(OH)_2$ [28]. In addition to that study, the principal criteria for the corrosion resistance of intermediate grade ferritic stainless steel(SS) were examined in a neutral chloride (Cl^-) solution [29]. Corrosion studies of welded type 444 stainless steel demonstrated [29] that dual stabilization with low individual concentrations of titanium and niobium provided optimum corrosion resistance, which was independent of the surface of the welded material. Also, passivation of stainless steel in hydrochloric acid was studied [30]. High alloyed stainless steels were polarized in 0.1M HCl +0.4 M NaCl solution for 10 min and 2 h between -75 and 800 mV vs. saturated calomel electrode (SCE) [30]. In this study, the composition of the passive films was analyzed by angle-resolved

XPS and showed that oxide particles are formed during the initial stage of passivation process. It is suggested that [30] they are formed by deprotonation of hydroxide layer and for prolonged exposure, a uniform oxide film is developed under the hydroxide layer. The composition of the film is strongly dependent on the potential, and the content of Cr, Fe and Ni increased while Mo decreased with the potential increase [30]. In another study, the effect of bicarbonate ions (HCO_3^-) on pitting corrosion of type 316L stainless steel was investigated in aqueous 0.5 M sodium chloride (NaCl) solution using potentiodynamic polarization, AC impedance spectroscopy combined with XPS, the abrading electrode technique and scanning electron microscopy (SEM) [31]. Addition of HCO_3^- ions to NaCl solutions decreased the pit growth rate and increased oxide film resistance[31]. Moreover, electrochemical molybdenum incorporation treatment is studied on a Fe-Cr ferritic steel in molybdate acid solutions [32]. In this study [32], the sample is first depassivated in 0.1 M H_2SO_4 then a low concentration molybdate solution is added and the passive layer is built by a slow increasing voltammetric sweep. Incorporation of molybdenum is confirmed by AES and XPS surface analysis. It is found that [32] the presence of molybdenum increases the pitting potential in neutral and acidified 0.5 NaCl solutions. On the other hand, the effects of copper (Cu), silicon (Si), molybdenum (Mo) and nitrogen (N) as alloying elements on the microstructure and corrosion behavior of type 304 austenitic stainless steel(SS) in deaerated dilute acidic chloride (Cl^-) solutions at 30 °C and 60 °C was investigated using potentiodynamic, SEM and energy dispersive x-ray analysis (EDXA) techniques[33]. It was observed that [33] the addition of 2% Cu decreased the

corrosion and critical current densities sharply. Also the presence of 3% Si and 0.8% Ni improved the general and pitting corrosion resistance. However, N addition shifted the pitting potential in the positive direction, extending the passive range of the steel [33]. Also, in another study, current oscillations have been found during anodic polarization of a stainless steel stationary electrode in concentrated H_2SO_4 solution or more dilute H_2SO_4 solution containing an appropriate amount of CrO_3 [34]. The potential range of current oscillations and the frequency were dependent on the potential scan rate, solution composition and concentration, and temperature [34]. This was due to a periodic sequence of dissolution and reformation of the $M(OH)_3$ film which was formed by the reaction of divalent metal ions dissolved in the earlier stage of polarization of the stainless steel [34]. Huang et al. [35] studied the electrochemical behavior of the laser-alloyed Fe-Cr-Ni-Si-N and Fe-Cr-Ni-Mo-Si-N stainless steels in a 3.5 wt. % NaCl solution. In this study [35], the authors performed cyclic potentiodynamic polarization tests and electrochemical impedance spectroscopy (EIS) measurements to evaluate the corrosion resistance of the alloyed layers in deaerated 3.5 wt. % NaCl solution at pH 4. The experimental results showed that the passivation and polarization resistance of laser-alloyed nitrogen containing stainless steels in chloride, containing solution could be improved by co-alloying molybdenum [35].

1.3 EIS measurements of oxide films formed on stainless steel surfaces

Electrochemical impedance spectroscopy (EIS) has been described by several authors as a technique to measure delamination of organic coatings[36].

The interpretation of EIS data can be performed in several ways. In this work [36], two methods are critically compared: the break point frequency method (BF) and the most probable impedance equivalent circuit method (MPI). On the other hand, corrosion prevention by organic coatings is not only obtained by resistance inhibition [37], but also the transport of water and corrosive species is also important. A low permeability of water gives no guarantee for an optimal anti-corrosion performances as this is likely to cause blistering when osmotic pressures occurred due to surface contamination [37]. A certain permeability is necessary to prevent blistering. In this case electrochemical impedance spectroscopy (EIS) can provide useful information in this field, such as calculating the water uptake from the results of impedance measurements [37]. In another study, a theoretical analysis; and non-liner impedance measurements of non-linear electric systems have been carried out [38]. It was found that [38] the frequency and amplitude analysis of obtained impedance spectra enabled the complex and unequivocal determination of the parameters of the tested model of electric systems. In this study [38] non-linear impedance measurements have been carried out of the process of carbon steel dissolution in a sulfuric acid environment. However, an EIS technique has been applied to estimate the corrosion rates of metals covered with a thin electrolyte layer[39]. Nishkata et al.[39] used for measuring the corrosion rates, a two electrode cell system, which consists of a pair of identical metal electrodes embedded in parallel in epoxy resin. In this study [39], the impedance measurements for type 304 stainless steel covered with a NaCl solution layer and ordinary carbon steels with an H_2SO_4 solution layer 10-1000 μm in thickness, were

carried out in the frequency 10 mHz to determine the equivalent circuit of a metal-thin electrolyte layer interface and the influence of current (potential) distribution over the electrode surface on the EIS data. It was found that the obtained EIS data can be described by a transmission line(TML) model, in which the current distribution over the electrode surface is considered [39]. Also, the use of EIS for characterization of protective films and their breakdown due to localized corrosion is demonstrated[40]. EIS has been used to determine the properties of passive films on stainless steels and Al alloys which had been treated by chemical and electrochemical processes to obtain improved corrosion resistance [40]. It is demonstrated that [40] the pitting model for Al alloys can be used to determine pit growth rates from EIS data obtained at the corrosion potential. Moreover, the solid/liquid interface can often be modeled by the familiar equivalent circuit consisting of a solution resistance is series with a parallel combination of the double layer capacitance C and the resistance to charge transfer $R_{(p)}$ [41]. For this model [41], when plots of the imaginary parts vs. the real part of the complex impedance produce depressed semicircles (Cole-Cole plots). The centers of semicircles lie below the real axis, then the relaxation time of the equivalent RC circuit is distributed around a most probable value tau(0)= $CR_{(p)}$. The degree of departure from ideality was given by an appropriate parameter alpha [41]. In addition to that, the effect of chloride concentration on early stage of pitting for type 304 stainless steel has been studied [42] by using an AC impedance method. It is found that [42] the Warburg impedance coefficient, which is calculated from Bode plots, increases with increasing chloride concentration at low potentials in

the passive region when the diffusion process begins to occur at the surface. For a pit which is nucleated under a given potential [42], there exists a minimum chloride concentration above which the pit on the surface of the steel can be activated into metastable propagation, and below which it cannot. It was found also that [42] the effect of chloride concentration is reflected qualitatively in the potential($E_{(m)}$) at which the metastable pit or pits start to grow on the surface of type 304 SS. The effect of bicarbonate ions (HCO_3^-) on pitting corrosion of type 316L stainless steel (SS), was investigated in aqueous 0.5 M NaCl solution using potentiodynamic polarization, the abrading electrode technique, EIS combined with XPS and SEM [31]. It was found that over the whole applied potential, the oxide film resistance was higher in the presence of HCO_3^- ions and pit number density decreased with increasing HCO_3^- ion concentration [31].

A renewed version of a surface charge approach to describe the impedance response of anodic film growth on passive metals in acidic solutions was presented by Bojinov et al. [43]. It is based on the point defect chemistry, the fact that oxygen vacancies are the main charge carriers in a range of anodic oxides and the suggestion of a constant field strength in the bulk of the barrier layer [43]. This new approach [43] explained either a capacitive or a pseudo-inductive relaxation of the metal/film/electrolyte system under small amplitude ac perturbation as follows: a negative surface charge due to accumulation of metal vacancies near film solution interface accelerates the oxygen vacancy transport in transient conditions, and a corresponding positive surface charge of oxygen vacancies at the opposite interface is shown to retard it. There is also a new technique which was introduced

for electrochemical measurements in low conductivity environments [44]. The ohmic drop was overcome by the specimen and counter electrodes across a 1μ m-range gap, while the potential was measured from the side of the specimen, and the electric field is negligible. An additional benefit of the new arrangement [44] is that the specimen and counter electrodes can be brought into a mechanical solid-contact impedance. In another study, the spectral-directional emittance of thermally oxidized 316 stainless steel was measured for angles from normal to grazing wavelengths between 2 and 10 μm, and temperatures between 773 and 973K [45]. It was found that the emittance decreases with angle away from the surface normal at the lower end of the measured spectral range and increases with angle at the higher end, also the emittance decreases with wavelength while the variation with temperature within the measured range is insignificant [45]. Moreover, the effect of nitrogen and carbon sputter coatings on the electrochemical behavior of 316L stainless steel in a simulated physiological solution was studied by electrochemical impedance spectroscopy with the aim of characterizing the surfaces and choosing the best coating [46]. The results showed that [46] the thicker sputter coating produce surfaces with higher charge transfer resistance and lower interface capacities, which indicates that these materials probably owe their high corrosion resistance to the formation of more protective films [46]. Surface modification of stainless steels using green technology for corrosion protection was done by Mansfeld et al. [47]. This new technology depends on replacing Cr^{6+}, which is a hazardous chemical element responsible for protection in conversion

coating by Ce and Mo such as Al 7075 and Al 2024 [47]. In this work [47], the results of applying these coatings to SS 304 and 316, using EIS and XPS for testing, showed improvement in corrosion behavior. Also, fretting corrosion of sensitized 316 stainless steel has been investigated as a function of the degree of sensitization in aqueous 0.01M NaCl solution at room temperature [48]. In this study, the squared rod specimens of 316 SS were thermally annealed at 700 °C for various durations :- [0h]: nonsensitized specimen A; [8h]: moderately sensitized specimen B; [96h]: severely sensitized specimen C, and then the pitting corrosion resistance of the three kinds of specimens was evaluated by potentiodynamic anodic polarization method, abrading electrode technique and EIS. It was shown that [48] the thin oxide film formed on the sensitized specimens B and C is less protective than that formed on the nonsensitized specimen A. Capobianco et al. [49] investigated the passive films on 304L and 446 stainless steels, after galvanostatic reduction in an equivolume mixture of 0.15 M borate/boric acid buffer solution or after gamma-ray irradiation in deaerated double-distilled water, by the EIS technique. The results [49] obtained indicated that gamma-ray irradiation can have significant effects on the stabilities of the passive films, due to the release of iron and corresponding enrichment in chromium oxides, specially in the external passive layers. Results obtained from the EIS data [49] indicated that the passive-films formed on 304L and 446 stainless steels have a compact structure, which, modified by the galvanostatic reduction leading to a film composed of two layers; the external one showing a spongy-like structure. Whereas, gamma-ray irradiation leads to a thinner film with a better capacitive

behavior compared to that of unirradiated sample [49]. Song et al. carried out an investigation on the transpassivation-repassivation of type 304 stainless steel in 0.5 mol/L H_2SO_4, and proposed a model concerned with electrochemical processes of the electrode [50]. The authors [50] found that in the high potential range the transpassive process is closely related with the electrochemical dissolution occurring at the interface between surface film and solution, and the repassivation is due to the sharp decrease in lower valence oxides. On the other hand, AC impedance and DC polarization tests of 304 stainless steels coated (CAPD) titanium nitride and zirconium nitride were conducted in aqueous chloride solution [51] suggested passive films were formed over the nitride coatings which are most likely hydrated titanium oxide and zirconium oxides. Also, the passivation current fluctuations have been studied for differently heat treated steels, after 20h of passivation in 0.2M H_2SO_4 at constant potentials +0.20V, +0.40V and +0.60V vs. SCE, respectively [52]. In this study [52] alternating passivation current have been monitored on the oscilloscope and transformed into a frequency domain by FFT, then power spectral density (PSP) value were calculated and represented in the dependence of frequency. It was found [52] that the curves (PSP vs. frequency) changed with heat treatment, passivation potential and the quality of the passive layers on the steel. In another study, the effect of applied D.C. potential and polarization time on the passivation of stainless steel 304 were investigated in deaerated 1M $NaHCO_3$ aqueous solutions at pH 8 [53]. Electrochemical impedance spectroscopy was used in conjunction with a rotating disc electrode. It was deduced that [53], the passive film present in the low region is partially dissolved

at 0.4 V vs. SCE and that a new passive film is formed in the higher potential region. And the reproducibility of the impedance spectra at constant potentials demonstrated that the passive film formation process is highly irreversible [53].

The effect of nitrogen on the electrochemical behavior of 301 Ln stainless steel in sulfuric acid solutions was investigated [54]. Electrochemical impedance spectroscopy data [54] indicates that the polarization resistance increased with increasing nitrogen content in the steel at open circuit potential and at +400 mV versus a saturated calomel electrode. Also, it was found that [54] the passive film formed on 301Ln stainless steel was more stable that that on 301 stainless steel. On the other hand, the inhibiting effect of octadecyclamine (ODA) on chloride induced localized corrosion of austenitic stainless steel type 321 was described at temperature ranging from 150 °C to 250 °C in deaerated aqueous solutions with chloride concentrations up to 10^{-1} M [55]. In this study [55], the increase of the corrosion resistance of the investigated materials is interpreted by an ODA-film on steel surface as a diffusion barrier, and the formation of a compact hot-water oxide layer, caused by the increase of pH resulted from ODA-cracking and dissociation.

An extremely thick and porous oxide film can be obtained on type 304 stainless steel [56]. In this study [56], the material was polarized in 5M H_2SO_4 solution at 50-80 °C with applied potential modulated as a square wave. The EIS and photoelectrochemical response were examined for two types of films: anodic type and cathodic type. The photo-current of both anodic and cathodic porous films exhibited p-type semiconductor responses, and the photo-current for anodic porous film increased with increasing film thickness. On the other hand, the photo-current

for the cathodic film remains approximately constant with increasing thickness [56]. Moreover, the passive state of Fe-12% Cr and Fe-25% Cr alloys in 1M sulfate solutions of pH 0 and 5 was studied with a combination of electrochemical techniques: impedance spectroscopy, photoelectrochemistry and dc resistance technique [57]. The steady-state passive film on the alloys (and on pure Cr) can be described as a thin, essentially insulating layer. Polarization of the steady-state metal/anodic film/electrolyte system to negative and positive potentials away from the potential region result in a substantial increase of the conductivity in the first layer adjacent to either the metal/film or the film/electrolyte interface [57]. Also, the electrochemical conditions for colored film formation on type 304 stainless steel with square wave polarization; was investigated by Fujimoto et al. [58]. In this study [58], a thick passive film which showing interference colors has been obtained in sulfuric acid solution. The deposited hydroxide, including mainly Cr^{3+}, formed at low potential loses protons and grows as a passive film under the high field provided. The colored film thus formed contains many diffusion path, which permit its further growth without any decrease in growth rate [58]. The alloys, Fe20Cr20Ni, Fe20Cr20Ni6Mo and Fe20Cr20Ni6Mo 0.2N, were polarized in 0.1 M HCl +0.4M NaCl at 22 °C and 70 °C [59]. At room temperature the Mo-alloyed steels are passivated in the potential range, -150 mV to 800 mV (SCE), where as the alloy without Mo has a break through potential at 0 mV(SCE), where pitting corrosion starts [59]. It is deduced that [59], the film consists of an inner oxide layer and an outer hydroxide layer where chromium in its three valence state is enriched in both phases. Molybdenum is slightly enriched in the oxide and

hydroxide layers in its six valence state. Nitrogen is enriched in the interface between the metal and the oxide as chromium nitride. The Ni contents are very low in the films formed at both temperatures [59]. Atres et al. [60] carried out an examination of the secondary passive film on type 304 stainless steel in 0.5 M H_2SO_4. The characterization techniques used were electrochemical (potentiodynamic; potentiostatic and film reduction experiments) and surface analytical techniques. It was found that [60] next to the metal, there was a modified passive film, which controls the electrochemical responses, i.e., governs the current for any applied potential. On top of this modified passive film, there was a porous corrosion-product film, which adds to the total film thickness but has little influence on the electrochemical response [60]. Looking to another study on SS 304, metastable and stable pitting on 304 stainless steel in 0.1-0.5 M NaCl aqueous solution (pH similar to 8) has been investigated using a potentiodynamic, a potentiostatic and a weak anodic current galvanostatic techniques[61]. The addition of bicarbonate (0.025-0.5 M) to the solution has an inhibiting effect. It was observed that [61], tile pit nucleation frequency and growth in the metastable and stable states, decreased as the $NaHCO_3$/NaCl molar concentration increased. On the other hand, corrosion of a sensitized high-nitrogen stainless steel (SS, nominally Fe-19% N) was studied by examining potentiodynamic polarization curves [62]. The SS was heat treated at temperatures of 600 °C to 1000 °C for times up to 1000 h. potentiodynamic polarization curves were generated in deaerated 1 M sulfuric acid (H_2SO_4) +0.01 M potassium thiocyanate (KSCN) at 30 °C at a scan rate of 100 mV/min [62]. Polarization curves region are two in the

passive region, and all were function of aging time and temperature [62]. Breslin et al. [63] described the influence of cerium treatments on the anodic and cathodic polarization behavior of type 316, 304 and 316L stainless steels. A decrease in the rate of oxygen reduction reaction was observed on treating the stainless steels by immersion in cerium-containing solutions at elevated temperatures followed by polarization in the deep cathodic region [63]. However, no inhibition of the oxygen reduction reaction was observed on simply treating the electrodes in the hot cerium-containing solutions. Looking to the results of this study, reduction in the passive current densities , increases in the polarization resistances and increases in the pitting potentials were observed for the stainless steels following treatment in boiling cerium solution [63]. Also, electrochemical properties of oxides formed on 250 maraging steel in steam at elevated temperatures were compared to standard phosphating treatment [64]. Polarization curves and time-to-pitting experiments established the advantage to these oxides over phosphating. Whereas the elongation of the oxide [64] was low, and diffusion coefficient of hydrogen was not dramatically smaller than for bare maraging steel, the threshold stress in stress corrosion cracking studies was significantly higher for oxidized steel. In another study, the corrosion behavior of the Fe-25Mn-5Al-0.15C alloy in different aqueous solutions of pH-0.8 to 15.3 and the corrosion protection mechanism induced by the presence of Al have been investigated by electrochemical measurements and AES/XPS analysis [65]. It was found that [65] the corrosion resistance of Fe-25 Mn-5Al-0.15 C steel in the aqueous solutions tested was comparable to that of mild steel. The outermost surface and the main part of the passive film formed on

the surface of Fe-25 Mn- 5Al steel in 30% NaOH solution are probably the bound water and a mixture of aluminum, iron and manganese oxides including metallic iron and Al, respectively [65]. Potentiodynamic polarization curves were measured for type AISI 304 and 316 stainless steels in 0.15 M NaCl solution at 4, 20, 40 °C [66]. The pitting potentials decreased with increasing temperatures. Results of surface enhanced Raman spectroscopy (SERS), which was carried out on SS 316, indicated that the corrosion films to be highly disordered and most likely to consist of a mixture of the oxides and hydroxides of the component elements of the stainless steel [66]. Moreover, the corrosion rates of AISI 304L and 316L stainless steels prepared by powder metallurgy (p/M) have been studied by continuous current electrochemical methods, in organic acid solutions(acetic, formic, latic and oxalic) at different concentrations [67]. The results revealed that the sintered AISI 304 L, and AISI 316L steels had the highest corrosion rates and the crevice corrosion attack was localized in the pore areas, close to the powder particle contact zone [67]. Luo et al. investigated the effects of hydrogen on the semiconductive properties and compositions of passive films on AISI 310 stainless steel (310 SS) and their corrosion behavior by Mott-Schottky plot, polarization, noise resistance analysis, and secondary ion mass spectroscopy (SIMS) [68]. The results indicated that, the susceptibility of 310 SS to pitting and electronic properties are strongly influenced by hydrogen present in the specimens, because the presence of hydrogen in 310 SS causes an inversion of conductivity type of a surface film from p-type to n-type, which consequently affect the susceptibility [68]. Passive films formed on sensitized stainless steel in sulfuric acid solutions

have been studied using photoelectrochemical techniques [69]. The results of the photocurrent measurement indicated that the passive films on sensitized stainless steel were characterized with n-type or p-type semiconductor in different potential regions. The difference in the photoelectrochemical behavior can be interpreted assuming that the passive film is an iron-chromium oxide solid solution associated with various hydration degrees of the Cr(III)-oxides at various potentials[69].

1.4 I-V characteristics of the oxide films formed at stainless steel surface:

Passive films formed on stainless steel in a borate buffer solution (pH 9.2) have been investigated by capacitance measurements and photoelectrochemistry [70]. The study was carried out on films formed on AISI type 304 and 316 stainless steels and high parity alloys with differing chromium, nickel, and molybdenum contents. Complementary research by Auger analysis [70] showed that the passive films were composed essentially of an inner chromium region in contact with the metallic substrate and an outer iron oxide region developed at the film/electrolyte interface. The semiconducting properties of the passive films are determined by those of the constituent chromium and iron oxides which are of p-type and n-type, respectively. Thus the influence of the alloying elements on the semiconducting properties of the passive films is explained by changes in the electronic structure of each of these two oxide regions [70]. Hakiki et al. studied the capacitance behavior of passive films formed on austenitic type 304 stainless steel and Fe-Cr alloys using the Mott-Schottky approach [71]. The results obtained

show that the films behave as n-type and p-type semiconductors in the potential range above and below the hat band potential, respectively. This behavior is assumed to be the semiconducting properties of the iron oxide and chromium oxide regions which compose the passive films [71]. Also, the action of the molybdenum on the electronic structure of the passive films formed on ferritic stainless steels was examined by capacitance measurements [72]. The research was supported by the mathematical analysis of a schottky barrier where the contribution of multiple bulk electronic states in the band gap was taken into account [72].

1.5 Surface characterization of the oxide films formed at stainless steel surface:

1.5.1 UV-visible light technique:

the influence of uv light (300 nm) on the nucleation of meta-stable pits on type 316 stainless steel in a neutral 0.5 M NaCl solution using current time measurements was described [73]. A significant increase in the induction periods and a decrease in the rate of pits nucleation were observed [73] for specimens pre-passivated under illumination conditions, indicating that illumination leaded to a modification of the passive film that persisted even after irradiation was removed. Also, ultra-violet (uv) light of wavelength 300 nm was irradiated on Fe-18 Cr alloy during passivation in a deaerated 0.1 M H_2SO_4 solution to modify the property of passive film [74]. In this study [74], XPS analysis of the passive film revealed that UV light irradiation during passivation enhanced Cr enrichment in the oxide layer

of the passive film which was correlated with an improved pitting corrosion resistance in the solution.

1.5.2 X-ray analysis (XRD,XPS):

Surface analysis methods, such as Auger electron spectroscopy (AES), x-ray photoelectron spectroscopy (XPS), secondary ion mass spectrometry (SIMS), glow discharge optical emission spectrometry and so on, have become indispensable to characterize surface and interface of many kinds of steel [75]. Although a number of studies on characterization of steel by these methods have been carried out, several problems still remain in quantification and depth profiling. Nevertheless, the methods have provided essential information on the concentration and chemical state of elements at the surface and interface [75]. An x-ray diffractometric technique has been used to determine the relative thicknesses of the two phases present in the duplex oxide formed on 20% Cr-25% Ni-Nb stabilized steel at 850 C in CO_2 [76]. Tempset et al. showed that at times less than 100 hr an outer spinel layer grows faster than an inner Cr_2O_3 rich layer, while after 500 hr the Cr_2O_3 layer was the faster growing. The results [76] indicated that parabolic kinetics do not pertain to the growth of the Cr_2O_3 layer during early oxidation (less than 500 hr). In another study [77], temperature resolved x-ray diffraction was applied to studies of high 100-1000 °C in air. With the measured series of diffraction patterns, the formation of the oxide layers was followed in situ, where the observed diffraction peaks enable the oxides to be identified [77]. An in-house grazing incidence x-ray scattering (GIXS) apparatus has been newly

developed for characterizing the surface structure at a microscopic level [78]. This system consists of an 18-kW relating anode x-ray generator, a flat or channel-cut Ge (111) single crystal monochromator and crossed double-axis diffractometers. Using this new apparatus [78], the x-ray reflection profiles of chromium oxide films grown on colored stainless steels were measured, the values of critical angle and thickness of films are estimated, and the density variation of chromium oxide films was suggested. The glow discharge optical emission spectrometry (GDS) was applied to determine the cobalt distribution accumulated in the corrosion films of type 304 stainless steel that was exposed to demineralized water with below 5 ppb of dissolved oxygen content at 561 k [79]. In this study [79], the structure and element depth distributions of the corroded specimen surfaces were analyzed by EPMA, XRD, XPS and GDS. Results showed that [79], tile corrosion film of the specimen exposed for 1000 hr had a clear double layer structure consisting of an iron-rich outer layer 3 μm in thickness and a chromium-rich layer 0.5 μm in thickness, where as the distribution of cobalt was peculiar in the corrosion film and its concentration tended to increase linearly with exposure time [79]. Also, oxidation of type 304 and 430 stainless steel for up to 1 hr was studied at 1273 k and the composition and structure of the oxide were determined by x-ray photoelectron spectroscopy (XPS) and x-ray diffraction (XRD) [80]. In the initial several tens of seconds, only iron-rich corundum-type oxide was formed, whereas the final oxide was composed of an inner chromium-rich corundum-type oxide layer and an outer mixed layer of corundum-type spinel-type oxides [80]. Lopez et al. [81] studied the structure and composition of passive films electrochemically

formed on AISI 304 and 316L stainless steels in a chloride-containing solution by soft x-ray absorption spectroscopy. The soft x-ray absorption spectra at the Cr 2p edges indicated that in all cases the passive film is mainly formed by Cr_2O_3, whereas spectra at the Fe and Ni 2p edges exhibited no significant contribution of Ni and Fe oxides to the passive layer composition [81]. However, differences in spectral shape with respect to metallic Ni and Fe suggested the presence of a small amount of hydroxides, which is maximum for the AISI 304 stainless steel polarized at the lowest scan rates [81]. In another study, the oxidation induced stoichiometric and morphological changes of the oxide film on a stainless steel surface were observed by x-ray photoelectron spectroscopy and atomic force microscopy for annealing temperatures in the range 400-500 °C in oxygen partial pressure of 10^{-4} to 10^{-4} torr [82]. It was found that [82] at 450 degrees c lower oxygen partial pressures found the formation of a smooth, pure chromium oxide, whereas at a high pressure the oxide formed mainly consists of iron oxide with distinct grains. Marijan et al. Also had been grown hydrous oxide film on stainless steel 304 under conditions of cycling voltammetry in 1 M NaOH solution [4]. A model, based on voltammetric, rotating ring-disc electrode and x-ray photoelectron spectroscopy measurements, implied that after hydrous oxide growth by potential cycling in an alkaline solution, the oxide placed in an acid solution remains enriched in chromium due to selective dissolution of nickel and iron [4]. Moreover, the structure and composition of chromium oxides films formed on 316 L stainless steel by immersion in a chromium electrolyte have been studied by SEM and XPS [83]. The chemical composition in the depth and thickness of the oxide layer have

been determined by XPS sputter profiles. It was found that [83], the oxide film can be described within the frame work of a double layer consisting of a thin outer hydrated layer and an inner layer of Cr_2O_3. Surface alloying of Al into AISI 310 austenitic stainless steel to increase its high temperature oxidation resistance was attempted by employing pack cementation process [84]. Oxidation resistances of AISI 310 stainless steel with or without aluminization treatment were evaluated by conducting thermal gravimetric analysis (TGA) in air at 700 and 1000 °C. After TGA, the oxides formed on the specimen surfaces were identified by x-ray diffraction analysis. The results [84] showed that the oxides formed on 310 stainless steel were composed of an outer spinal of Fe/Mn oxide and an inner layer of chromium oxide. Moreover, characterization of the structure and chemical composition of nickel oxide films formed on AISI 316L stainless steel by electrochemical anodic treatment in an aqueous electrolyte containing 560 g/L NaOH was made by electron microscopy and x-ray photoelectron spectroscopy (XPS) [85]. The depth chemical composition, thickness and duplex character of the oxide layer were determined by XPS sputter profiles using 3 keV Ar^+ ions [85]. The thickness of these layers was found to depend on he electrochemical conditions (current density or working time of the electrolyte).

1.5.3 Electron microscopy: (SEM, TEM, EDAX, ESCA and AES)

The oxide film formed on type 304 stainless steel in high temperature, high purity water containing oxygen, hydrogen, and hydrogen peroxide (H_2O) was analyzed by auger electron spectroscopy (AES), scanning electron microscopy (SEM), and transmission electron microscopy (TEM) [86]. AES data indicated a thicker oxide

was formed under 200 ppb O_2 or 200 ppb H_2O_2 conditions than less than 150 ppb H_2. The oxide film consisted of two layers: the outer oxide layer with different particle sizes and the inner, fine-grained layer [86]. Also, Sputter-deposited 304 stainless steel was electrochemically treated in 0.1 M H_2SO_4 aqueous solution [87], and was observed in air at atomic resolution with a scanning tunneling microscope. This study suggested that the surface is covered with a single oxide phase, which was initially rather disordered but crystallized with time[87]. Shibagaki et al. [88] analyzed an oxide thin film formed on a stainless steel by microfocused Auger electron spectroscopy (mu AES): the oxide film consisted of five sublayers of 2 to 4 nm in thickness. A recently built position-sensitive atom probe (POSAP) was used to visualize the 3D atom-by-atom microstructures of the oxide-alloy interface of a type 316 stainless steel [89,90]. It was found that[90], the oxide film formed at 350 °C and at 475 °C consisted of mostly iron oxide, whereas in the topmost part of the film at 475 °C, chromium oxide is predominant. The oxide film tend to grow only in the region just above where molybdenum does not exist [90]. Yen et al. [91] had been investigated the early oxidation (t less than or equal to 120 min) of AISI 430 stainless steel by thermal gravimetric analysis and Auger electron spectroscopy. Through analysis of the components of the oxide film and mathematical modeling, a critical temperature, Tc, above which a chromium-rich oxide film is formed was determined to be 947k. The corrosion resistance of the oxidized metal was enhanced at T greater than or equal to T_c but was worse at $T<T_c$ [91]. In another study, electrochemical scanning tunneling microscopy have been used to observe, in situ and in real time, the early stages of corrosion on

duplex stainless steel in aqueous NaCl solution [92]. With the specimens polarized in the transpassive region, the in situ techniques monitored clearly a process involving first a progressive etching of the damage layer, second the appearance of austenite and ferrite phases, and finally the formation of corrosion pits [92]. Also, oxidation behavior of 321 was studied [93]. TEM, SEM ,ESCA (surface chemical analysis) and EDS(electron diffraction spectroscopy) were used to study oxidation behavior. According to the results of TEM analysis after 500 DGC oxidation treatment, it was found that thin amorphous Fe oxide was formed on the surface and polycrystalline $(Cr, Fe)_2O_3$ was formed below the amorphous Fe oxide layer [93].

1.5.4 Infrared spectroscopy (IR):

Fourier transform infrared (FT-IR) spectroscopy was utilized in the analysis of various materials as a complementary technique to scanning electron microscopy during microstructural characterization[94]. Applications included: (1) detection of thin lubricating oil films on stainless steel; (2) characterization of the oxidation of stainless steel as a function of temperature and exposure time; (3) characterization of the aqueous corrosion of stainless steel during exposure in 0.1 M sodium chloride [94]. Also, reflectance infrared studies of the oxidation of types 304, 316 and 410 stainless steel, in oxygen at various temperatures, are described [95]. The value of the technique is in providing a record of oxide composition; changes with time and temperature. Pecharroman et al. [96] had determined the infrared complex permittivity functions of three varieties of maghemite, gamma-

Fe_2O_3; having different degrees of vacancy ordering, from their IR reflectance spectra, measured at near to normal incidence on pressed powder pellets. In this study, all calculations were based on a procedure for the estimation of the effective dielectric function of a mixture, which incorporates percolation features, recently developed by the authors [96].

AIM OF THESIS

The present thesis deals with the study of the formation of relatively thick oxide layer at the surface of stainless steels type 316 and 310 in highly acidic media. The possibility of using potential step programming for film deposition will be investigated. Several inquiries will be seek out of this work:

- What is/are the effect(s) of thickening the oxide film at the surface of stainless steel on its electronic properties?
- What are the electrochemical characteristics of the film formed in acidic medium and chloride-containing acidic medium?
- To devise an equivalent circuit for modeling the experimental data obtained.
- To fit the experimental data obtained to the devised model and deduce the electronic parameters of the film.
- To study the effect of changing the bath composition during film formation on its properties.
- To examine the morphological structure of the films formed under different experimental conditions.
- To analyze the surface composition of the film using x-ray photoelectron spectroscopy and energy dispersive x-ray analysis.
- To estimate the film thickness from electrochemical parameters and surface reflectance FT-IR spectroscopy.
- To compare the electronic and surface structure of the films formed at both stainless steel types 316 and 310.

- To examine the photo-electrochemical response of different films in acidic medium.

II. EXPERIMENTAL SECTION

II. EXPERIMENTAL SECTION

II. Experimental

1. Materials and Reagents

1.1 Stainless Steel Samples

Two types of stainless steels were investigated: AISI 310 (SS 310) and AISI 316 (SS 316). The stainless steel samples were purchased from Goodfellow (Huntingdon, England). The compositions of the stainless steels used in this study are given in Table III according to the data sheet provided by the supplier.

1.2 Reagents and Solutions Preparation

Sulfuric acid, sodium chromate, ammonium molybdate, and sodium chloride used in this study were high purity grade reagents. All chemicals purchased were used as received and were supplied by Aldrich Chem. Co. (Wisconsin, USA).

Test solutions were prepared from stock and diluted using de-ionized water supply. Water was first distilled then de-ionized using Millipore water purification system. The conductivity of water used in this study is 18.3 μS.

1.3 Electrode Mounting and Electrochemical Cells

AISI 310 and AISI 316 stainless steel specimens were in the form of rods and foils. Rod specimens were prepared and mounted according to the following steps: stainless steel rods were cut in the dimensions of 2.0 cm long and 0.60 cm diameter. The stainless steel specimen was then grooved and threaded for electrical contact and connection. A copper rod 12.0 cm long and 0.35 cm diameter

Table III. **Weight Percentage chemical composition of SS 310 and SS 316**

Element	SS 310	SS 316
Cr	25	16.9
Ni	19.3	10.9
Si	0.65	0.75
Mn	1.79	1.24
P or N	0.021 (P)	0.025 (N)
S	0.006	0.027
Cu	0.17	0.20
Mo	0.43	2.11
V	0.13	-
C	0.018	0.053
Fe	Balance	Balance

was used for establishing electrical contact. The whole assembly was finally inserted in a glass tube 10.0 cm long and 0.8 cm inner diameter. Epoxy resin (Torr Seal, from Varian, MI, USA) was used to ensure the exposure of a determined apparent surface area of 0.282 cm^2 (see figure II1 for details). This specimen configuration was used for electrochemical oxide growth and characterization.

Flat specimen configuration was used for samples prepared for surface examination. In this setup, the stainless steel foils in the dimensions of 5 cm x 5 cm and 2 mm thick were cut and mounted on a flat cell holder as shown in figure II2. The surface area exposed is either 1.0 cm^2 or 5.0 cm^2 according to the cell used (Figure II2b and Figure II2c, respectively).

Prior to oxide film formation, the surface of the steel specimen was prepared according to the following steps: the surface was polished mechanically using metallurgical papers of successive grades (120 - 600 - 1200 μm). Then the surface was polished using alumina paste (0.3 μm) dispersed on a soft cloth paper until a scratch-free surface is obtained. The surface was rinsed with distilled water, degreased in ethanol and was thoroughly rinsed with de-ionized water.

Two types of electrochemical cells were used in this investigation. A three-electrode one compartment glass cell, with a saturated Ag/AgCl reference electrode and a platinum sheet (2 x 2 cm^2) counter electrode was used for oxide film formation and subsequent electrochemical characterization of the stainless steel working electrode (see figure II2).

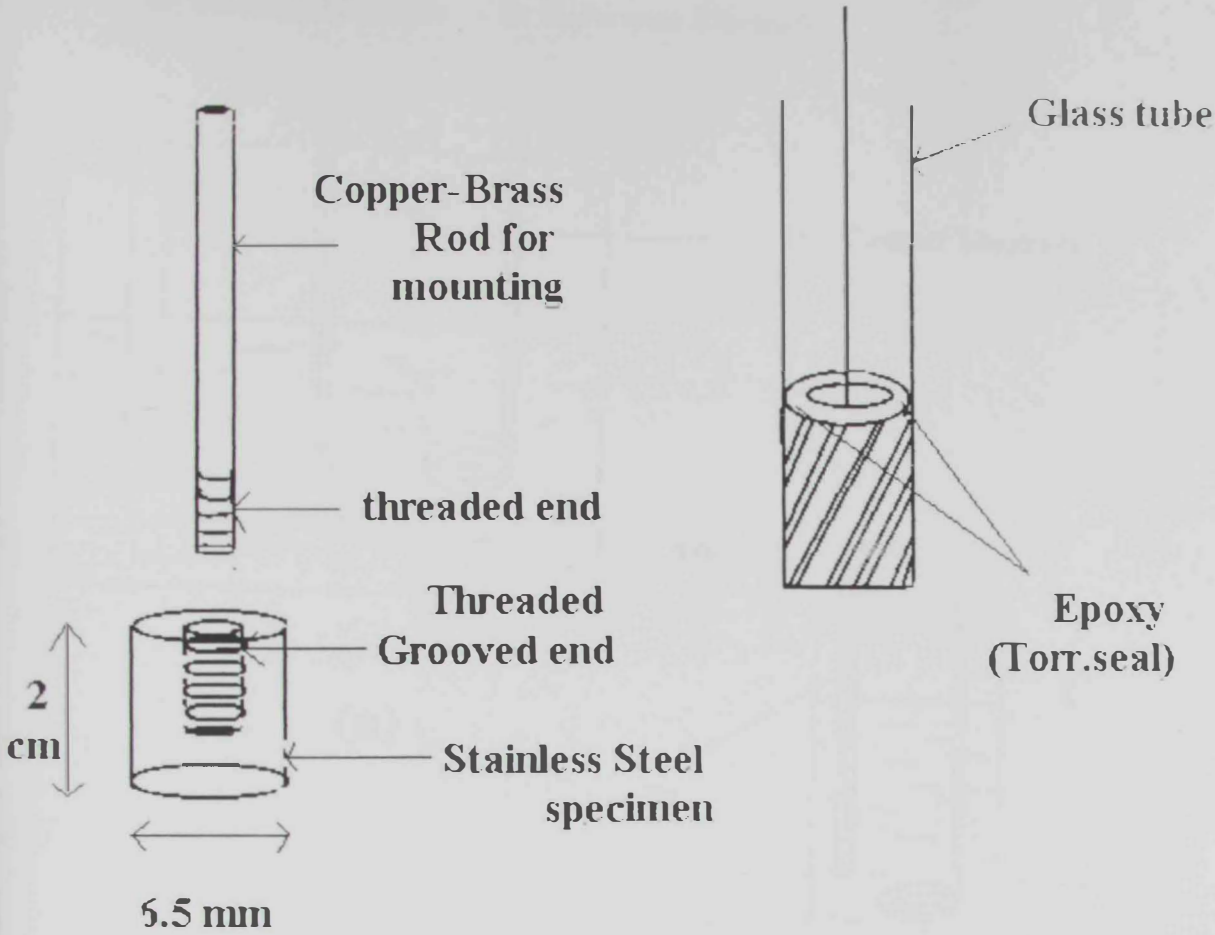

Top View

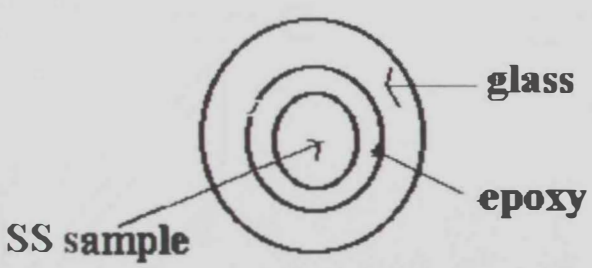

Figure II1. Stainless Steel Electrode Mounting

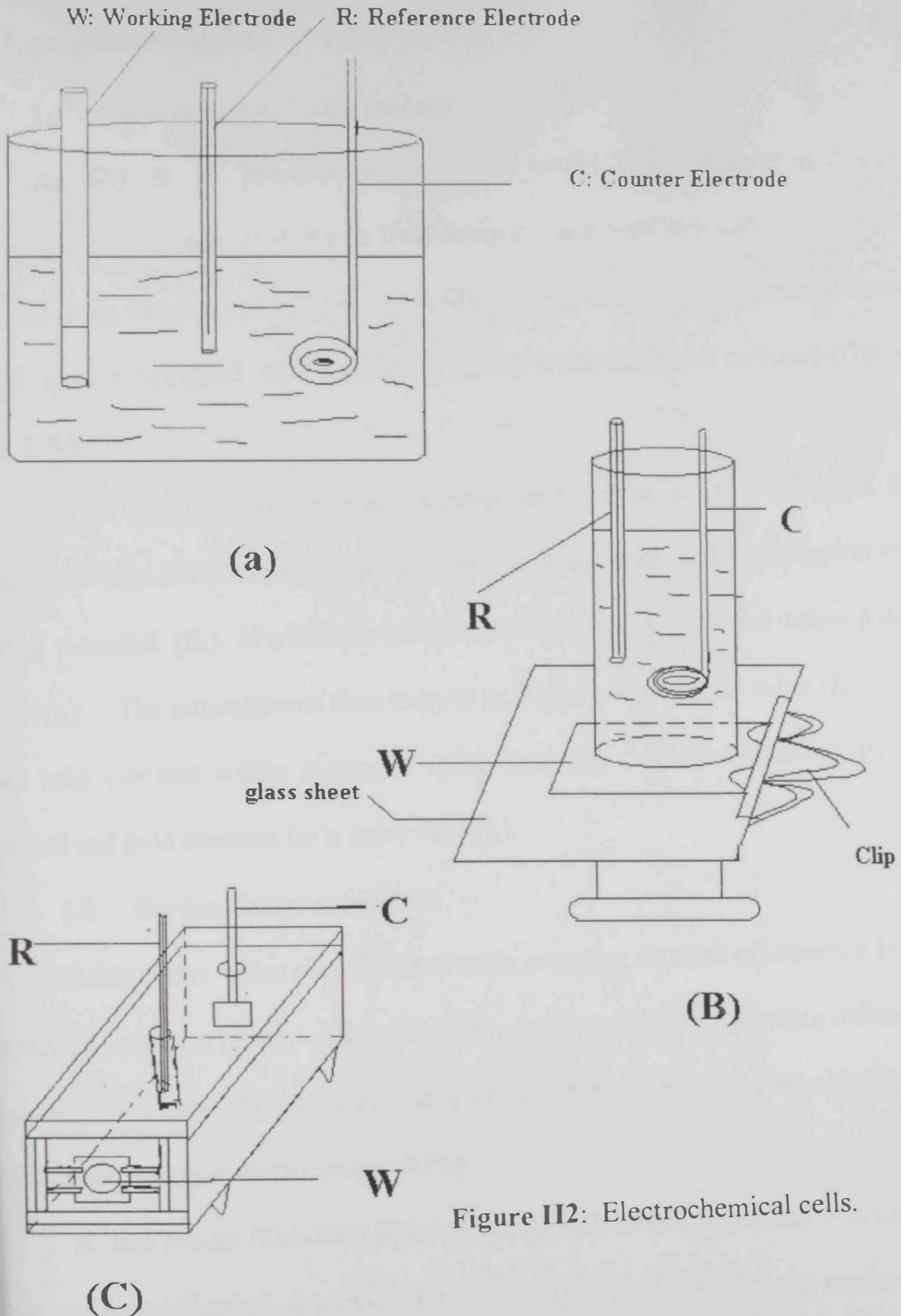

Figure II2: Electrochemical cells.

2. Equipments and Instrumentation

2.1 Electrochemical Equipments

An EG & G potentiostat/galvanostat model 371A (Princeton Applied Research, USA) controlled by an IBM computer and *SoftCorr* software was used for the oxide film formation. The oxide film formed was examined using a Gamry CMS system equipped with a PC and a Gamry control/analysis software (Gamry, Inc., USA).

Oxide film formation was accomplished using a three potential step program. The EG & G instrument was programmed to allow the application of an initial potential (E_1) at which the electrode surface was maintained within a delay time (t_1). The potential was then stepped to the second potential value (E_2) which was held constant within a second delay time (t_2). A final potential (E_3) was applied and held constant for a delay time (t_3).

2.2 Surface Instrumentation

Oxide films were characterized using scanning electron microscopy (SEM) equipped with an energy dispersive x-ray analyzer (EDXA), surface reflectance Fourier transform infra-red spectroscopy (SRFTIRS), x-ray diffraction (XRD) and x-ray photoelectron spectroscopy (XPS).

A Jeol Model JSM-5600 SEM equipped with EDXA capability was used for surface morphological determination. The instrument is fully computerized with 18 - 300,000 times magnification power, with guaranteed resolution of 3.5 nm, acquisition of both secondary and back-scattered electron images. The samples

were coated with a thin film of gold to eliminate the effect of charging during measurements. A Jeol JFC-1200 fine coater was used for this purpose and a current of 20 mA was applied for 150 s coating period.

SRFTIRS experiments were achieved using a Nicolet Magna-IR spectrometer, Nic-Plan IR-microscope and a Spectra Tech stage controller. All results were analyzed using an Omnic software and library.

For XRD experiments, a Philips analytical x-ray instrument equipped with a diffractometer type PW1840 was used. The instrument is equipped with a Cu anode, with a generator tension of 40 kV, a generator current of 30 mA. The receiving slit was set at 0.2. Other conditions for the experiment setup is listed in table II6.

XPS experiments were performed using a Perkin-Elmer ESCA-5300 spectrometer with a pass energy of about 25 eV (ΔE = 0.5 eV). Measurements were accomplished using a high x-ray flux density.

3. Solutions Preparations

All solutions were prepared from reagent grade chemicals and distilled/deionized water. The 0.1 M H_2SO_4 was prepared by the dilution from the 5 M H_2SO_4 solution. The solutions prepared and used are:

(1) For the Oxidation step, 5 M H_2SO_4, 5 M H_2SO_4 + 0.01 M Na_2CrO_4, 5 M H_2SO_4 + 0.01 M $(NH_4)_2MoO_4$.

(2) For the Testing step, 0.1 M H_2SO_4, 0.1 M H_2SO_4 + 0.1 M NaCl, 0.1 M H_2SO_4 + 0.01 M NaCl, 0.1 M H_2SO_4 + 0.001 M NaCl.

4. Arrangement for Oxidation step

The oxidation step experiments were conducted in a three-electrode system cell containing a platinum counter electrode, a saturated Ag/AgCl electrode as a reference electrode, and the stainless steel (310 or 316) as the working electrode. The electrolyte used was mainly 5 M H_2SO_4. In some experiments the solutions: [5 M H_2SO_4 + 0.01 M Na_2CrO_4] and [5M H_2SO_4 + 0.01 M $(NH_4)_2MoO_4$] were also used to determine the effect of changing the oxidizing bath.

The EG & G potentiostat/galvanostat equipped with a personal computer were used for oxide layer formation on the surface of the working electrode with different thicknesses.

The following potential step programs were used for oxide growth onto the stainless steel surface:

- For SS 310; the oxide formation program was:

E_1 = -1.4 V, t_1 = 60 s

E_2 = -0.9 V, t_2 = 100 s – 600 s

E_3 = -0.8 V, t_3 = 60 s

For SS 316; the major oxide formation program was:

Program 1:

E_1 = -1.2 V, t_1 = 60 s

E_2 = -0.5 V, t_2 = 100 s – 600 s

E_3 = 0.6 V, t_3 = 60 s

Other programs were used for SS 316 in order to study the effect of changing the oxide formation programs on the characteristics of the oxide film. The following programs were also employed:

Program 2:

E_1 = -1.2 V, t_1 = 60 s

E_2 = -0.9 V, t_2 = 100 s – 600 s

E_3 = -0.5 V, t_3 = 60 s

Program 3:

E_1 = -1.2 V, t_1 = 60 s

E_2 = -0.5 V, t_2 = 100 s – 600 s

E_3 = 0.0 V, t_3 = 60 s

The scanning rate for potential step programs in all experiments was 100 mV/s and the applied potential was modulated as a square wave.

5. Oxide Characterization

5.1 EIS Measurements

The EIS measurements on oxide-covered stainless steel were performed at room temperature in a 0.1 M H_2SO_4 test solution. Some experiments were carried out in an aggressive media of 0.1 M H_2SO_4 and different concentrations of NaCl. A three-electrode electrochemical cell, with a saturated Ag/AgCl reference electrode vs. SHE and a platinum counter electrode, was also used for all measurements. The exposed sample area was 0.282 cm^2.

The EIS measurements were carried out with a CMS 100 electrochemical impedance system. The measurements were performed under potentiostatic control at the open circuit potential. The test conditions are listed in Table 112.

After the determination of the open circuit potential (E_{open}) from the open circuit delay that lasts for 1200 s, sine wave voltages (10 mV/s) peak to peak, at the frequencies between 5 x 10^3 Hz to 10^{-2} Hz, were superimposed on the open circuit potential. All the measurements were automatically controlled with the aid of the computer program provided by Gamry.

Table 112. EIS test conditions

Reference Electrode	Ag/AgCl
Counter Electrode	Platinum
Electrolyte	H_2SO_4
Electrolyte Concentration	0.1 M
Tested Area	0.282 cm^2
Frequency Range	10^{-2}~ 5000 Hz
AC Potential	10 mV
DC Potential	0 mV (E_{open})

5.2 Other Electrochemical Measurements

Other electrochemical experiments were performed in the same three-electrode cell used for the EIS measurements with the same testing electrolyte at room temperature. Three types of electrochemical measurements were done: Tafel, Polarization Resistance, and Potentiodynamic Polarization measurements. All measurements were carried out with the Gamry CMS 100 software. Test conditions for each electrochemical method are listed in Table II 3, Table II4, and Table II5, respectively. The potentiodynamic polarization measurements were performed first in order to determine the potentials at which oxides can be formed and built up for both SS 310 and SS 316.

5.2.1 Tafel Method

Tafel experiment were conducted according to the conditions listed in Table II3.

5.2.2 Polarization Resistance

Polarization experiments were conducted according to the conditions listed in Table II4.

5.2.3 Potentiodynamic Polarization

Potentiodynamic polarization experiments were conducted according to the conditions listed in Table II5.

Table II3. Test conditions for Tafel experiments

Reference Electrode	Ag/AgCl
Counter Electrode	Platinum
Elecrolyte	H_2SO_4
Electrolyte Concentration	0.1 M
Tested Area	0.282 cm^2
E_I	-250 mV vs. E_{open}
E_f	+250 mV vs. E_{open}
Scan Rate	1 mV/s

Table II4. Test conditions for Polarization Resistance experiments

Reference Electrode	Ag/AgCl
Counter Electrode	Platinum
Elecrolyte	H_2SO_4
Electrolyte Concentration	0.1 M
Tested Area	0.282 cm^2
E_I	-20 mV vs. E_{open}
E_f	+20 mV vs. E_{open}
Scan Rate	1 mV/s

Table 115. Test conditions for Potentiodynamic experiments

Reference Electrode	Ag/AgCl
Counter Electrode	Platinum
Elecrolyte	H_2SO_4
Electrolyte Concentration	0.1 M
Tested Area	0.282 cm^2
E_I	-0.5 V vs. $E_{reference}$
E_f	+1.2 V vs. $E_{reference}$
Scan Rate	1 mV/s

6. Surface Analysis

A flat type three-electrode electrochemical cell (cf. figures 2b and 2c), with saturated Ag/AgCl reference electrode and a platinum counter electrode, was used to prepare the samples for surface analyses. The working electrode was in the form of sheet with surface area about 1.0 or 5.0 cm^2 according to the cell used. The electrochemical cell was a pyrex glass cylinder with a flat circular piece of glass fused on each end. Two small holes on the top of the cylinder connected with two plastic tubes were used to accommodate the gas bubbler. A platinum sheet counter electrode of large area was housed inside the chamber. A cavity was left at the top of the chamber to be filled with the testing solution and to insert the reference electrode. The cavity is connected to the working electrode through a Luggin capillary tube. Oxide film formation was carried out in 5.0 M H_2SO_4. EG & G potentiostat/Galvanostat was used for oxide film formation in all cases for subsequent surface measurements.

6.1 X-Ray Diffraction

AISI 316 stainless steel sheets of surface area 1.0 cm^2 were investigated after the oxide layer had been formed on the surface with different thickness and using different potential step programs (basically: program 1 and 2). Also the effect of changing the oxidation bath on the structure of the oxide layer was investigated by X-ray diffraction measurements. Test conditions are listed as indicated in Table II6.

Table 116. Test conditions for X-Ray Diffraction experiments

Diffractometer type	PW1840
Tube anode	Cu
Generator tension	40 KV
Generator current	30 mA
Wavelength α_1	1.54056 A°
Wavelength α_2	1.54439 A°
Intensity ratio(α_1/α_2)	0.500
Monochromator used	No
Full scale of recorder	10 Kcount/s
Time constant of recorder	0.5
Start angle	2.010° 2θ

6.2 Scanning Electron Microscope (SEM)

Samples investigated by SEM of both AISI 310 and AISI 316 were in the form of sheets with surface area of about $1 cm^2$. For each type of stainless steel two different thickness were studied (films grown for 200 s and 600 s, respectively). In addition, the effect of changing the oxidizing bath was studied for both types (for films grown at 600 s).

6.3 Surface Reflectance FT-IR Spectroscopy

The effect of changing the thickness of the oxide layers formed on the surface of AISI 316 stainless steel under investigation were determined using this technique. Oxide film formation was achieved as indicated in previous sections. Films were formed on AISI 316 stainless steel using potential step program number 1. Films with variable thickness, were formed by holding E_2 applied to the working stainless surface in 5.0 M H_2SO_4 for different time periods, ca. 100 s, 200 s, 300 s, 500 s and 600 s, respectively. Absorption peak due to the oxide film was measured as a function of thickness.

III. RESULTS AND DISCUSSION

Potentiodynamic Polarization Data at Stainless Steel Surfaces

1. Polarization Curves of Stainless Steel in Strong Acidic Solutions

One important goal for this work is to form a stable oxide film over stainless steel surfaces. As described in the experimental section, oxide film formation at stainless steel surfaces was accomplished using a potential step program in acidic solutions. Therefore, it was essential first to determine the regions at which the formation of the oxide film is conceivable. Studying the potentiodynamic polarization behavior would clarify the current/potential (I/V) characteristics for the stainless steel in the acid medium. Thus, figures IIIIa and IIIIb show the potentiodynamic curves of stainless steel type 316 and stainless steel type 310 exposed to aerated 5.0 M H_2SO_4 solution, respectively. The sweep rate used was 5 mV/s, and potentials recorded vs. Ag/AgCl. The following conclusions could be withdrawn from the data of figures IIIIa and IIIIb:

- The polarization behavior of the different types of stainless steels studied is strongly dependent on the steel structure.

  In both figures, region A is the immune region in which the metal specimen is protected from dissolution as the applied potential is much lower than the corrosion potential (E_{corr}), region B is the active region in which the metal specimen corrodes as the applied potential is made more positive. At C further increase in the rate of corrosion (as measured by the current) ceases and the onset of passivation begins.

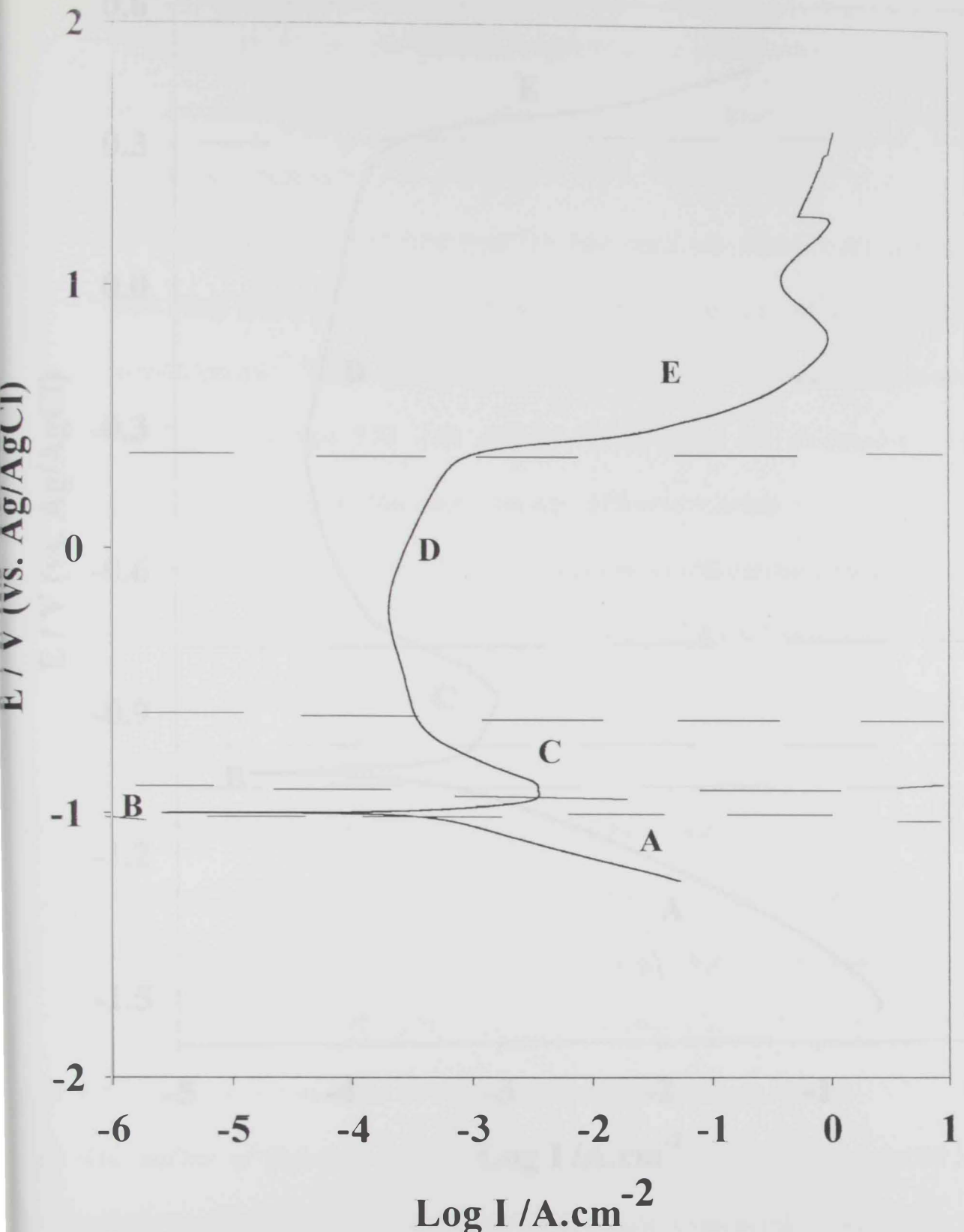

figure III1a: Potentiodynamic Polarization curve for SS 316 in 5 M H_2SO_4

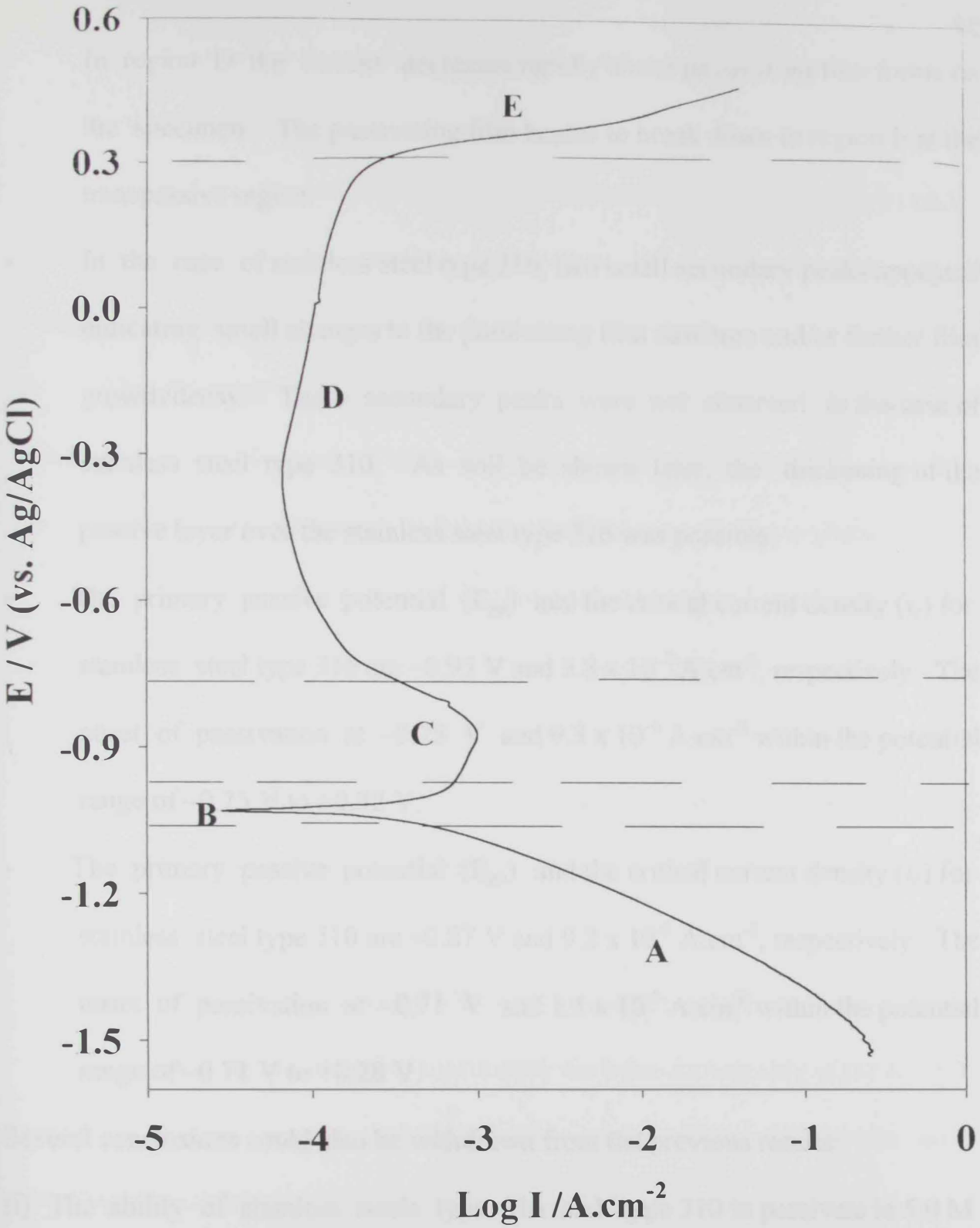

Figure III1b: Potentiodynamic Polarization curve for SS 310 in 5 M H_2SO_4

In region D the current decreases rapidly as the passivating film forms on the specimen. The passivating film begins to break down in region E at the transpassive region.

- In the case of stainless steel type 316, two small secondary peaks appeared indicating small changes to the passivating film structure and/or further film growth/decay. These secondary peaks were not observed in the case of stainless steel type 310. As will be shown later, the thickening of the passive layer over the stainless steel type 316 was possible.
- The primary passive potential (E_{pp}) and the critical current density (i_c) for stainless steel type 316 are –0.95 V and 5.8×10^{-3} A.cm^{-2}, respectively. The onset of passivation at –0.75 V and 9.3×10^{-4} A.cm^{-2} within the potential range of –0.75 V to +0.32 V.
- The primary passive potential (E_{pp}) and the critical current density (i_c) for stainless steel type 310 are –0.87 V and 9.2×10^{-4} A.cm^{-2}, respectively. The onset of passivation at –0.71 V and 1.1×10^{-4} A.cm^{-2} within the potential range of –0.71 V to +0.28 V.

Several conclusions could also be withdrawn from the previous results:

(i) The ability of stainless steels type 316 and type 310 to passivate in 5.0 M sulfuric acid is realized and stabilized within a relatively wide range of potential. However, passivating current in the case of stainless steel type 316 is relatively higher than that shown for stainless steel type 310.

(ii) Both stainless steels studied showed a stable passive oxide layer over a potential window of ca. 1.0 V.

(iii) Oxide film formed over stainless steel type 316 is relatively more stable than that formed over stainless steel type 310 surfaces under similar experimental conditions, as will be shown in next sections.

(iv) The structure of stainless steel type 316 with relatively less Cr and Ni and with more Mo content than that for stainless steel type 310 is a possible explanation for the differences in the potentiodynamic polarization behavior.

In this respect, the choice of the programmed potential step was to ensure the following aspects in the applied potential: (i) the first applied potential is in the immune region where hydrogen evolution is taking place, (ii) the second applied potential step is at the maximum rate at which the oxide film is formed, and (iii) the final potential lays in the passive region or beyond.

2. Polarization Curves of Oxide Films formed at Stainless Steel Surfaces

At this stage it was advisable to examine the behavior/stability of the formed oxide. In this respect, potentiodynamic polarization experiments were conducted at stainless steel type 316 and type 310 after oxide film formation.

- In this part of the work the electrochemical behavior of the oxide film formed on each type of stainless steels was examined. Thus, oxide film formation using potential step program #1 was used for stainless steel type

316. Film thickening was achieved by varying the time at which the second applied potential was held constant in the potential program, ca. between 100 and 600 seconds. Figure III2 depicts the Tafel plots for stainless steel type 316 after oxide film formation in 5.0 M sulfuric acid using program (1) with variable oxide thickening time and tested in 0.1 M sulfuric acid. Scan rate used was 5 mV/s. The following observations could be drawn from the data of figure III2:

- Corrosion potential (E_{corr}) values for oxide covered stainless steel increased towards anodic values considerably when compared to the corrosion potential of bare stainless steel (ca. –1.24 V and –0.48 V to –0.38 V for bare and oxide-covered stainless steel with different thickness, respectively). Moreover, corrosion current density (I_{corr}) values decreased appreciably when comparing the Tafel curve of the bare surface to that with oxide formed with time of deposition of 100 s. Moreover, the value of I_{corr} decreased as the oxide film thickness increases (as indicated by the increase in the time of oxide film deposition at the second applied potential value, E_{app2}). Typical change in the value of I_{corr} is from 1.2×10^{-4} A.cm^{-2} to 1.1×10^{-6} A.cm^{-2} for oxide-free and oxide-covered surfaces, respectively.
- Anodic and cathodic Tafel constants, (β_a and β_c), showed different trends. Anodic Tafel slopes increased with oxide thickness, while cathodic Tafel

slopes showed merely unchanged values. Electrochemical parameters for polarization data of stainless steel type 316 are given in table IIII.

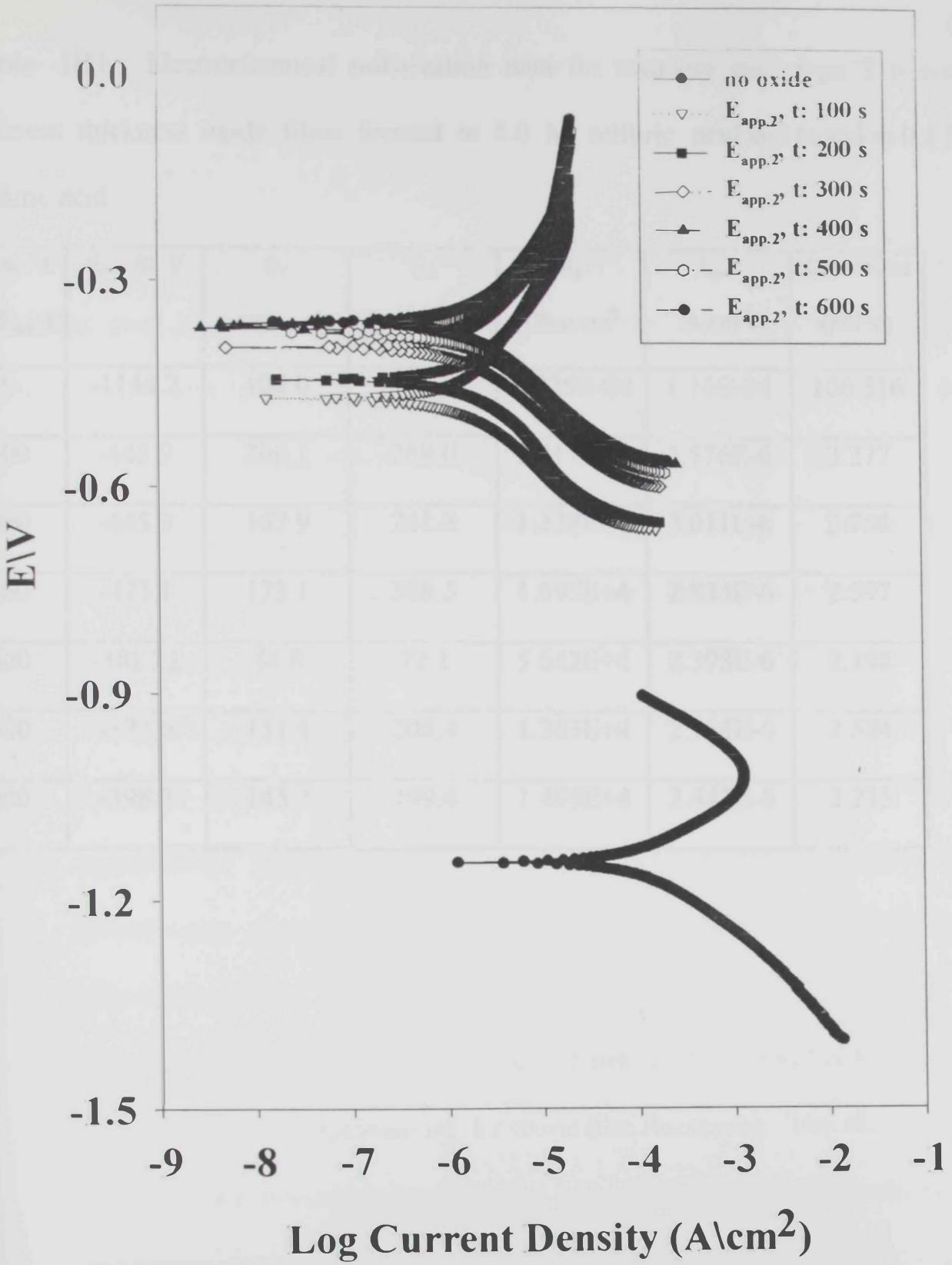

Figure III2. Tafel Plots for SS 316 tested in 0.1 M H_2SO_4 after Oxide Formation in 5 M H_2SO_4 $E_{app.2}$, t: 100 s - 600 s

Table IIII. Electrochemical polarization data for stainless steel type 316 with different thickness oxide films formed in 5.0 M sulfuric acid and tested in 0.1 M sulfuric acid.

Time / s (at E_{app2})	E_{corr} /m V	β_c mV/Decade	β_a mV/Decade	R_p Ohm.cm^2	I_{corr} A.cm^{-2}	Corr. Rate (MPY)
0	-1144.2	108.0	98.1	1.925E-04	1.16E-04	106.316
100	-445.9	206.1	269.0	1.417E+4	3.576E-6	3.277
200	-445.9	167.9	241.3	1.428E+4	3.011E-6	2.760
300	-473.1	173.1	306.5	1.695E+4	2.834E-6	2.597
400	-381.22	54.8	72.1	5.642E+4	2.398E-6	2.198
500	-377.6	151.4	208.4	1.383E+4	2.754E-6	2.524
600	-398.7	145.3	199.4	1.495E+4	2.442E-6	2.235

Where R_p is the polarization resistance and calculated from the relation [100]

$$R_p = \frac{\Delta E}{\Delta i} = \frac{\beta_a \beta_c}{2.3(I_{CORR})(\beta_a + \beta_c)} \qquad (1)$$

On the other hand, figure III3 shows the data obtained for oxide-covered stainless steel type 310 obtained under similar experimental conditions as the data obtained for stainless steel type 316. The following conclusions could be withdrawn from figure III3 and compared to those depicted in figure III2:

- Corrosion potential (E_{corr}) values showed irregular trend as well as the corrosion current (I_{corr}) values. Thus, (E_{corr}) showed most cathodic values for constant potential value applied for 100 s and 200 s during oxide film formation. On the other hand, most anodic values for (E_{corr}) were observed for oxide films formed at constant applied potential for 300 s and 400 s, respectively. Corrosion current (I_{corr}) values showed similar trend and the lowest value observed was for the oxide film formed at constant applied potential for 300 s.
- Constant applied potential for extended times, ca. 500 s and 600 s, showed no indication of improvement for oxide film thickening. This observation will also be confirmed in later sections when examining the electrochemical impedance spectroscopic data.

Anodic and cathodic Tafel constants, (β_a and β_c), showed distinct values only in the ase of oxide films formed for 300 s and 400 s at constant applied potentials.

lectrochemical parameters for polarization data of stainless steel type 310 are given n table III2.

3. Polarization Curves of Oxide Films in Presence of Chloride Ions

The presence of chloride ions namely, in acidic media affects the stability of the film ayer formed at the surface of the stainless steel [97] that mainly led to pit formation nd the inclusion of the chloride ion within the oxide film. It has been shown that Cl^- ons are incorporated in the passive layer when the passivation is taking place in Cl^- - ontaining electrolyte [98]. No chloride is detected in passive film when the steel is irst prepassivated in Cl^- -free environment and then exposed to Cl^- containing acid 99]. Figure III4A shows the results obtained for stainless steel type 316 exposed to ifferent concentrations of chloride ions in 0.1 M H_2SO_4 after oxide film formation nd passivation in 5.0 M H_2SO_4. The electrochemical parameters for the stainless teel and the oxide-covered steel are included in table III3.

Table III2. Electrochemical polarization data for stainless steel type 310 with different thickness oxide films formed in 5.0 M sulfuric acid and tested in 0.1 M sulfuric acid.

Time / s (at E_{app2})	E_{corr} / mV	β_c mV/Decade	β_a mV/Decade	R_p Ohm.cm^2	I_{corr} A.cm^{-2}	Corr. Rate (MPY)
0	-925.1	75.9	124.8	2.081E+3	9.85E-6	9.027
100	-960.0	136.1	316.5	9.39E+2	4.403E-5	40.351
200	-947.1	123.3	281.1	8.934E+2	4.403E-5	38.178
300	-699.8	123.3	281.1	8.934E+2	4.166E-7	0.676
400	-729.5	296.6	243.2	9.175E+3	6.325E-6	5.797
500	-868.2	100.8	227.7	1.041E+3	2.914E-5	26.709
600	-871.0	133.2	235.5	1.192E+3	3.10E-5	28.412

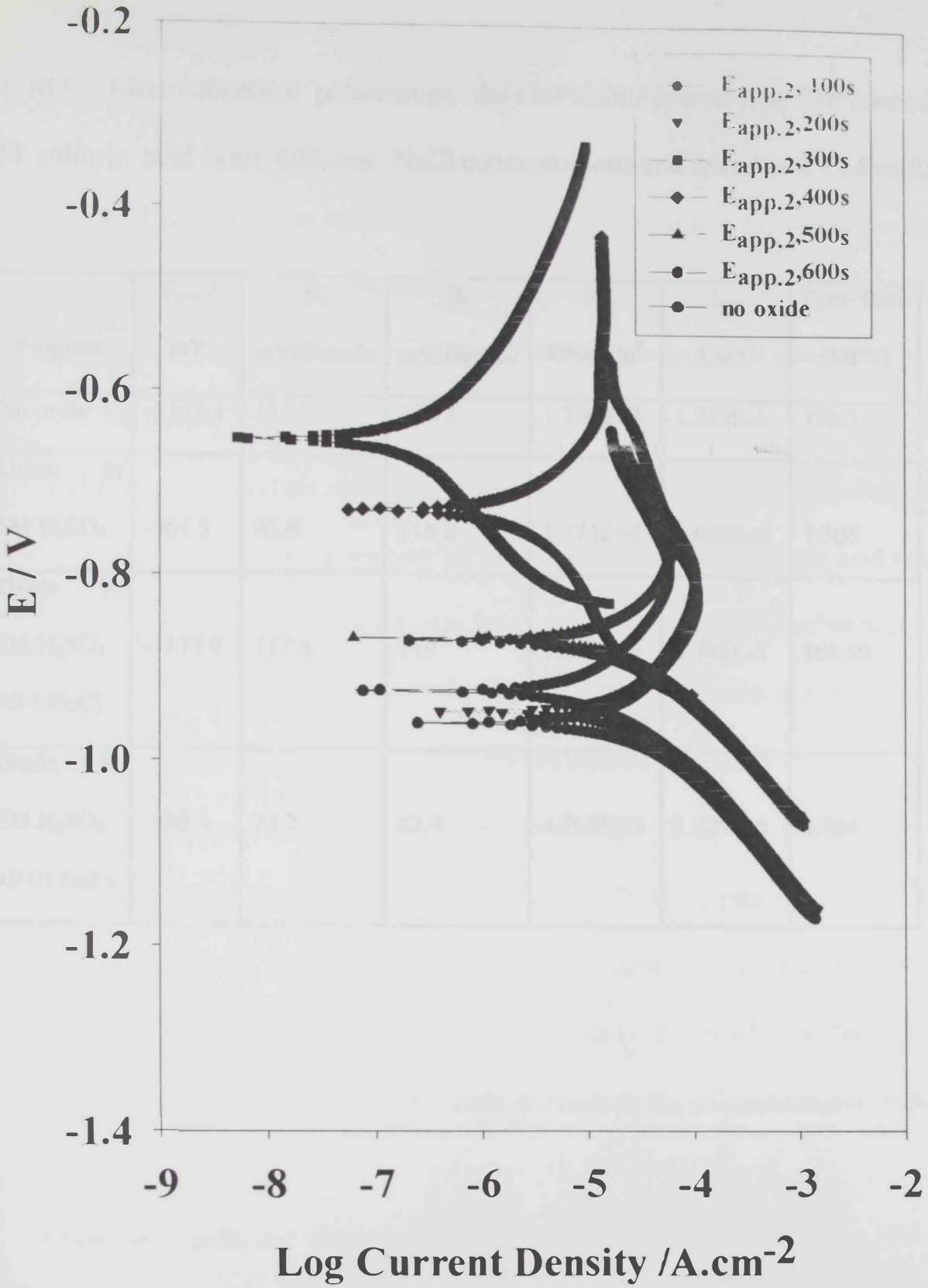

Figure III3. Tafel Plots for SS 310 tested in 0.1 M H_2SO_4 after Oxide Formation in 5 M H_2SO_4 $E_{app.2}$, t: 100 s - 600 s

able III3 Electrochemical polarization data for stainless steel type 316 formed in .0 M sulfuric acid with different NaCl concentrations and tested in 0.1 M sulfuric cid.

Program	E_{corr} / mV	β_c mV/Decade	β_a mV/Decade	R_p Ohm.cm^2	I_{corr} A.cm^{-2}	Corr. Rate (MPY)
No oxide	-1144.3	133.7	179.2	1.766E+2	1.234E-4	172.5
Oxide in 5M H_2SO_4	-361.5	93.9	116.3	1.374E+4	1.642E-6	1.505
Oxide in 5M H_2SO_4 +0.1 NaCl	-1177.9	117.4	119	1.438E+2	1.785E-4	163.59
Oxide in 5M H_2SO_4 +0.01 NaCl	-430.5	33.7	43.4	4.767E+3	1.728E-6	1.584

The following observations and conclusions could be withdrawn from the data of table III3:

- The highest corrosion rate in this aggressive medium was for the oxide-free surface. Moreover, the corrosion current, I_{corr}, showed a gradual decrease in the order of oxide-free surface in 0.1 M H_2SO_4 > oxide-covered surface in 0.1 M H_2SO_4 > oxide-covered surface in 0.1 M H_2SO_4 and 0.1 M NaCl > oxide-covered surface in 0.1 M H_2SO_4 and 0.01M NaCl. It is evident that oxide layer imparts protection to the stainless steel in sulfuric acid when comparing the data in figure III4A for curves a, and b. On the other hand, in presence of chloride ions, a slight increase in the corrosion rate is observed in case of a ten-fold increase in the concentration of chloride.
- Both anodic and cathodic Tafel constants (β_a and β_c) showed a relative increase when comparing the oxide-free surface to oxide-covered surface tested in 0.1 M H_2SO_4. Similar result is shown in the case of the oxide tested in H_2SO_4 + 0.01 M NaCl and that tested in H_2SO_4 + 0.1 M NaCl. The result is manifested in the noticeable increase in the polarization resistance, R_p, value.
- Opposite results are observed in the case of stainless steel type 310 as depicted in figure III4b. The results showed that the corrosion rate increased considerably with the chloride ion in the medium. Moreover, the

-

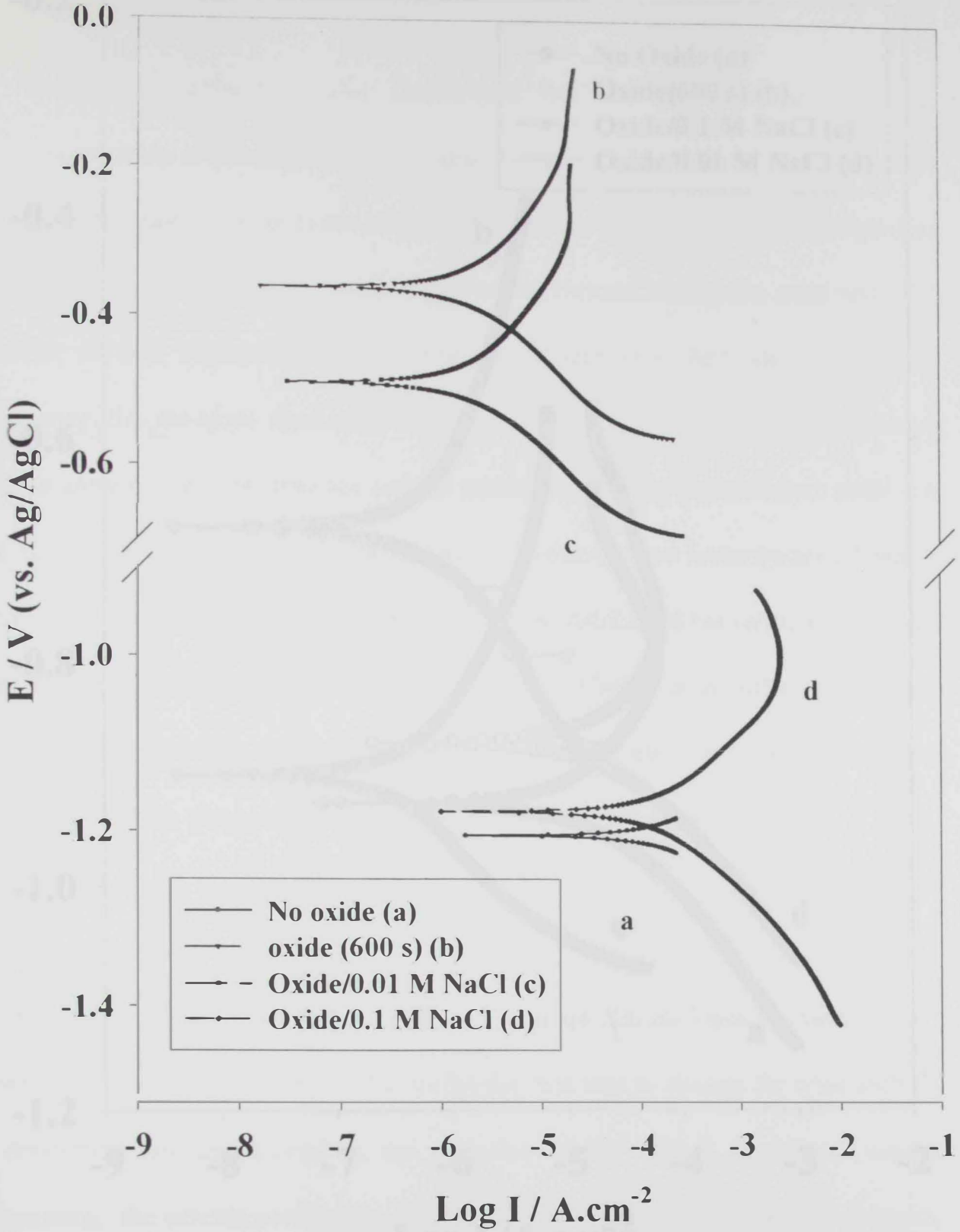

Figure III4a: Effect of Chloride on the Polarization of SS 316 in 0.1 M H_2SO_4 after Oxide Formation in 5 M H_2SO_4

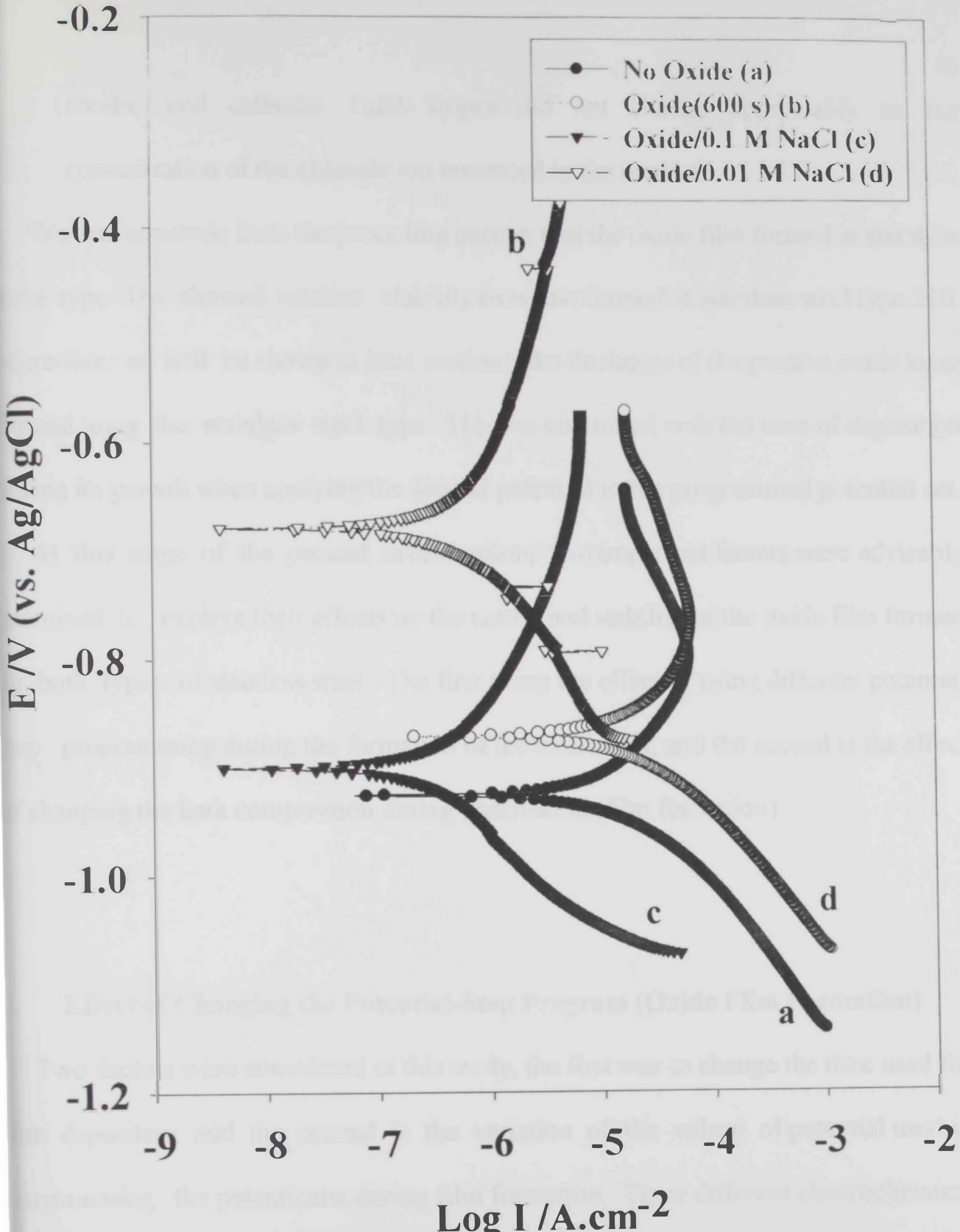

Figure III4b. Effect of Chloride on the Polarization of SS 310 in 0.1 M H_2SO_4 after Oxide Formation in 5 M H_2SO_4

anodic and cathodic Tafel slopes did not change appreciably as the concentration of the chloride ion increased in the medium.

We can conclude from the preceding section that the oxide film formed at stainless steel type 316 showed relative stability over that formed at stainless steel type 310. Moreover, as will be shown in later sections, the thickness of the passive oxide layer formed over the stainless steel type 316 was controlled with the time of deposition during its growth when applying the second potential in the programmed potential set.

At this stage of the present investigation, two important factors were advisably examined to explore their effects on the nature and stability of the oxide film formed on both types of stainless steel. The first being the effect of using different potential step programming during the formation of the oxide film, and the second is the effect of changing the bath composition during passivation (film formation).

. Effect of Changing the Potential-Step Program (Oxide Film Formation)

Two factors were considered in this study, the first was to change the time used for film deposition and the second is the variation of the values of potential used in programming the potentiostat during film formation. Three different electrochemical techniques were used to study these effects, namely, polarization resistance, Tafel plots, and electrochemical impedance spectroscopy (EIS).

anodic and cathodic Tafel slopes did not change appreciably as the concentration of the chloride ion increased in the medium.

We can conclude from the preceding section that the oxide film formed at stainless steel type 316 showed relative stability over that formed at stainless steel type 310. Moreover, as will be shown in later sections, the thickness of the passive oxide layer formed over the stainless steel type 316 was controlled with the time of deposition during its growth when applying the second potential in the programmed potential set.

At this stage of the present investigation, two important factors were advisably examined to explore their effects on the nature and stability of the oxide film formed on both types of stainless steel. The first being the effect of using different potential step programming during the formation of the oxide film, and the second is the effect of changing the bath composition during passivation (film formation).

4. Effect of Changing the Potential-Step Program (Oxide Film Formation)

Two factors were considered in this study, the first was to change the time used for film deposition and the second is the variation of the values of potential used in programming the potentiostat during film formation. Three different electrochemical techniques were used to study these effects, namely, polarization resistance, Tafel plots, and electrochemical impedance spectroscopy (EIS).

4.1. Effect of Changing Film Thickness

The potential program used for stainless steel type 316 was program # 1 as described in the experimental section (E_1 = -1.2 V, t_1 = 60 s, E_2 = -0.5 V, t_2 = 100 s – 600 s, E_3 = 0.6 V, t_3 = 60 s) while that used for stainless steel type 310 was (E_1 = -1.4 V, t_1 = 60 s, E_2 = -0.9 V, t_2 = 100 s – 600 s, E_3 = -0.8 V, t_3 = 60 s). Figure III5a shows the electrochemical data of the polarization resistance of the oxide films tested in 0.1 M H_2SO_4 for stainless steel type 316. The oxide films were formed in 5.0 M H_2SO_4. In these experiments, the potential was scanned through a potential range of ca. 50 mV close to E_{corr}. The resulting current plotted versus potential, as depicted in figure III5a, is a straight line.

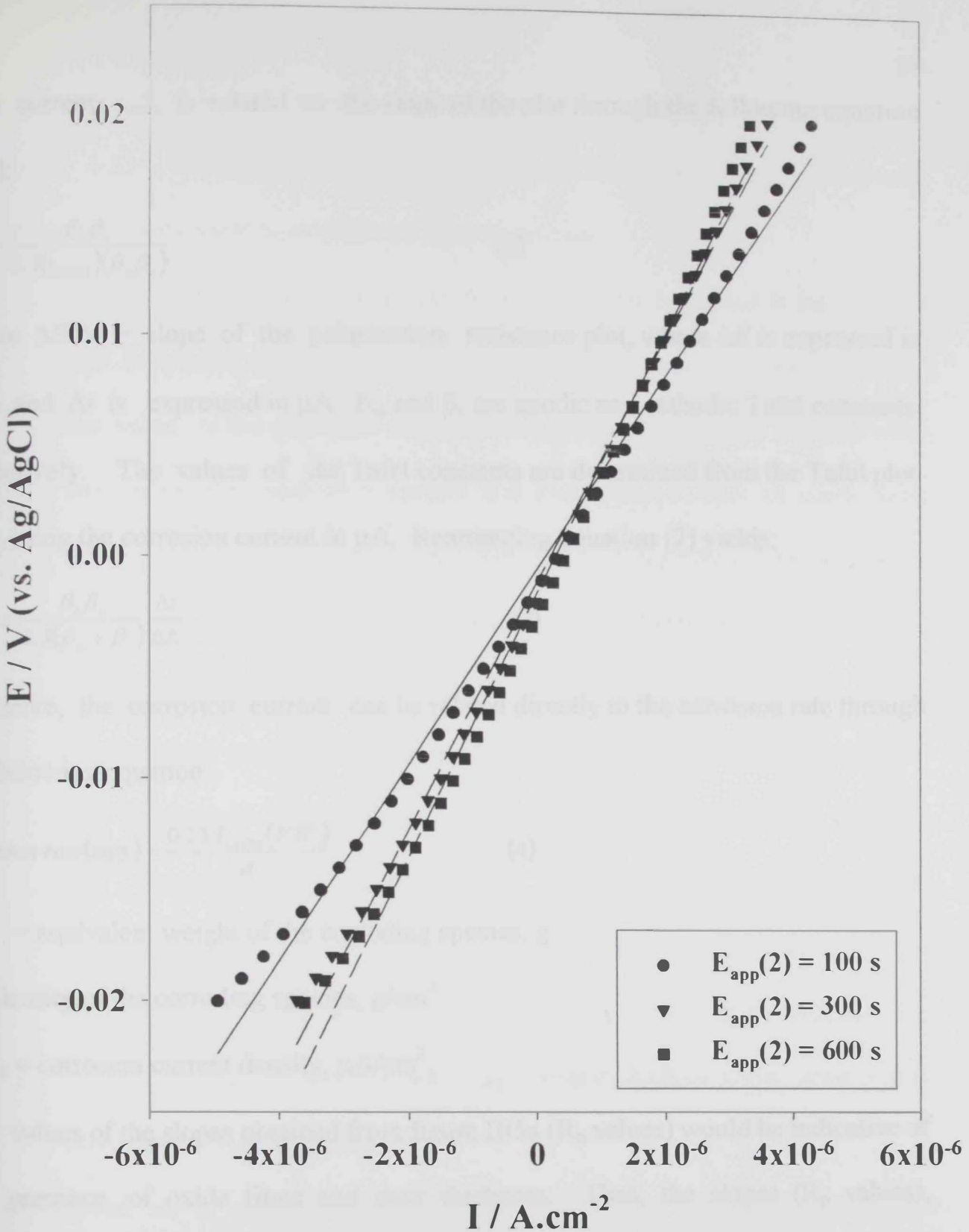

Figure III5a. Polarization Resistance of Oxide-Covered SS 316 with Different Thickness in 0.1 M H_2SO_4

Film Formation in 5.0 M H_2SO_4 using Potential Program # 2

The current, i_{corr}, is related to the slope of the plot through the following equation [100]:

$$\frac{\Delta E}{\Delta i} = \frac{\beta_a \beta_c}{2.3(i_{CORR})(\beta_a \beta_c)} \qquad (2)$$

Where $\Delta E/\Delta i$ = slope of the polarization resistance plot, where ΔE is expressed in volts and Δi is expressed in μA. β_a, and β_c are anodic and cathodic Tafel constants, respectively. The values of the Tafel constants are determined from the Tafel plot. i_{CORR} being the corrosion current in μA. Rearranging equation (2) yields:

$$i_{CORR} = \frac{\beta_a \beta_c}{2.3(\beta_a + \beta_c)} \frac{\Delta i}{\Delta E} \qquad (3)$$

Therefore, the corrosion current can be related directly to the corrosion rate through the following equation:

$$Corrsion\ rate(mpy) = \frac{0.13\, I_{CORR}(E.W.)}{d} \qquad (4)$$

E.W. = equivalent weight of the corroding species, g.

d = density of the corroding species, g/cm^3.

i_{CORR} = corrosion current density, μA/cm^2.

The values of the slopes obtained from figure III5a (R_p values) would be indicative of the presence of oxide films and their thickness. Thus, the slopes (R_p values), corrosion current values (i_{corr}) and corrosion rates for the tested specimens are as follows: 9.59 x 10^1 Ohm.cm^2, 2.72 x 10^{-4} A.cm^{-2}, 248.8 mpy for oxide-free surface, 4.52 x 10^3 Ohm.cm^2, 5.76 x 10^{-6} A.cm^{-2}, 5.283 mpy for oxide formed for 100 s, 5.03 x

10^3 Ohm.cm^2, 5.18 x 10^{-6} A.cm^{-2}, 4.748 mpy for oxide formed for 300 s, 6.01 x 10^3 Ohm.cm^2, 4.33 x 10^{-6} A.cm^{-2}, 3.972 mpy for oxide formed for 600 s, respectively. Several conclusions could be withdrawn from these data:

- The corrosion current decreases as the oxide film is formed at the surface. The corrosion current decreased as the film thickness increases. However, the value of the corrosion current shows a dramatic decrease in value when comparing the oxide-free surface and that covered with an oxide layer formed by applying a potential value of –0.9 V for 100 s. The subsequent values of corrosion currents showed a slight difference as the time of deposition of the oxide layer increases.
- Similar trend was observed in the noticeable decrease in the corrosion rate and increase in the polarization resistance. We can conclude at this stage that the oxide film formation at the stainless steel surface exhibits an immediate blockage to the surface from corrosion in sulfuric acid. Moreover, the thickening of the anodic film formed upon increasing the time of deposition did not show appreciable changes to corrosion current and polarization resistance values.

The second set of experimental results that proved the evidence of the oxide formation at the stainless steel type 316 and its effect on the electrochemical parameters of the oxide is given in figure III5b.

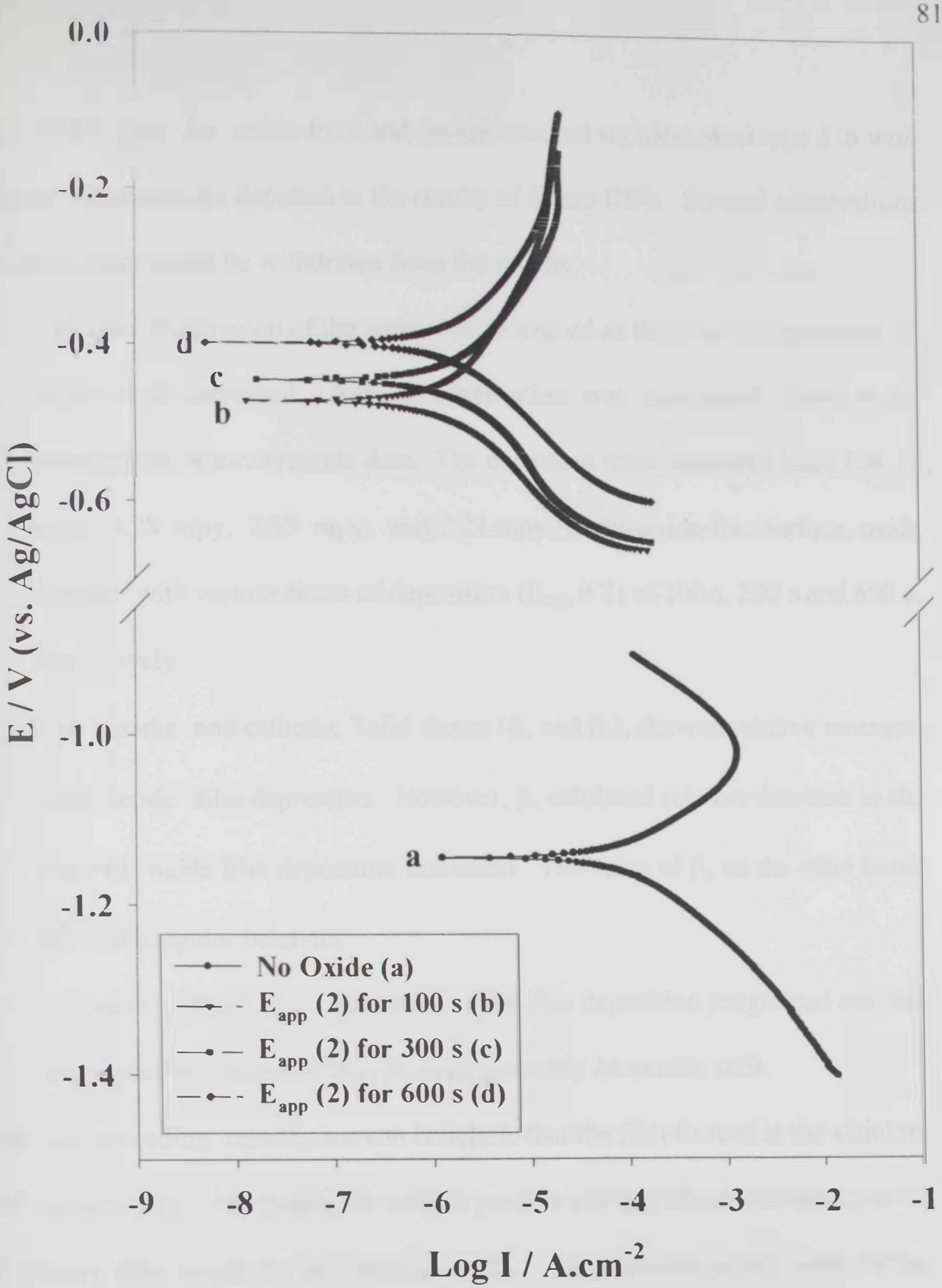

Figure III5b. Tafel Plots of Oxide-Covered SS 316 with Different Thickness in 0.1 M H_2SO_4
Film Formation in 5.0 M H_2SO_4 using Potential Program # 1

Thus, Tafel plots for oxide-free and oxide-covered stainless steel type 316 with different thickness are depicted in the results of figure III5b. Several observations and conclusions could be withdrawn from the results:

- The rate of corrosion of the specimen decreased as the time of deposition of oxide layer increased. Similar observation was mentioned above in the polarization measurements data. The corrosion rates measured were 106.32 mpy, 3.28 mpy, 2.59 mpy, and 2.24 mpy for the oxide-free surface, oxide formed with various times of deposition (E_{app} # 2) of 100 s, 300 s and 600 s, respectively.
- Both anodic and cathodic Tafel slopes (β_a and β_c), showed relative increase upon oxide film deposition. However, β_c exhibited relative decrease as the time of oxide film deposition increased. The value of β_a on the other hand, showed irregular behavior.
- Corrosion current, i_{corr}, decreased as the film deposition progressed and the corresponding values of E_{corr} showed generally an anodic shift.

From the preceding results, one can conclude that the film formed at the stainless steel surface type 316 renders the surface passive and that the electronic nature of the passive film ought to be characterized. The semiconducting nature of the passive film formed on stainless steels is now well recognized [101, 102]. However, the exact electronic structure of these films is not fully described and should be dependent on several factors including the method adopted for their

formation. In this respect, electrochemical impedance spectroscopy (EIS) experiments were conducted in order to estimate the electronic parameters of the film-covered stainless steel. Figures III5c, III5d, and III5e show typical impedance diagrams for the oxide-free stainless steel type 316 surface and that covered with film layer with different thickness. The impedance spectra revealed imple capacitive response as is usually observed for the passive film on stainless steel surfaces [103]. The morphological structure of the passive film formed on stainless steel has partial porous characteristics as will be shown in a later section from the scanning electron microscopy measurements. Thus, it was expected that a diffusion-controlled response would be displayed in the impedance measurements. Figures III5c, III5d and III5e show that the modulus and phase angle of the impedance change considerably when an oxide film is grown at the stainless steel surface. However, the variation of impedance parameters is not strongly dependent on film thickening. The polarization resistance, R_{po} that strongly depends on the passive film, is a measure of corrosion resistance of the material in the tested environment. In the higher frequency region (1-5 kHz), the Bode plot exhibits a constant (horizontal line) log Impedance (Z) versus log frequency (f) with phase angle values near 0°. This is the response of the electrolyte resistance R_s (resistive region). In the broad low middle frequency range, the diagrams display a linear slope of about –1 in log Z as log f decreases, while phase angle values approach -80° for the oxide-covered surfaces.

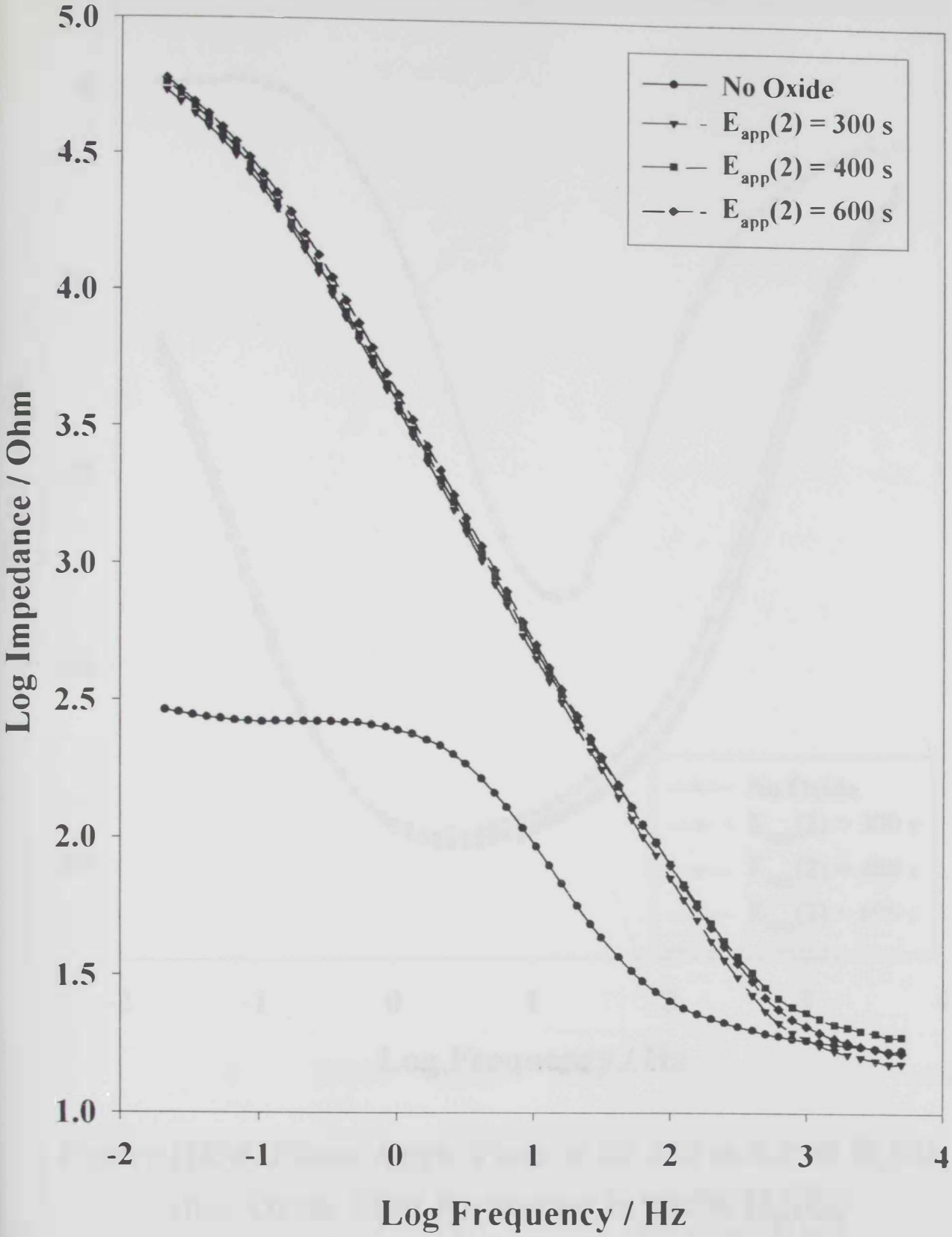

Figure III5c. EIS Plots of SS 316 in 0.1 M H_2SO_4 after Oxide Film Formation in 5.0 M H_2SO_4 with Different Thickness

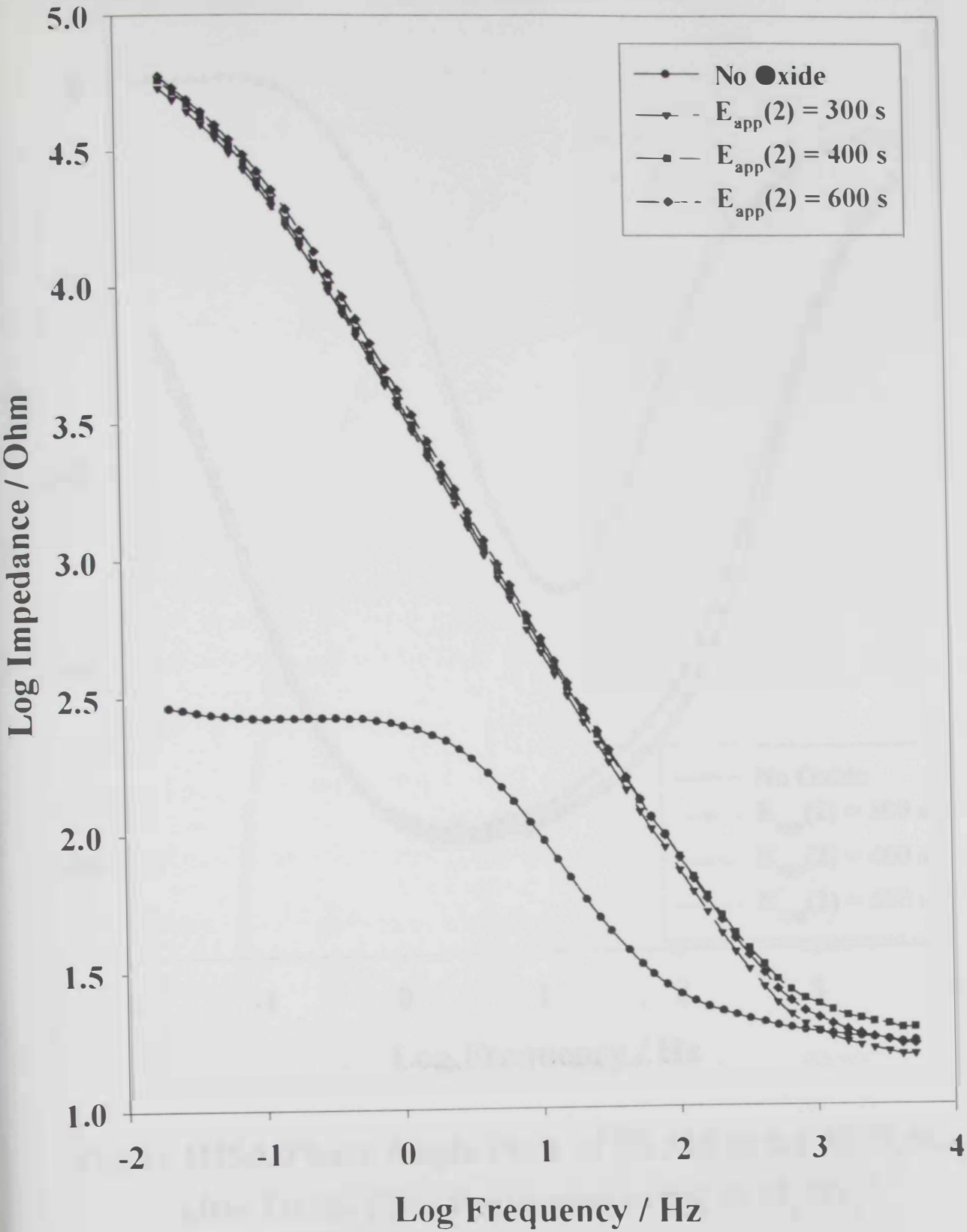

Figure III5c. EIS Plots of SS 316 in 0.1 M H_2SO_4 after Oxide Film Formation in 5.0 M H_2SO_4 with Different Thickness

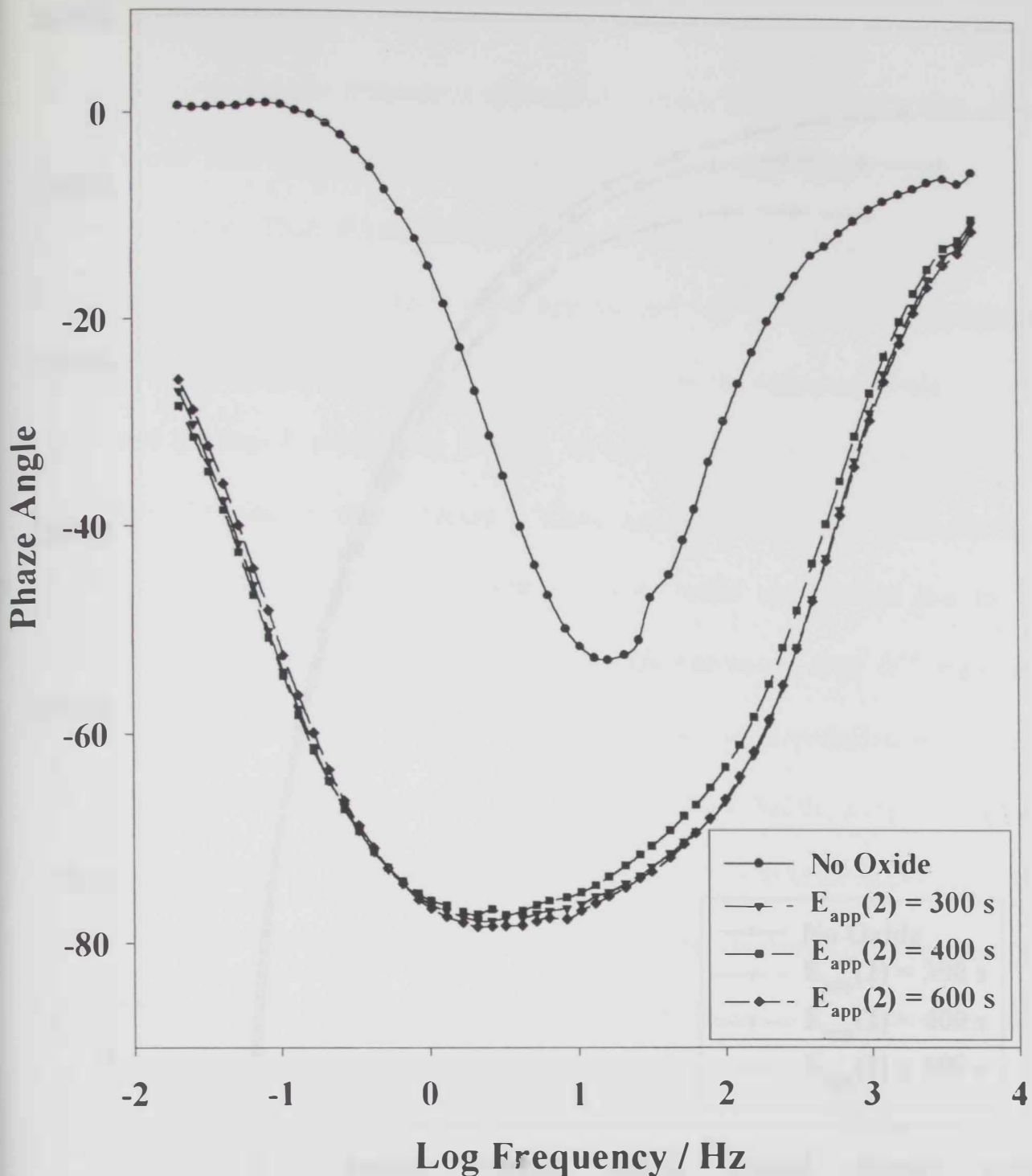

Figure III5d. Phase Angle Plots of SS 316 in 0.1 M H_2SO_4 after Oxide Film Formation in 5.0 M H_2SO_4 with Different Thickness

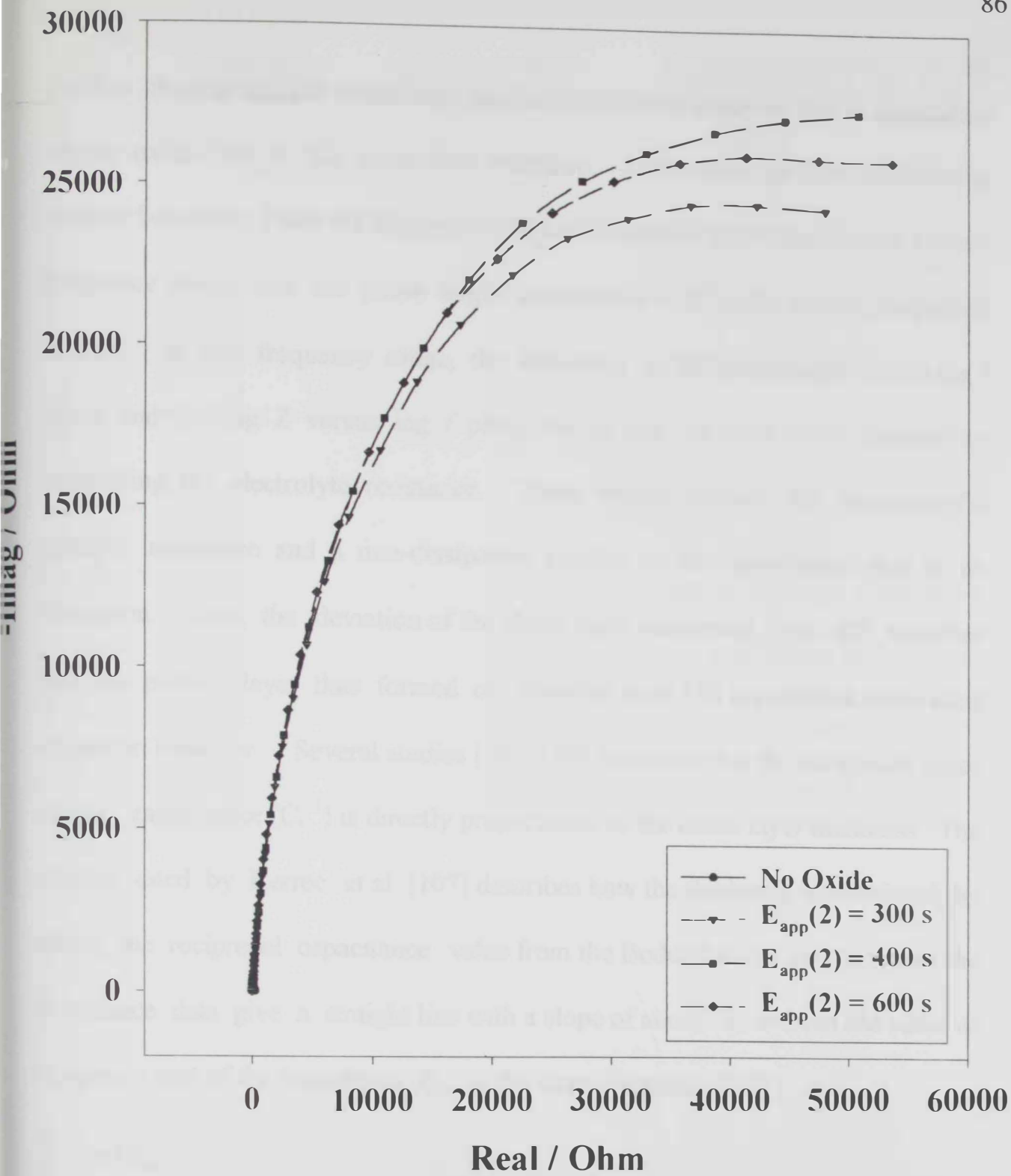

Figure III5e. Nyquist Plots of SS 316 in 0.1 M H_2SO_4 after Oxide Film Formation in 5.0 M H_2SO_4 with Different Thickness

At low frequencies, the impedance approaches a linear behavior that is equivalent to the oxide film at the electrolyte interface. Oxide-free surface exhibited a distinct behavior. Thus, the negative slope log Z versus log *f* extended over a short frequency range, and the phase angle approached -50° in the middle frequency domain. In this frequency range, the inflection in the phase angle versus log *f* curve and the log Z versus log *f* plots, which can be more easily obtained by subtracting the electrolyte resistance. These results indicate the presence of a parallel resistance and a non-dissipative passive oxide capacitance due to its formation. Also, the deviation of the phase angle maximum, near -80°, signifies that the passive layer thus formed on stainless steel 316 approaches more ideal capacitor behavior. Several studies [104–106] indicated that the reciprocal space charge capacitance (C_c^{-1}) is directly proportional to the oxide layer thickness. The relation cited by Kerrec et al. [107] describes how the thickness is calculated, by taking the reciprocal capacitance value from the Bode plot at 0.16 Hz, where the impedance data give a straight line with a slope of about –1, or from the value of imaginary part of the impedance, Z_{im}, at the same frequency [107]:

$$\frac{1}{C} = 2\pi f Z_{im} \qquad (5)$$

$$d = \frac{\varepsilon \varepsilon_o r}{C_C} \qquad (6)$$

Where d is the oxide layer thickness, r the roughness factor, ε the relative dielectric constant of the oxide, ε_0 the permitivity of free space (8.9×10^{-14} F.cm^{-1})

and C_c the oxide layer capacitance. The relative dielectric constant of the oxide could not be measured directly. Therefore, we calculated the amount of charge consumed during the formation of the oxide during the potential step programming. It was assumed that the oxide layer is stable and no dissolution took place thereafter. From the Faraday's law, the oxide layer thickness, *d*, is calculated according to [107]:

$$d = \frac{QM}{nF\rho r} \qquad (7)$$

Where Q is the amount of Coulombs, M is the mean molar mass of the oxide (assumed 159 [108]), n is the mean number of electrons required to form passive oxide and ρ the oxide density (assumed 5.2 $g.cm^{-3}$ [108]). The values of passive oxide capacitance (C_c) were calculated for different film formation time and programs as depicted in table III4.

Table III4. Electrochemical Impedance Spectroscopy data for stainless steel type 316 with different thickness oxide films formed in 5.0 M sulfuric acid and tested in 0.1 M sulfuric acid in three different programs.

System	R_s Ohm	C_c F	R_{po} Ohm	C_{dl} F	R_{ct} Ohm
400 s,Pg1	21.23	3.75E-5	3.5E+4	8.3E-5	4.5E+4
1000s,Pg1	21.41	3.68E-5	3.5E+4	1.334E-4	3.8E+4
400 s,Pg2	22.48	6E-5	2.5E+2	1.119E-4	4.2E+2
1000s,Pg2	17.64	6.7E-5	1.9E+2	1.699E-4	4E+2
400 s,Pg3	19.97	7.6E-5	2.7E+2	1.12E-4	2E+2
1000s,Pg3	23.45	6.9E-5	4E+4	8.653E-5	5E+2

The equivalent circuit depicted in figure III6 describes the electrochemical impedance data. The choice of this circuit was a compromise between a reasonable fitting of the experimental values, the limitation of the software used, and keeping the number of circuit elements at a minimum. In the equivalent circuit, a capacitance (C_c) and a parallel capacitance (C_{dl}) and resistance (R_{ct}) were used instead of a constant phase element. The double-layer capacitance (C_{dl}) and the passive film capacitance (C_c) determine the interfacial capacitance. When the influence of the passive film is dominant, that is the passive film capacitance is small compared to the double-layer capacitance, the capacitance data obtained from bode plot can be used to estimate the passive film thickness using the following equation [102]:

$$C = \frac{\varepsilon_o . \varepsilon . A}{d_{ox}} \qquad (8)$$

Where C is the measured capacitance, ε_o is the permitivity of vacuum (ε_o =8.85 x 10^{-14} F/cm), ε is the dielectric constant, A the effective area and d_{ox} is the thickness of the film layer. It is worth to mention that accurate film thickness could be difficult to determine using this relation since the double layer capacitance may not be negligible when the passive layer is thin and the dielectric constant is not well established. However, it is the purpose of the EIS measurements to show the variation of the capacitance values with film thickening.

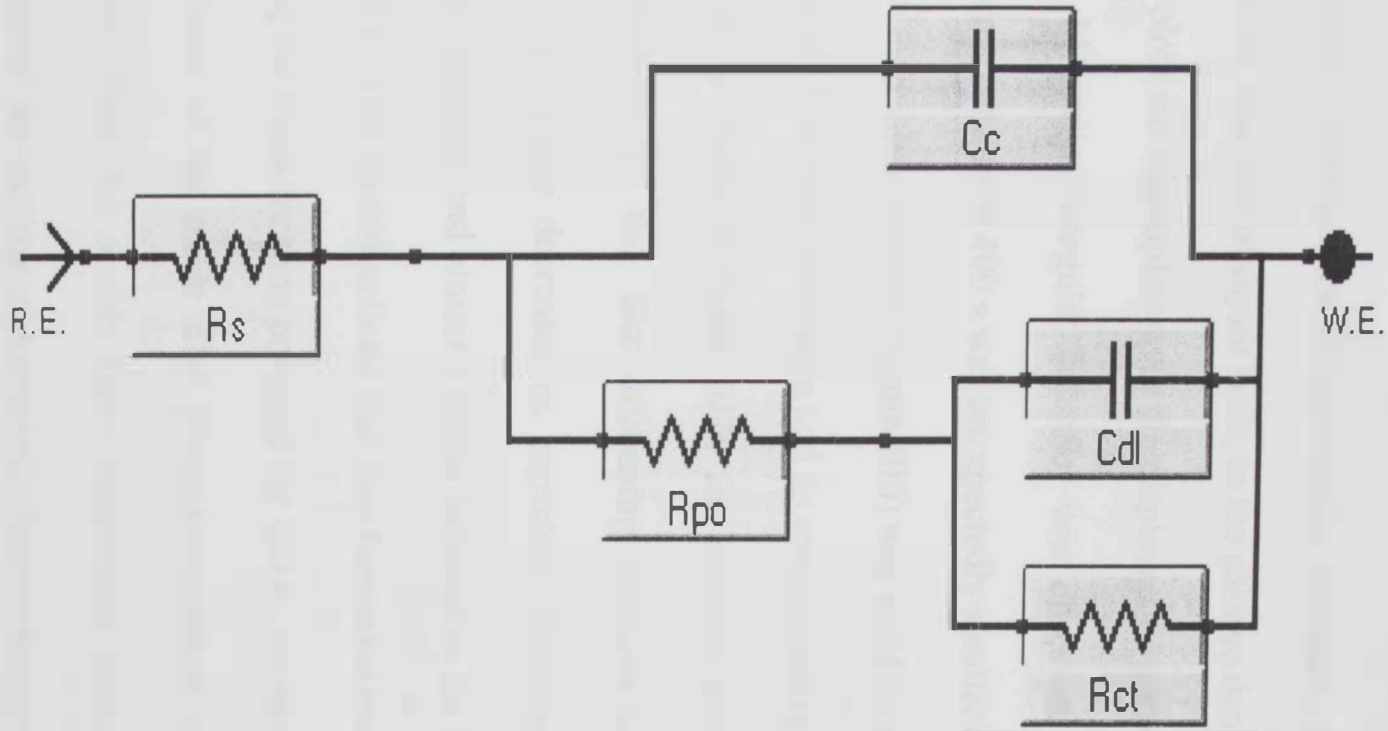

Figure1116 . **Equivalent Circuit used for Electrochemical Impedance Data Analysis**

The equivalent circuit shown in figure III6 still allows the association of the elements therein to the phenomena probably taking place at the stainless steel specimen. The symbols used in figure III6 are as follows: R_s is the solution resistance, R_{po} is the pores resistance, C_c is the film capacitance, C_{dl} is the double layer capacitance, and R_{ct} is the charge transfer resistance, respectively. As could be noticed from the data of figure III5e, in the passive domain, the semicircles in the Nyquist plots are incomplete over the displayed frequency domain to be easily interpreted. Moreover, irregular behavior was observed, as the radius of the semicircle corresponding to 400 s was unexpectedly smaller than that for 600 s.

The assumed equivalent circuit (figure III6) was valid for all EIS measurements. The variation of film pore resistance and its corresponding capacitance with film thickening time is given in figure III7a for stainless steel type 316. The pore resistance increases as the film thickening increases and the corresponding capacitance of the oxide decreases as expected. However, the two data show a "mirror image" behavior and almost a stable behavior as the time of film formation exceeded 200 s. This should indicate that film formation reaches a "mature" stage after applying the oxide forming potential for 200 s. As shown in figure III7b, the coating resistance of the oxide film formed at stainless steel 316 increases with thickening time while the double layer capacitance decreases. The later is an expected behavior as the water/electrolytic layer is being substituted by the film coating.

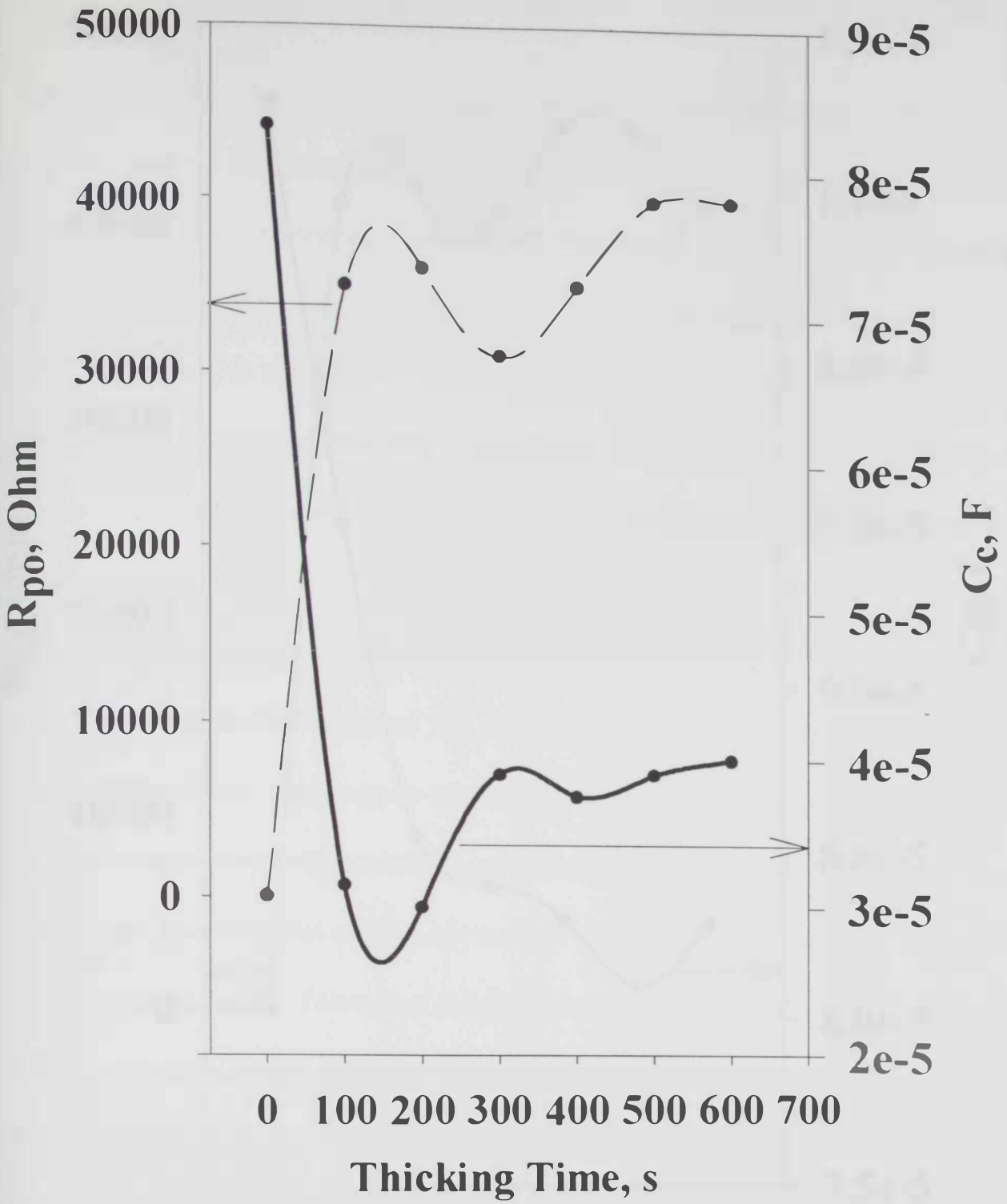

Figure III7a:Effect of thickening time during oxide film formation on the pore resistance andCapacitance of the oxide film formed at SS 316 surface

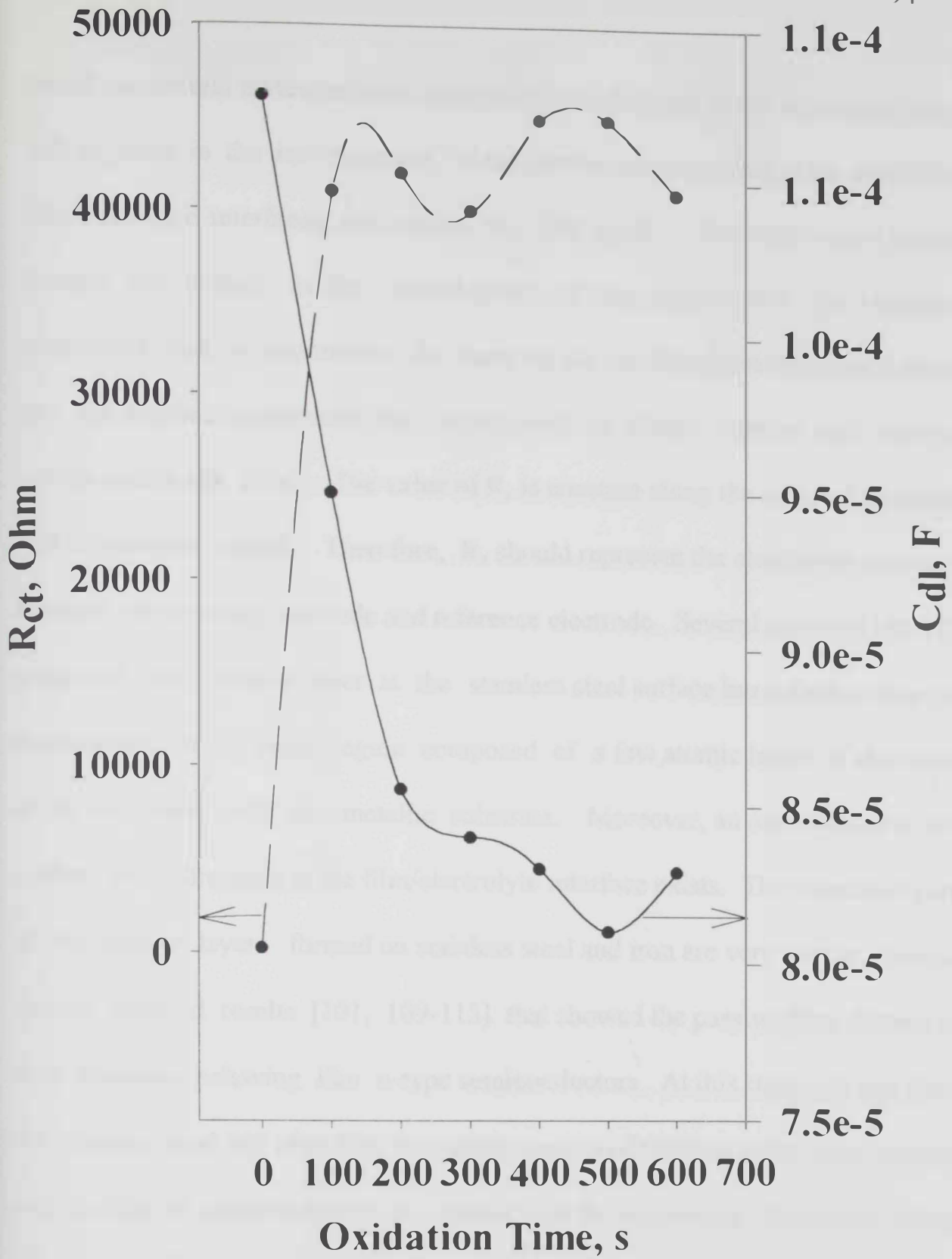

Figure III7b. Double Layer Capacitance and Coating Resistanceof the Oxide Layer vs. Thicking Time Plots for SS 316

Based on several review articles, analysis of the elements of the equivalent circuit will be used in the interpretation of the phenomena occurring at the metal/film, film/electrolyte interfaces and within the film itself. The total current passing through the system is the contribution of two components: the capacitive component, that is responsible for charging the two interfaces mentioned above, and the faradaic component that corresponds to charge transfer and transport events within the film. The value of R_s is constant along the range of potentials and frequencies tested. Therefore, R_s should represent the electrolyte resistance between the working electrode and reference electrode. Several authors [108-112] suggested that, passive layer at the stainless steel surface has a duplex structure that consists of an inner region composed of a few atomic layers of chromium oxide in contact with the metallic substrate. Moreover, an outer region of iron oxides and hydroxides at the film/electrolyte interface exists. The outermost parts of the passive layers formed on stainless steel and iron are very similar. Several authors reported results [101, 109-113] that showed the passive films formed on both materials behaving like n-type semiconductors. At this stage, we can claim that stainless steel 316 after film formation consists of the base metal alloy covered with a film of semiconductor in contact with the electrolyte. Moreover, charge alignment at the metal/film interface should be established due to the difference of the Fermi level on each side of the interface. Thus, this interface was considered as a capacitor C_{MF}.

On the other hand, a charge alignment at the film/electrolyte interface is also expected. However, the charge carrier density in semiconductors is much smaller than in metals. The accumulated charge at this surface will not be easily compensated that generates a depletion region inside the film. The latter could be called "space-charge layer." Across this layer a potential barrier is established that prevents or, at least, diminishes substantially the flux of charge carriers. This barrier facilitates a deformation of both conduction and valence bands of film during polarization. This layer can also be considered as a capacitor C_{FE}. Also, is it well established that at the film/electrolyte interface a Helmholtz double layer capacitance C_{dl} is established. The combination of these three series capacitances results in the system (metal/film, film, film/electrolyte, and double layer interfaces) capacitance, C_{sys} that can be expressed as:

$$\frac{1}{C_{sys}} = \left(\frac{1}{C_{MF}} + \frac{1}{C_{FE}} + \frac{1}{C_{dl}} \right) \qquad (8)$$

The two capacitances C_{MF}, C_{FE} constitute the passive film capacitance C_C of figure 1116. The values of C_{dl} cited in the literature [114] for different metals and alloys are around 5.0×10^{-5} F.cm^{-2}. The capacitance for the semicircle of the Nyquist plots can be calculated from:

$$C = \frac{1}{(2\pi f_{max} R_2)} \qquad (9)$$

Where R_2 is the diameter of the semicircle of the Nyquist diagram and f_{max} is the frequency corresponding to the maximum of this semicircle. This value equal 5.3 x 10^{-6} F.cm^{-2} for the film formed for 400 s. Thus, it seems reasonable to propose that this value mainly represents the term ($1/C_{MF} + 1/C_{FE}$) since the value of C_{dl} is high, the term $1/C_{dl}$ could be neglected. Therefore, the equivalent circuit should include a capacitive contribution that represents the film capacitance: $1/C_C = 1/C_{MF} + 1/C_{FE}$ to which an impedance can be associated and can be calculated from: $Z_C = (1/jw)(1/C_C)$.

The potential program used for stainless steel 310 was as indicated in the experimental section: (E_1 = -1.4 V, t_1 = 60 s, E_2 = -0.9 V, t_2 = 100 s – 600 s, E_3 = -0.8 V, t_3 = 60 s). Figure III8a shows the electrochemical data of the polarization resistance of the oxide films formed in 5.0 M H_2SO_4 and tested in 0.1 M H_2SO_4. A potential window of 50 mV close to E_{corr} was selected and through which the scanning was performed. The resulting current-potential behavior is a straight line as was previously shown with the data of figure III5a. The values of the slope would again be indicative of the presence of oxide films and more importantly of their thickness. The slopes (R_p values), corrosion current values (i_{corr}) and corrosion rates for the tested specimens are as follows: 3.267 x 10^3 Ohm.cm^2, 8.415 x 10^{-6} A.cm^{-2}, 7.310 mpy for oxide-free surface, 4.293 x 10^4 Ohm.cm^2, 5.321 x 10^{-7} A.cm^{-2}, 0.488 mpy for oxide formed for 300 s, 3.983 x 10^4 Ohm.cm^2, 8.44 x 10^{-7} A.cm^{-2}, 0.851 mpy for oxide formed for 400 s, 8.352 x 10^3 Ohm.cm^2.

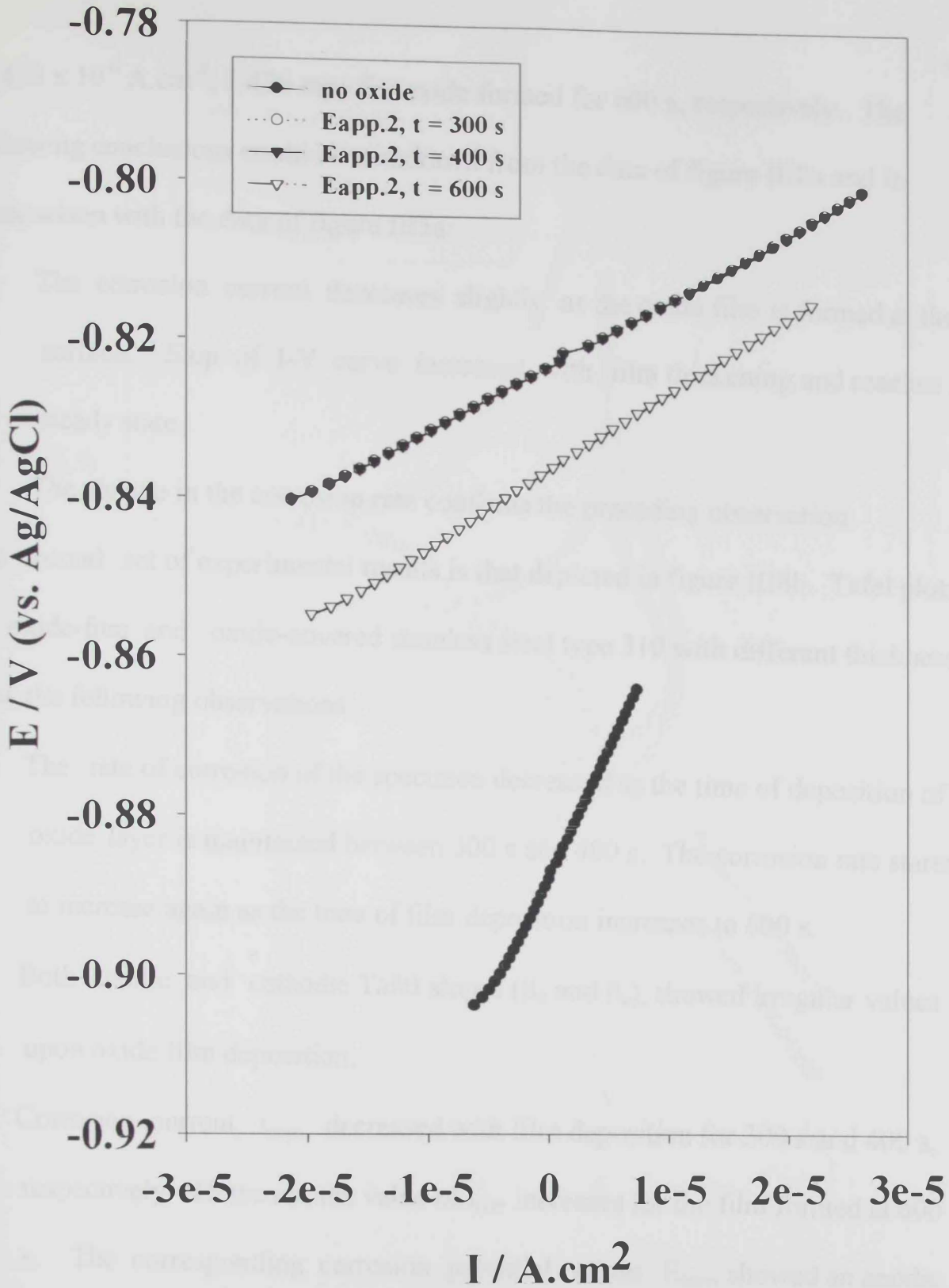

Figure III8a. Polarization Resistance of Oxide-Covered SS 310 with Different Thicknesses in 0.1 M H_2SO_4 Film Formation in 5.0 M H_2SO_4

1.425×10^{-6} A.cm^{-2}, 1.426 mpy for oxide formed for 600 s, respectively. The following conclusions could be withdrawn from the data of figure III8a and in comparison with the data of figure III5a:

- The corrosion current decreases slightly as the oxide film is formed at the surface. Slop of I-V curve increases with film thickening and reaches a steady state.
- The change in the corrosion rate confirms the preceding observation.

The second set of experimental results is that depicted in figure III8b. Tafel plots for oxide-free and oxide-covered stainless steel type 310 with different thickness show the following observations:

- The rate of corrosion of the specimen decreased as the time of deposition of oxide layer is maintained between 300 s and 400 s. The corrosion rate starts to increase again as the time of film deposition increases to 600 s.
- Both anodic and cathodic Tafel slopes (β_a and β_c), showed irregular values upon oxide film deposition.
- Corrosion current, i_{corr}, decreased with film deposition for 300 s and 400 s, respectively. However, the value of i_{corr} increases for the film formed at 600 s. The corresponding corrosion potential values E_{corr}, showed an anodic shift followed by a cathodic shift as the film formation time is increased.

We can conclude from the preceding section that the oxide film formed at the stainless steel type 310 is not stabilized as the time of film deposition increases.

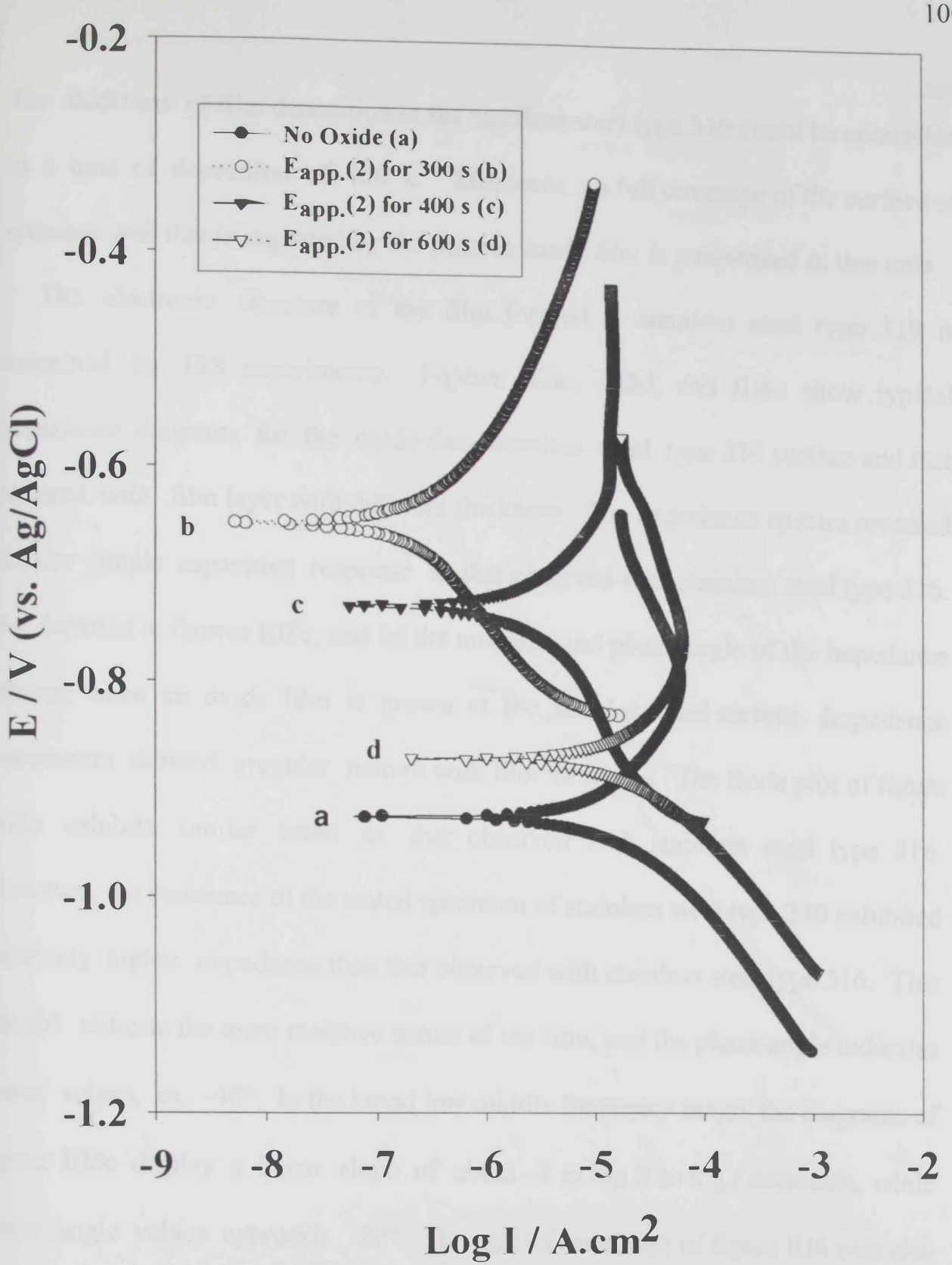

Figure III8b. Tafel Plots of Oxide-Covered SS 310 with Different Thicknesses in 0.1 M H_2SO_4 Film Formation in 5.0 M H_2SO_4

The thickness of film deposition at the stainless steel type 310 could be controlled to a time of deposition of 400 s. Moreover, no full coverage of the surface of stainless steel that is imparted by the passive oxide film is guaranteed in this case.

The electronic structure of the film formed at stainless steel type 310 is examined by EIS experiments. Figures III8c, III8d, and III8e show typical impedance diagrams for the oxide-free stainless steel type 310 surface and that covered with film layer with different thickness. The impedance spectra revealed similar simple capacitive response as that observed with stainless steel type 316. As depicted in figures III8c, and 8d the modulus and phase angle of the impedance change when an oxide film is grown at the stainless steel surface. Impedance parameters showed irregular pattern with film thickness. The Bode plot of figure III8c exhibits similar trend as that observed with stainless steel type 316. However, the resistance of the tested specimen of stainless steel type 310 exhibited relatively higher impedance than that observed with stainless steel type 316. This should indicate the more resistive nature of the film, and the phase angle indicates lower values, ca. -40°. In the broad low middle frequency range, the diagrams of figure III8c display a linear slope of about -1 in $\log Z$ as $\log f$ decreases, while phase angle values approach -80°. The equivalent circuit of figure III6 was also used for the data fitting of EIS experiments shown in figures III8c – III8d. However, noticeable deviations were observed in the fitting results.

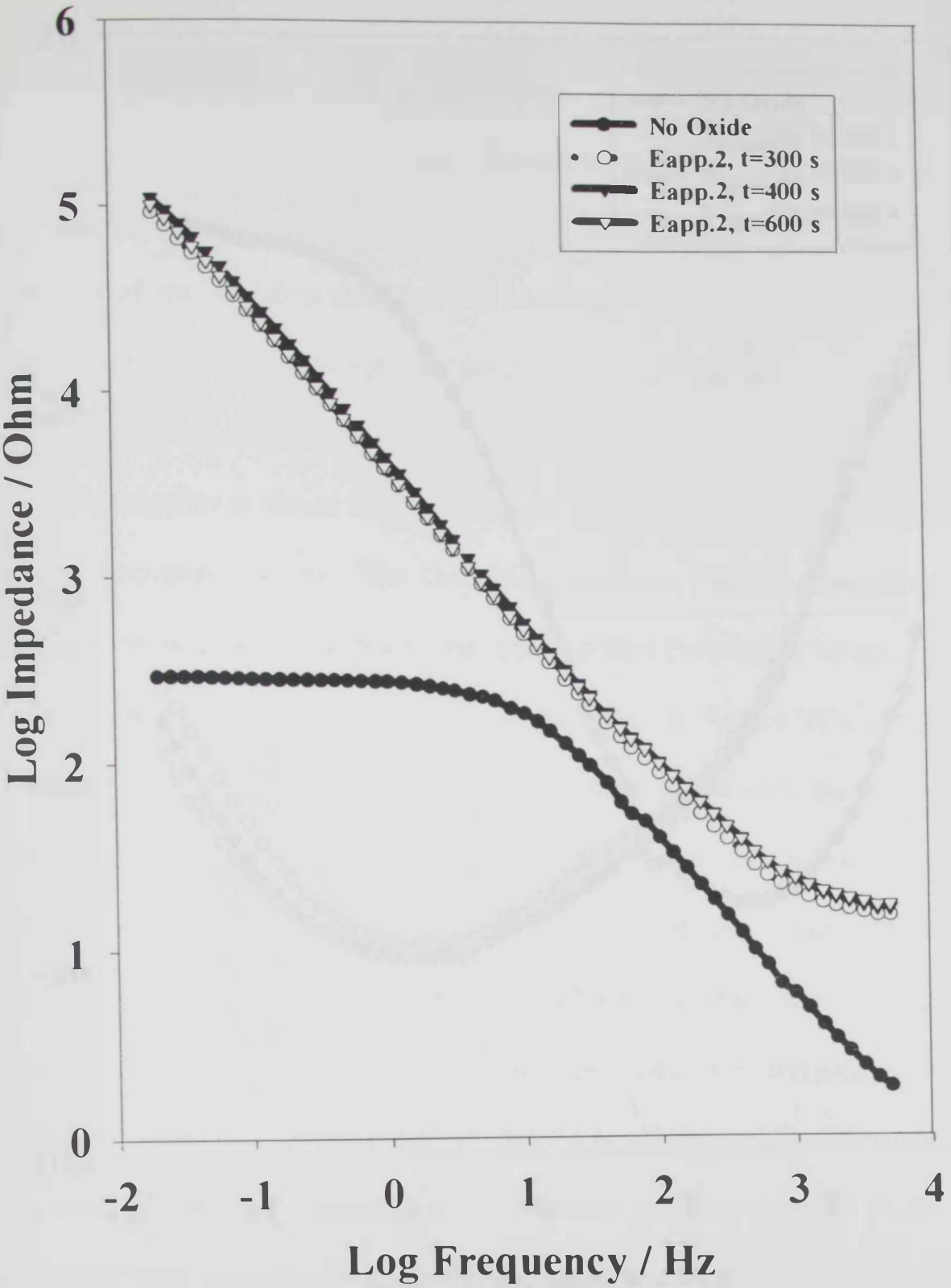

Figure III8c. EIS Plots of SS 310 in 0.1 M H_2SO_4 after OxideFilm Formation in 5.0 M H_2SO_4 with Different Thicknesses

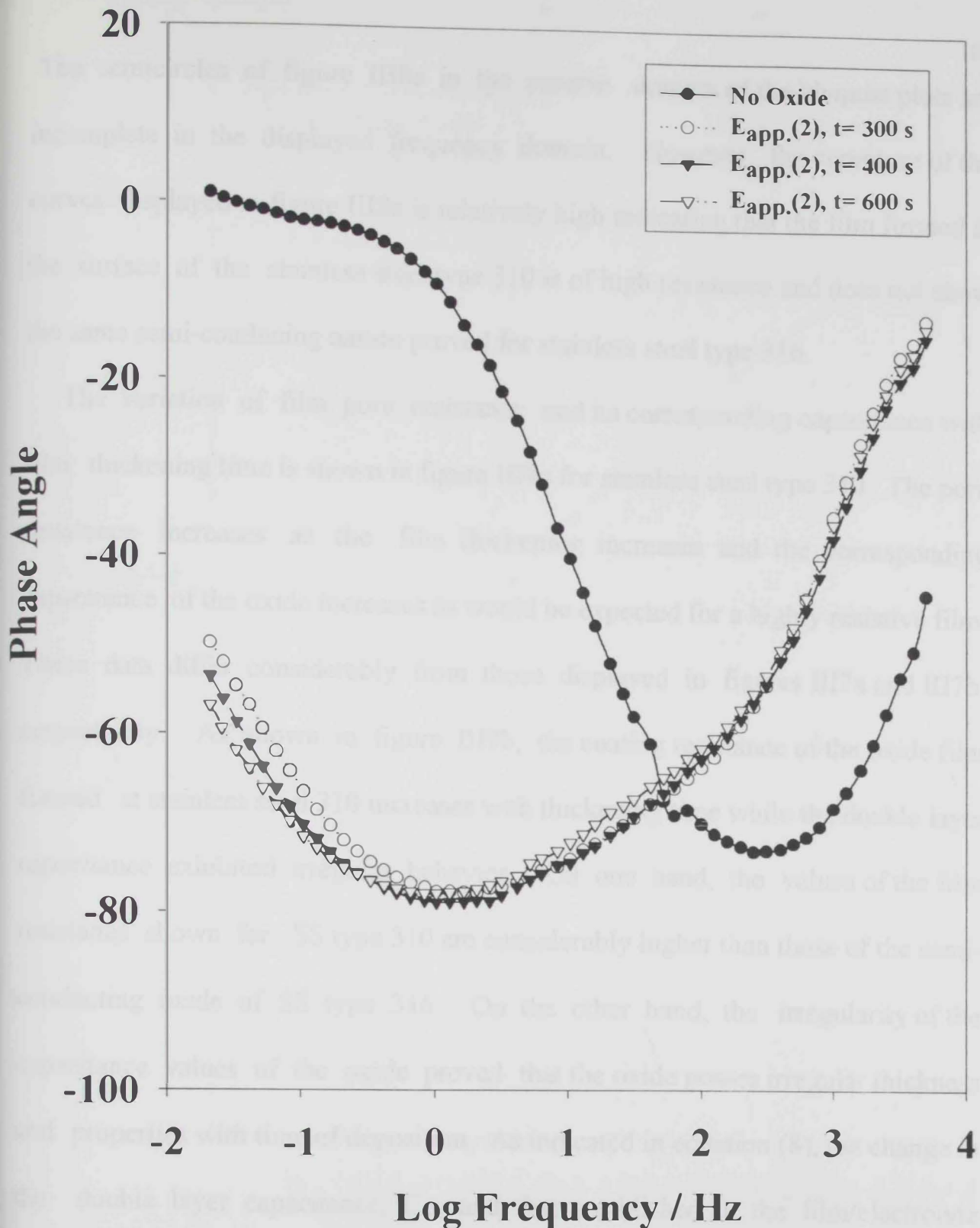

Figure III8d. Phase Angle Plots of SS 310 in 0.1 M H_2SO_4 after Oxide Film Formation in 5.0 M H_2SO_4 with Different Thicknesses

The semicircles of figure III8e in the passive domain of the Nyquist plots are incomplete in the displayed frequency domain. However, the curvature of the curves displayed in figure III8e is relatively high indicating that the film formed at the surface of the stainless steel type 310 is of high resistance and does not show the same semi-conducing nature proved for stainless steel type 316.

The variation of film pore resistance and its corresponding capacitance with film thickening time is shown in figure III9a for stainless steel type 310. The pore resistance increases as the film thickening increases and the corresponding capacitance of the oxide increases as would be expected for a highly resistive film. These data differ considerably from those displayed in figures III7a and III7b, respectively. As shown in figure III9b, the coating resistance of the oxide film formed at stainless steel 310 increases with thickening time while the double layer capacitance exhibited irregular behavior. On one hand, the values of the film resistance shown for SS type 310 are considerably higher than those of the semi-conducting oxide of SS type 316. On the other hand, the irregularity of the capacitance values of the oxide proved that the oxide posses irregular thickness and properties with time of deposition. As indicated in equation (8), the change in the double layer capacitance, C_{dl}, and that established at the film/electrolyte interface, C_{FE}, should appreciably affect the value of the film capacitance.

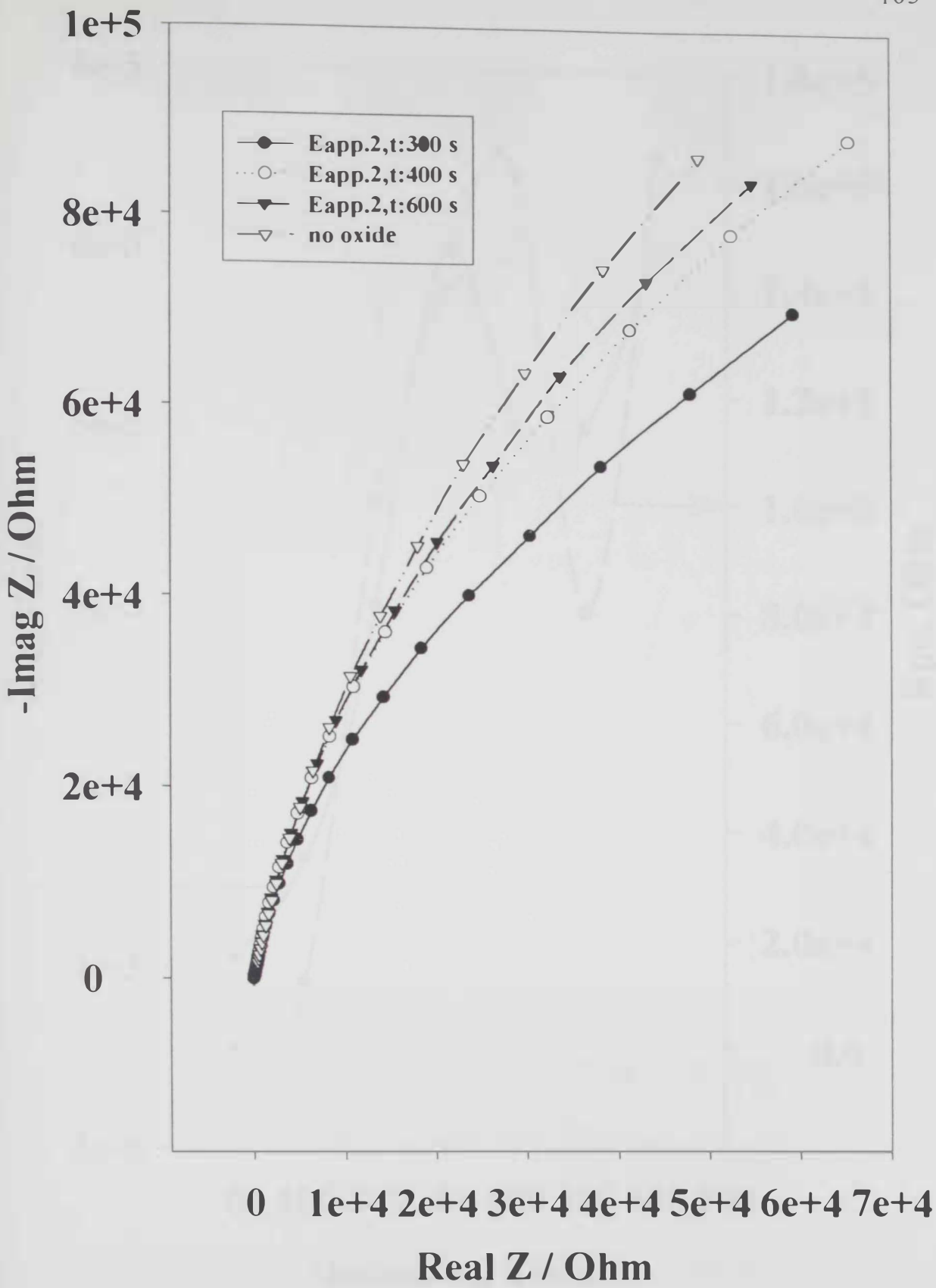

Figure III8e: Nyquist plots of SS 310 in 0.1 M H2SO4 after oxide film formation in 5.0 M H2SO4 with different thicknesses

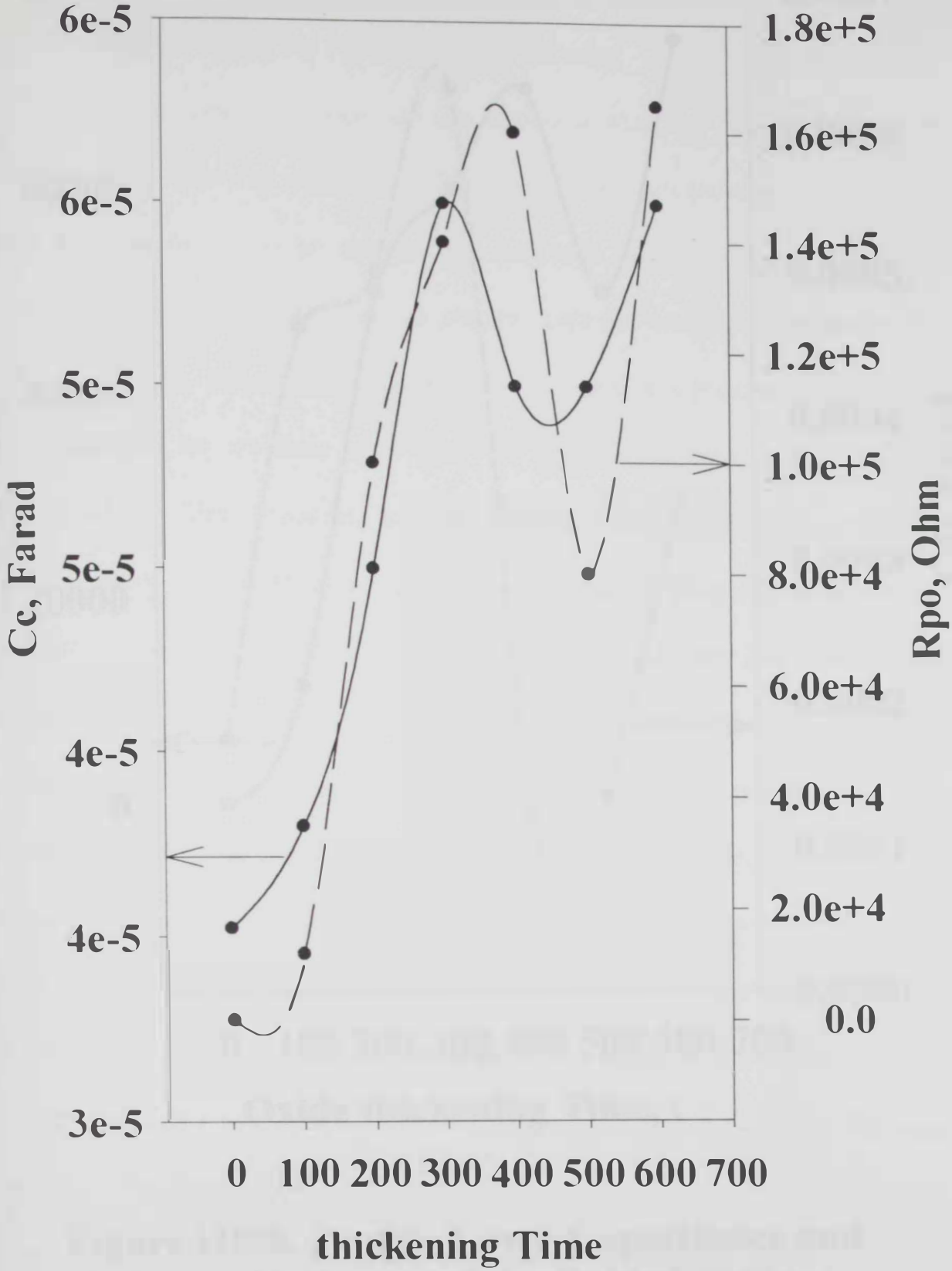

Figure 1119a: Effect of thickening time during oxide film formation on the pore resistance and capacitance of the oxide film formed at SS 310 surface.

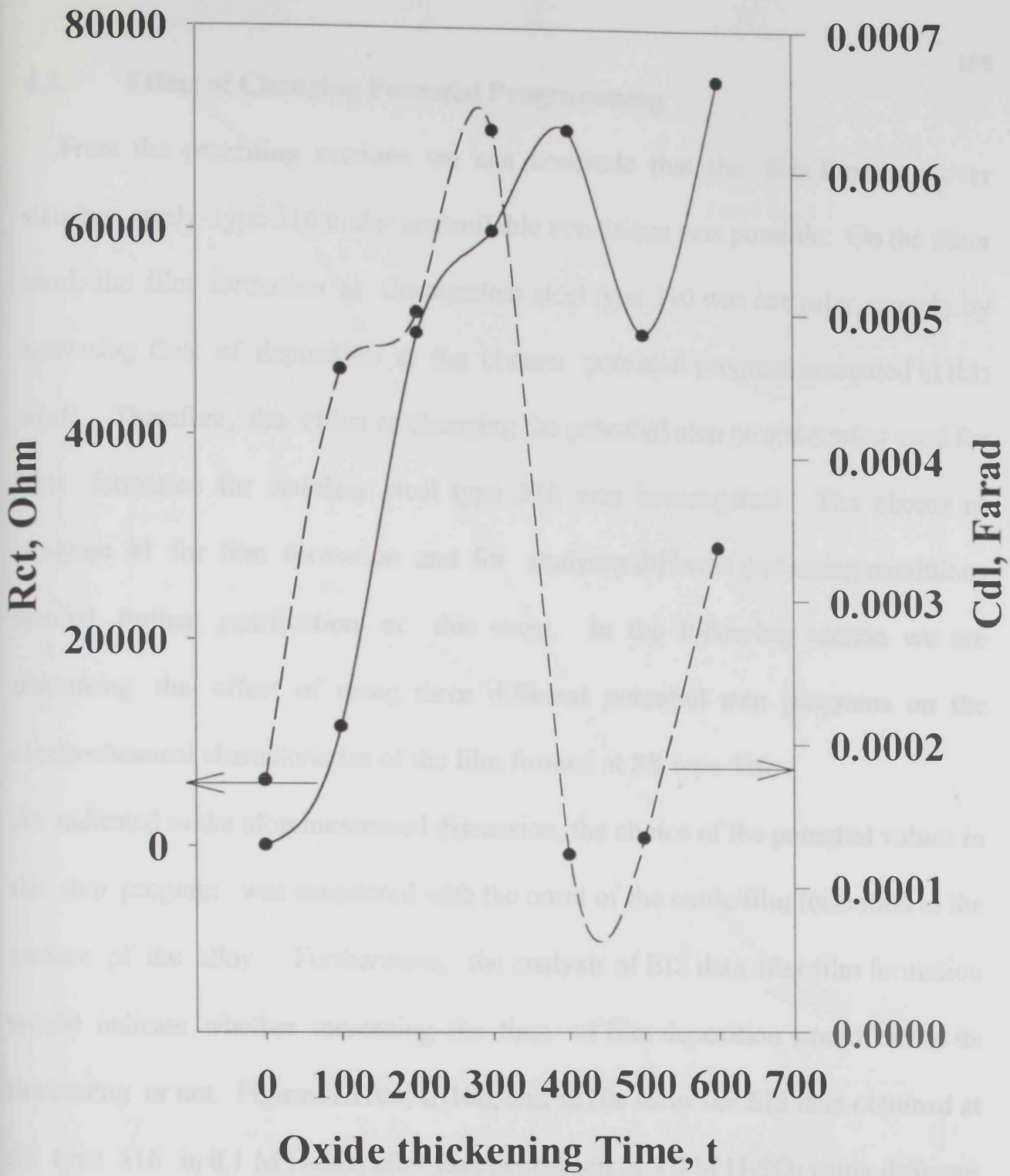

Figure III9b. Double Layer Capacitance and Coating Resistanceof the Oxide Layer vs. Thicking Time Plots for SS 310

4.2. Effect of Changing Potential Programming

From the preceding sections we can conclude that the film formation over stainless steely type 316 under controllable conditions was possible. On the other hand, the film formation at the stainless steel type 310 was irregular, namely by increasing time of deposition at the chosen potential program presented in this work. Therefore, the effect of changing the potential step programming used for film formation for stainless steel type 316 was investigated. The choice of program #1 for film formation and for studying different pertaining conditions needed further justification at this stage. In the following section we are discussing the effect of using three different potential step programs on the electrochemical characteristics of the film formed at SS type 316.

As indicated in the aforementioned discussion, the choice of the potential values in the step program was associated with the onset of the oxide/film formation at the surface of the alloy. Furthermore, the analysis of EIS data after film formation would indicate whether increasing the time of film deposition would lead to its thickening or not. Figures III10a, III10b, and III10c show the EIS data obtained at SS type 316 in 0.1 M H_2SO_4 after film deposition in 5.0 M H_2SO_4 using different programs. The description of the programs used is listed in the experimental section. It is worth to mention that the difference between program # 1 and program # 2 is the final applied potential, E_3, +0.6 V and 0.0 V, respectively. The potential program # 3 being different than the two others in the second and final

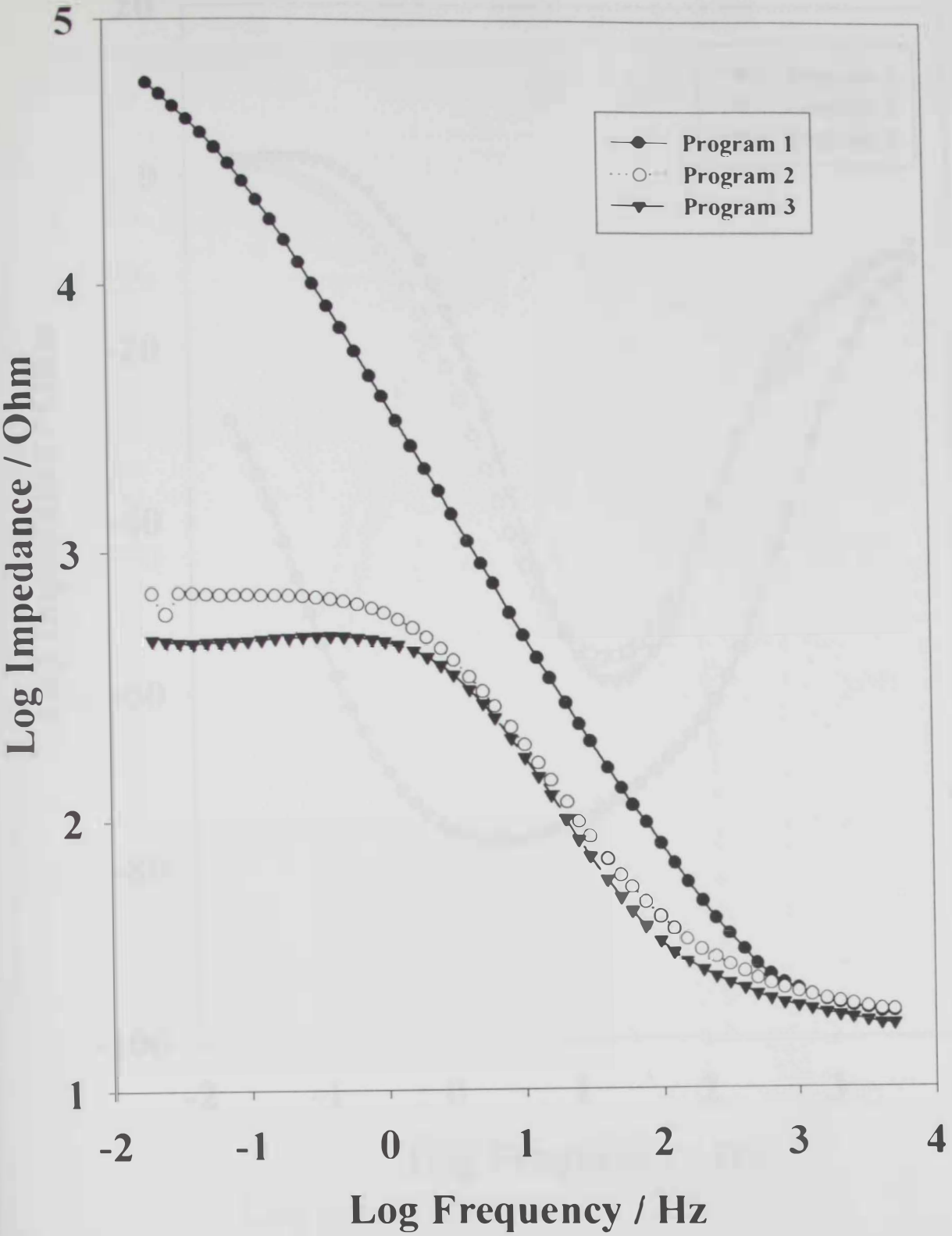

Figure III10a. EIS Plots of SS 316 in 0.1 M H_2SO_4 after Film Formation in 5.0 M H_2SO_4 with Different Programs, $E_{app.}$(2), t = 400 s

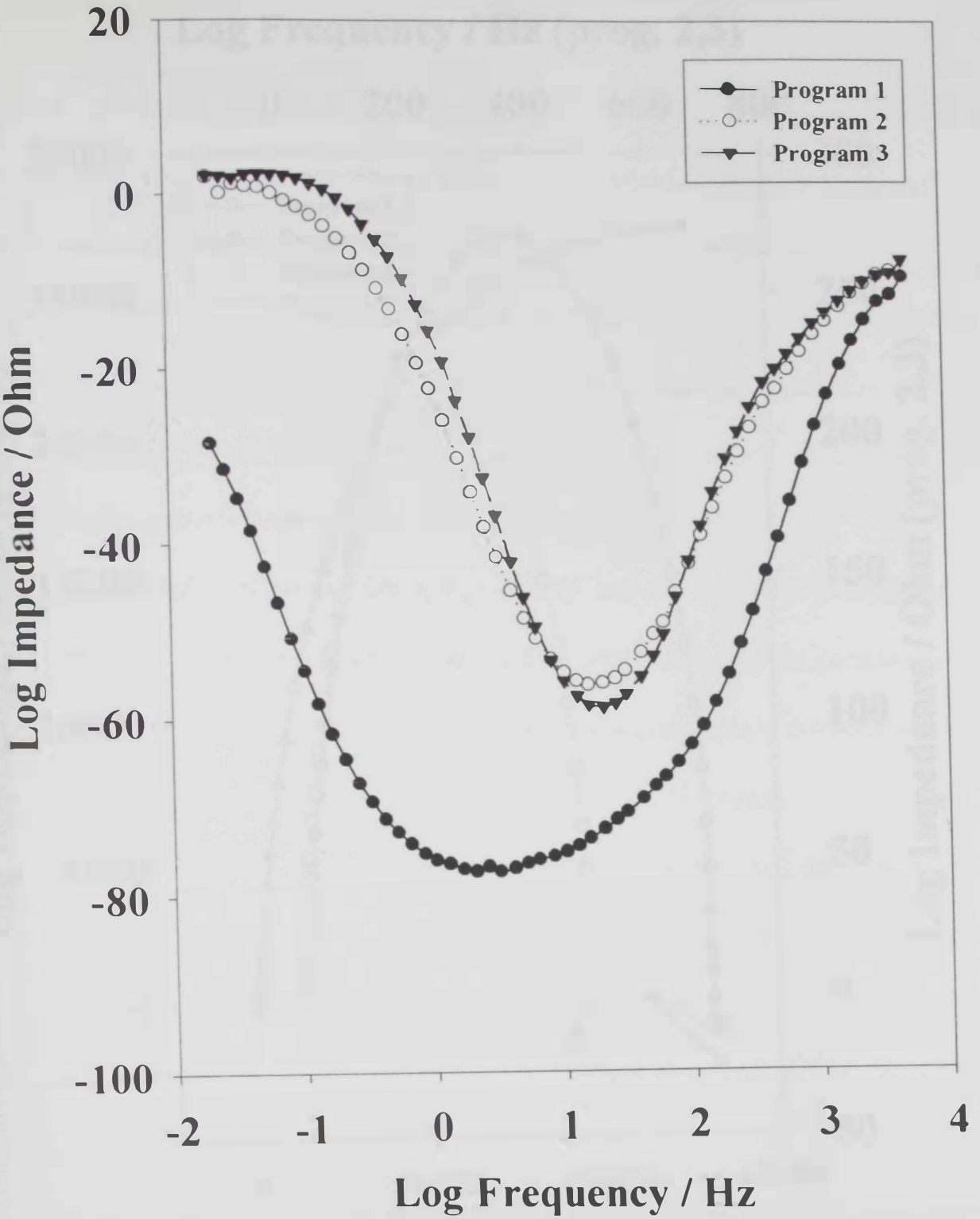

Figure III10b. Phase Angle Plots of SS 316 in 0.1 M H_2SO_4 after Oxide Film Formation in 5.0 M H_2SO_4 with Different Programs, $E_{app.}$(2): t = 400 s

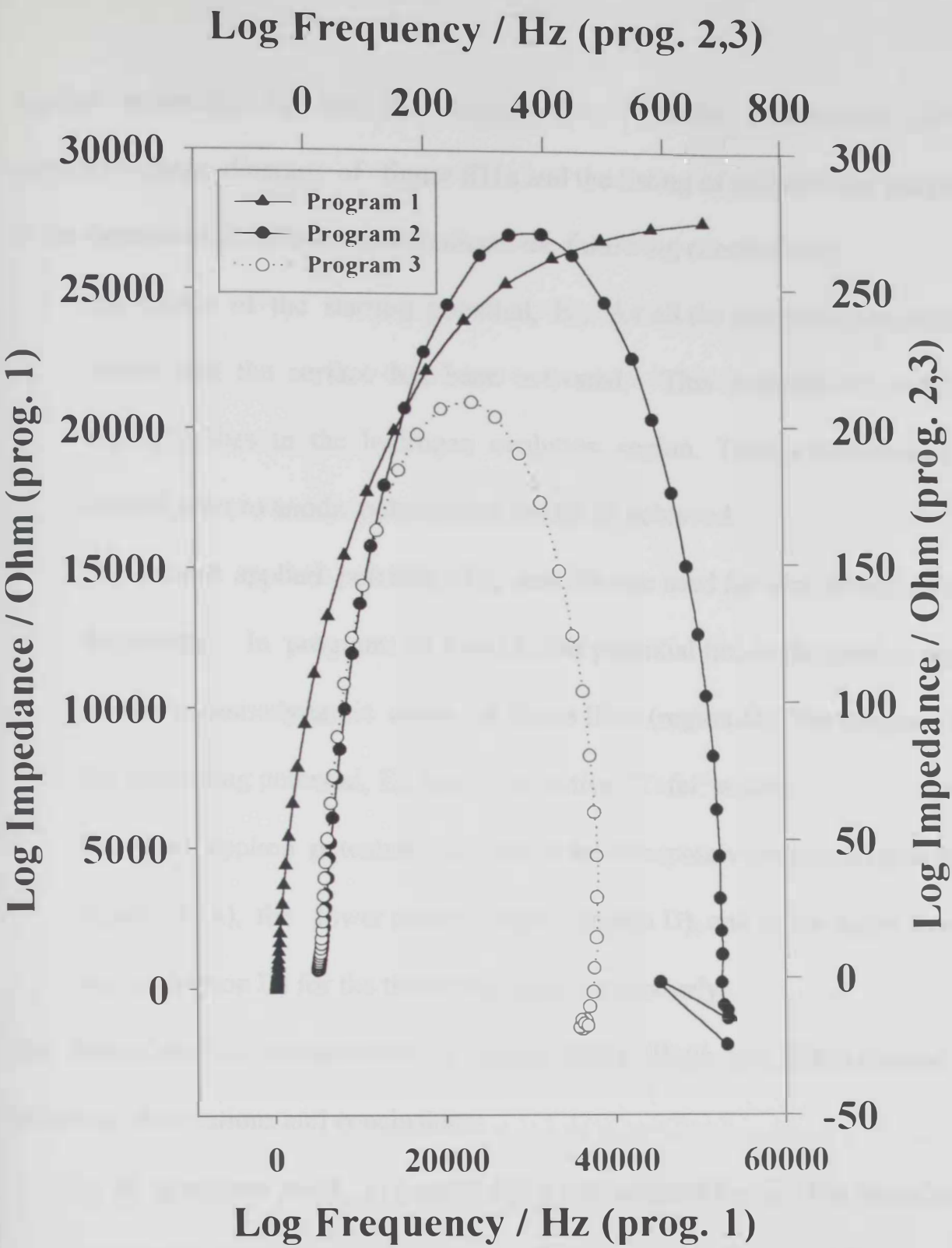

gure III10c. Nyquist Plots of SS 316 in 0.1 M H_2SO_4 after Oxide Film Formation in 5.0 M H_2SO_4 with Different Programms, $E_{app.}$(2), t = 400 s

applied potentials, E_2 and E_3, respectively. Careful examination of the potentiodynamic diagram of figure III1a and the listing of the potential programs in the experimental section would indicate the following conclusions:

- The choice of the starting potential, E_1, for all the programs used was to ensure that the surface has been activated. This potential, $E_1 = -1.2$ vs. Ag/AgCl, lies in the hydrogen evolution region. Thus, a reduction of the surface prior to anodic polarization would be achieved.
- The second applied potential, E_2, was the one used for film formation and thickening. In programs #s 1 and 3, this potential lies in the passive region of the potentiodynamic curve of figure III1a (region D). For program # 2, the thickening potential, E_2, lies in the active "Tafel" region.
- The third applied potential, E_3, lies in the transpassive region (region E of figure III1a), the lower passive region (region D), and in the upper passive region (region D) for the three programs, respectively.

The data of the EIS measurements of figures III10a, III10b, and III10c showed the following observations and conclusions:

- In all programs used, a time of 400 s was adopted for E_2. The impedance spectra is simple capacitive in nature as would be expected for a passive film covering the surface of a metal substrate.
- The modulus measured at the low frequency end (ca. below 1 Hz) would indicate the electronic nature of the film. Thus, the film formed using

program # 1 exhibited the highest resistance. The value of the modulus mounts to about 10^5 ohms. The lower values of impedance exhibited by those films formed using programs #s 2 and 3 are indicative of a film of smaller thickness. We can conclude that it would be possible to control the thickness of oxide/film forming over stainless steel type 316 using program # 1.

- For all programs used, in the higher frequency range, the Bode plot exhibited a constant horizontal line of log Impedance (Z) versus log frequency (f) with the phase angle approaching 0°.
- In the low to middle frequency region, the diagrams exhibited the regular linear slope of –1 in log Z as log f decreases. The phase angle approached -80° in case of program # 1 and was restricted at about -60° for both programs #s 2 and 3.
- In the low frequency domain, the impedance of the film formed with program # 1 showed higher value over those formed using programs 2 and 3. Also, the phase angle inflected to reach about -25° in case of film formed using program # 1 versus a value near 0° in case of the films formed using the other two programs. This should be indicative of the presence of a parallel resistance and a non-dissipative passive oxide capacitive layer of considerable thickness for the first film. The approach of the ideal capacitive behavior of the films as observed from the inflection around –80°

for the first film and near –60° for the second and third films could also be observed. However, the inflection in the phase angle versus log *f* curve is shown to take place at two different frequency ranges. Thus, the inflection took place for the first film in the frequency range of 100 Hz to about 0.1 Hz, while in the region of 70 Hz to 30 Hz for the second and third films. This would explain the size of the oxide layer that is proportional to the reciprocal of space charge capacitance (C_C^{-1}) [104-106].

The semicircles of figure III10c represent the Nyquist plots for the same set of experiments depicted in figures III10a and III10b. As indicated previously, the diameters of the semicircles ascertain the previously mentioned conclusions. Thus, as the diameter of the semicircle increases in the order of using the programs 1 > 2 > 3, the capacitance at the frequency that corresponds to a maximum in the Nyquist plot decreases, cf. equation (9). In conclusion, the data given in figure III10c showed that film thickening took place more efficiently when using program # 1 of the potential step.

5. Effect of Changing Bath Composition on Film Formation

It is well established that high temperature materials degradation or protection of Fe-Cr alloys are often related to the nature of their oxide scale formation [115]. Breakdown of passive oxide film lead to localized corrosion. Various alloying elements are often incorporated in these alloys to prevent high temperature oxidation [116, 117]. The addition of selected alloying elements is cumbersome and not always cost effective. Thus, the electrochemical molybdenum incorporation treatment is studied on stainless steel types 316 and 310. The study is compared to that of chromium at the same alloys using similar experimental conditions. In this respect, 0.01 M $(NH_4)_2MoO_4$ was added in the bath containing 5.0 M H_2SO_4 during film formation using potential program # 1 and a time of deposition of 400 s for E_{app2}. Similarly, the bath composition for the chromium incorporation is 0.01 M Na_2CrO_4 and 5.0 M H_2SO_4. The validity of incorporation treatments was evaluated by means of corrosion tests in 0.1 M H_2SO_4 and controlled by surface analysis. And since the deposition of Mo is greatly influenced by pH of solution, the acid concentration was kept at the 5.0 M level. Figure IIII1a shows the polarization resistance data for the stainless steel type 316 with films deposited using different bath composition and tested in 0.1 M H_2SO_4. It could be noticed that the slope of the V-I curves increases in the order of films formed in molybdate-containing > chromate-containing > sulfuric only-containing baths.

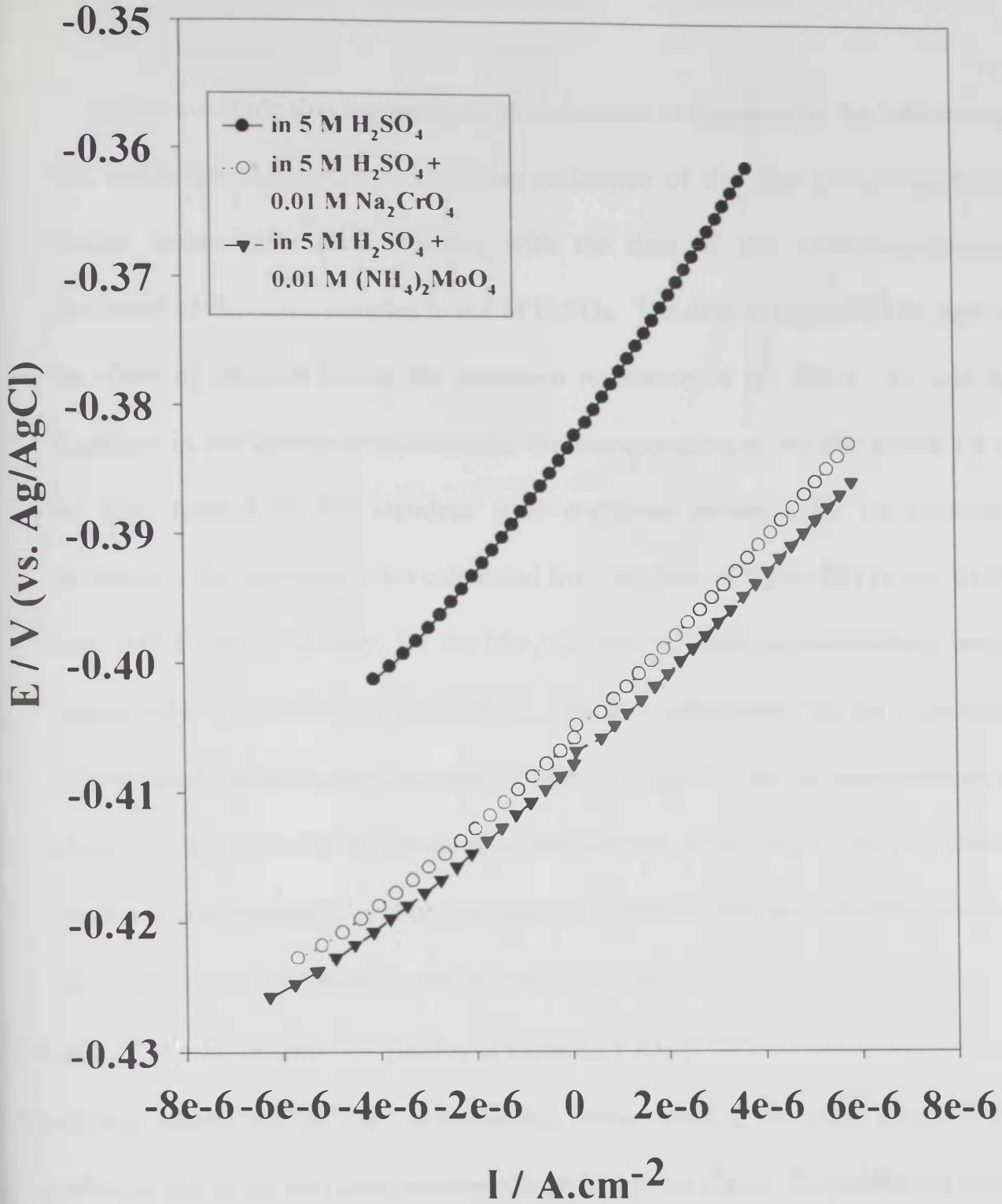

Figure III11a. Polarization Resistance Plots for SS 316 tested in 0.1 M H_2SO_4 after Oxide Formation in Different Bath Composition, $E_{app.2}$, t: 400 s

We can conclude that the presence of molybdate or chromate in the bath during film deposition enhances the corrosion resistance of the film in acid medium. Similar trends were also observed with the data of the Tafel experiments performed on the same samples in 0.1 M H_2SO_4. The data of figure III 11b depicts the effect of Mo and Cr on the corrosion resistance of the films. As will be explained in the surface measurements, the incorporation of the Mo and/or Cr to the film formed at the stainless steel enhances substantially its corrosion resistance. The corrosion rates calculated from the data of figure III 11b are, 0.099 mpy, 0.088 mpy, 27.8 mpy, for the Mo-, Cr- and sulfuric only-containing baths, respectively. The corrosion potential, E_{corr}, shifted cathodically for the same order of baths used. A mechanistic sequence could be suggested for the incorporation of Mo to the film deposited at the stainless steel surface at this stage. The first step of the deposition reaction is probably a reduction reaction, like the reduction reaction of octamolybdate according to the following reaction:

$$[Mo_8O_{26}]^{4-} + mH^+ + 2ne^- \rightarrow [HMo_{8-2n}(VI)Mo_{2n}(V)O_{26}]^{4+2n-m}$$

Thereafter, deposition of the corresponding oxide with a chemical precipitation equilibrium that is pH and concentration dependent takes place. The inhibiting effect on the active dissolution current of steel may be due to this insoluble oxide or to an insoluble Fe or Cr compound formed from the reduced anion of the above reaction. Thus, Mo incorporation in the passive layer of the alloy takes place after the electrochemical treatment during film formation.

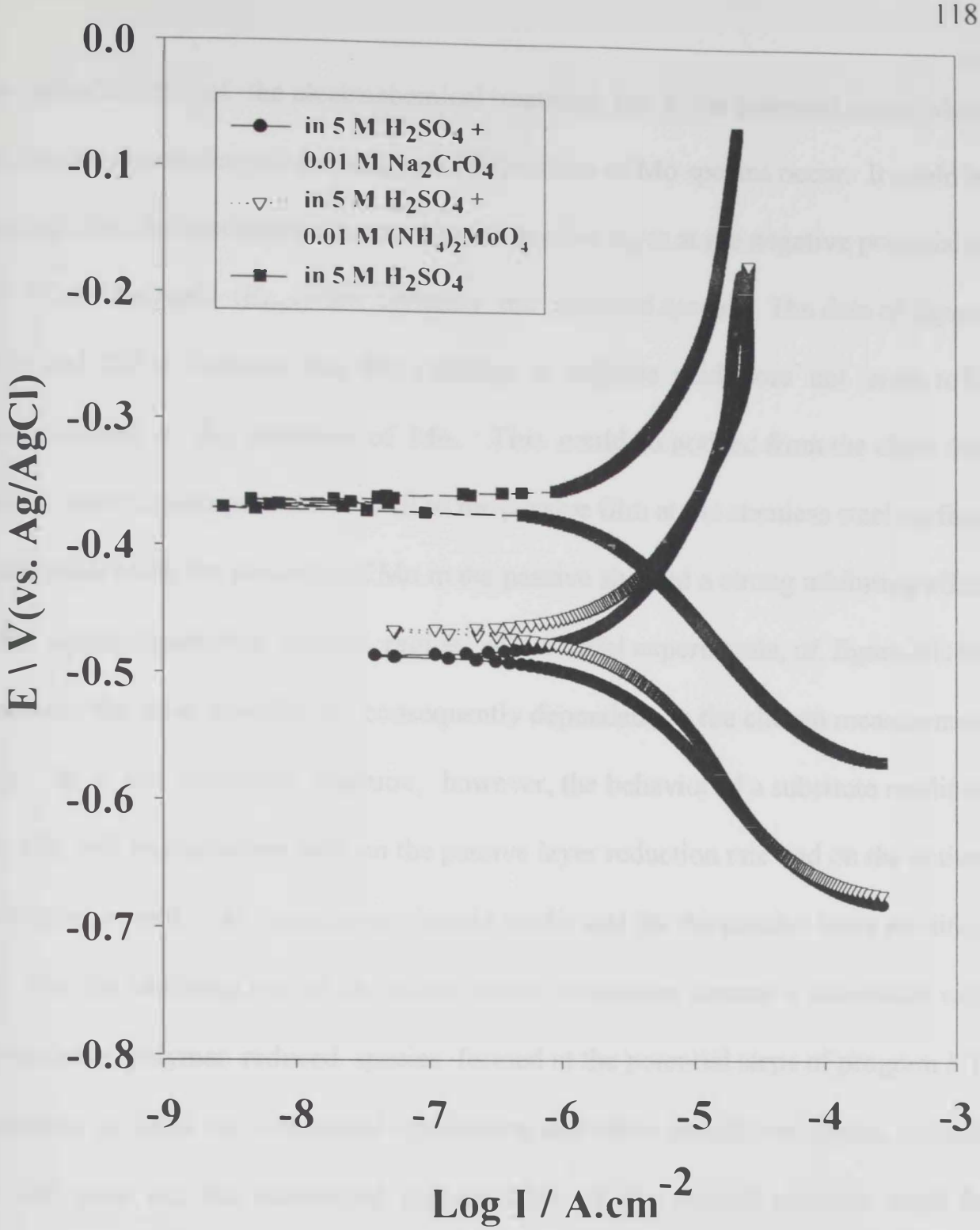

Figure III11b. Tafel Plot for SS 316 tested in 0.1 M H_2SO_4 after Oxide Formation in Different Bath Composition, $E_{app.2}$, t: 400 s

The cathodic limit of the electrochemical treatment lies in the potential range where both active dissolution of the alloy and deposition of Mo species occur. It could be expected that the species incorporated in the passive layer at the negative potential of –1.2 V vs. Ag/AgCl (E_{appl}) are certainly the reduced species. The data of figures III11a and III11b indicate that the stability in sulfuric acid does not seem to be directly related to the presence of Mo. This could be noticed from the close data obtained with Cr incorporation as well to the passive film at the stainless steel surface. On the other hand, the presence of Mo in the passive showed a strong inhibiting effect on the active dissolution current region of the Tafel experiments, cf. figure III11b. Therefore, the acid stability is consequently dependent on the chosen measurement setup. In a real corrosion situation, however, the behavior of a substrate modified with Mo, will be dependent both on the passive layer reduction rate and on the active-dissolution current. In conclusion, in acid media and for the passive layer modified with Mo, the inhibiting role of Mo on the active dissolution current is associated with the insoluble polymer reduced species formed at the potential steps of program # 1. Deposition is fixed by a chemical equilibrium and when dissolution occurs, in order that Mo may act, the superficial concentration of the formed polymer must be sufficient to form by reduction an insoluble species. Therefore, Mo has to have a minimum concentration within the passive film to have effect. For instance, the Mo concentration in the alloy must be at least 2%. Alternatively, when the Mo content in

the passive layer is too large, the layer becomes less protective because Mo would be present as MoO_3 that is poorly protective.

A similar set of experiments was performed using stainless steel type 310. The data are given in figures III12a and III12b, respectively. The same contradictory behavior was also observed in the case of incorporating Mo or Cr in the film deposition bath. Thus, the polarization resistance, Rp, value is relatively higher for films formed in presence of 5.0 M H_2SO_4 only when compared to those formed in presence of Mo or Cr. The same surprising results were also observed when examining the data of figure III12b. Thus, corrosion currents, i_{CORR}, and corrosion rates are relatively higher for the oxides presumably containing Mo or Cr.

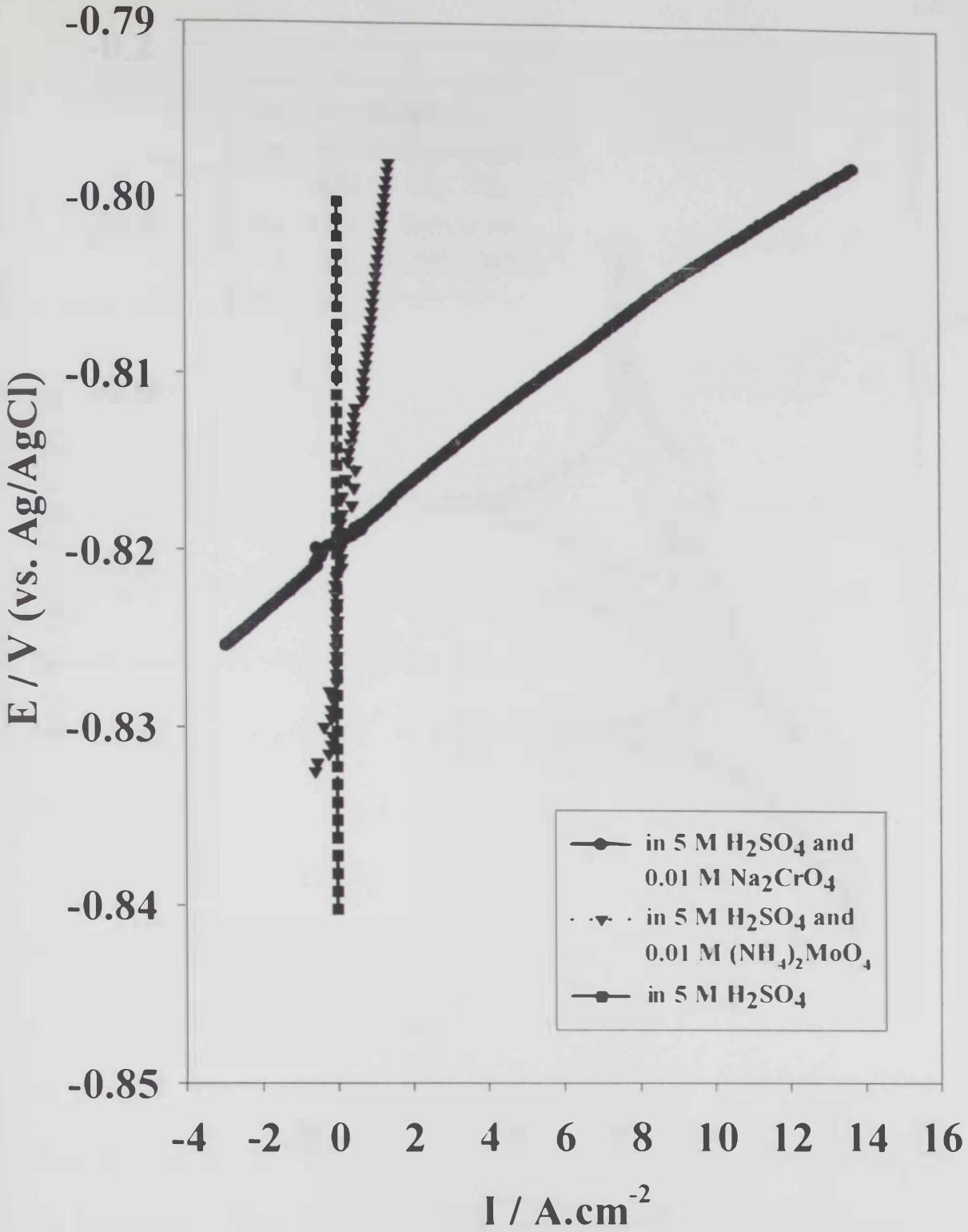

Figure III12a. Polarization Resistance Plots for SS 310 tested in 0.1 M H_2SO_4 after changing the bath composition in oxide formation step, $E_{app.}$2 ,t: 400 s

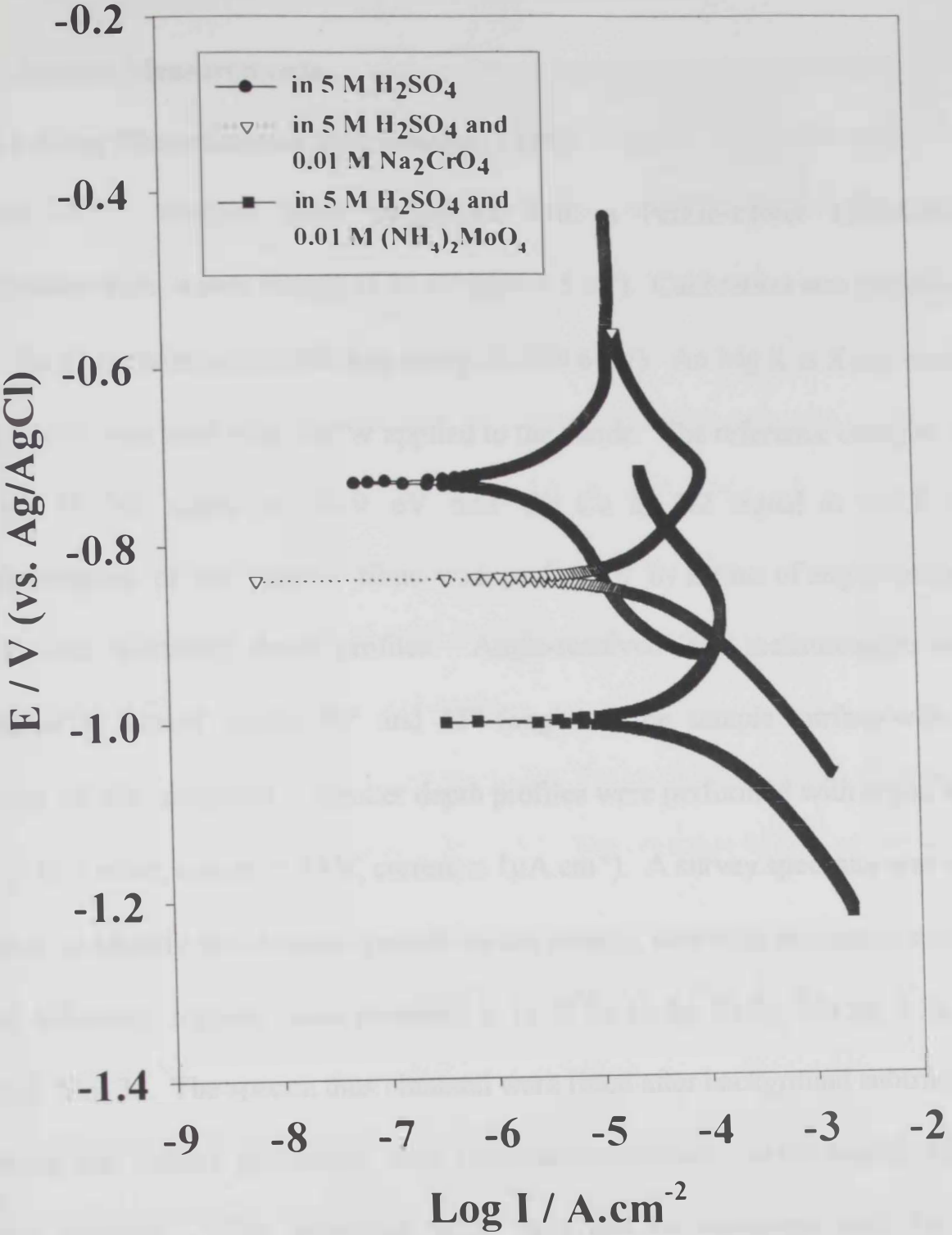

Figure III12b. Tafel Plots for SS 310 tested in 0.1 M H_2SO_4 after Oxide Formation at $E_{app.}$2, t: 400 s with different bath composition

6. Surface Measurements

6.1 X-ray Photoelectron Spectroscopy (XPS)

The XPS analyses were performed with a Perkin-Elmer ESCA-5300 spectrometer with a pass energy of 25 eV (ΔE=0.5 eV). Calibration was performed using the C 1s component (binding energy is 284.6 eV). An Mg K α X-ray source (1 253.6 eV) was used with 300 W applied to the anode. The reference energies are the Au 4f 7/2 signal at 83.9 eV and the Cu 2p 3/2 signal at 932.8 eV. Characterization of the passive films was performed by means of angle-resolved analysis and sputtering depth profiles. Angle-resolved XPS measurements were performed at takeoff angles 90° and 45° (angle of the sample surface with the direction of the analyzer). Sputter depth profiles were performed with argon ions (P_{Ar} = 10-5 mbar, energy = 3 kV, current $\cong$ 1μA.cm^{-2}). A survey spectrum was first recorded to identify the elements present on the surface, then high resolution spectra of the following regions were recorded: C 1s, O 1s, Fe 2p, Cr 2p, Mn 2p, S 2p, Ni 2p, and Mo 3d. The spectra thus obtained were fitted after background subtraction following the Shirley procedure, with Guassian-Lorentzian curves modified by a tailored function. The reference XPS data and the equations used for the quantitative analysis of passive films have been published previously [118].

The survey spectrum of the non-treated stainless steel type 316 showed that the elements present were iron, chromium, oxygen, sulfur, manganese and carbon. The carbon peak strongly decreased after a short ion sputtering, which proved that it is

present as contaminant on the surface. The data are depicted in figure III13a for a SS type 316 degreased in alcohol and washed thoroughly in de-ionized water. Iron is present as metallic iron (706.8 eV) and mainly as divalent oxide (709.5 eV). Chromium is present mainly as the metallic chromium (574.2 eV). Oxygen is present as O^{2-} in oxide (530.3 eV). Sulfur is present as elemental sulfur (163.1 eV). Figure III13b depicts the XPS survey for SS type 316 after polarization using the potential program step # 2 with E_{app2} = 400 s in 5.0 M H_2SO_4. Important conclusions could be withdrawn by comparing the data of figures III13a and III13b:

- The appearance of the Ni peak indicating the incorporation of the Ni in the passive film, in form of nickel oxide.
- The peak of chromium in the multiplex spectrum indicates the presence of chromium as trivalent oxide (576.7 eV). The presence of Cr^{6+} in the passive film was not observed.
- Oxygen is present as OH^- in hydroxide (531.6 eV) and O^{2-} in H_2O and SO_4^{2-} (532.2 eV).
- Iron is present mainly in the trivalent oxidation state (710.3 eV).

The third experiment was to polarize the stainless steel type 316 using the same experimental procedure described above in presence of chromate and molybdate in the film-forming bath and in 5.0 M H_2SO_4. The data are depicted in figure III13c.

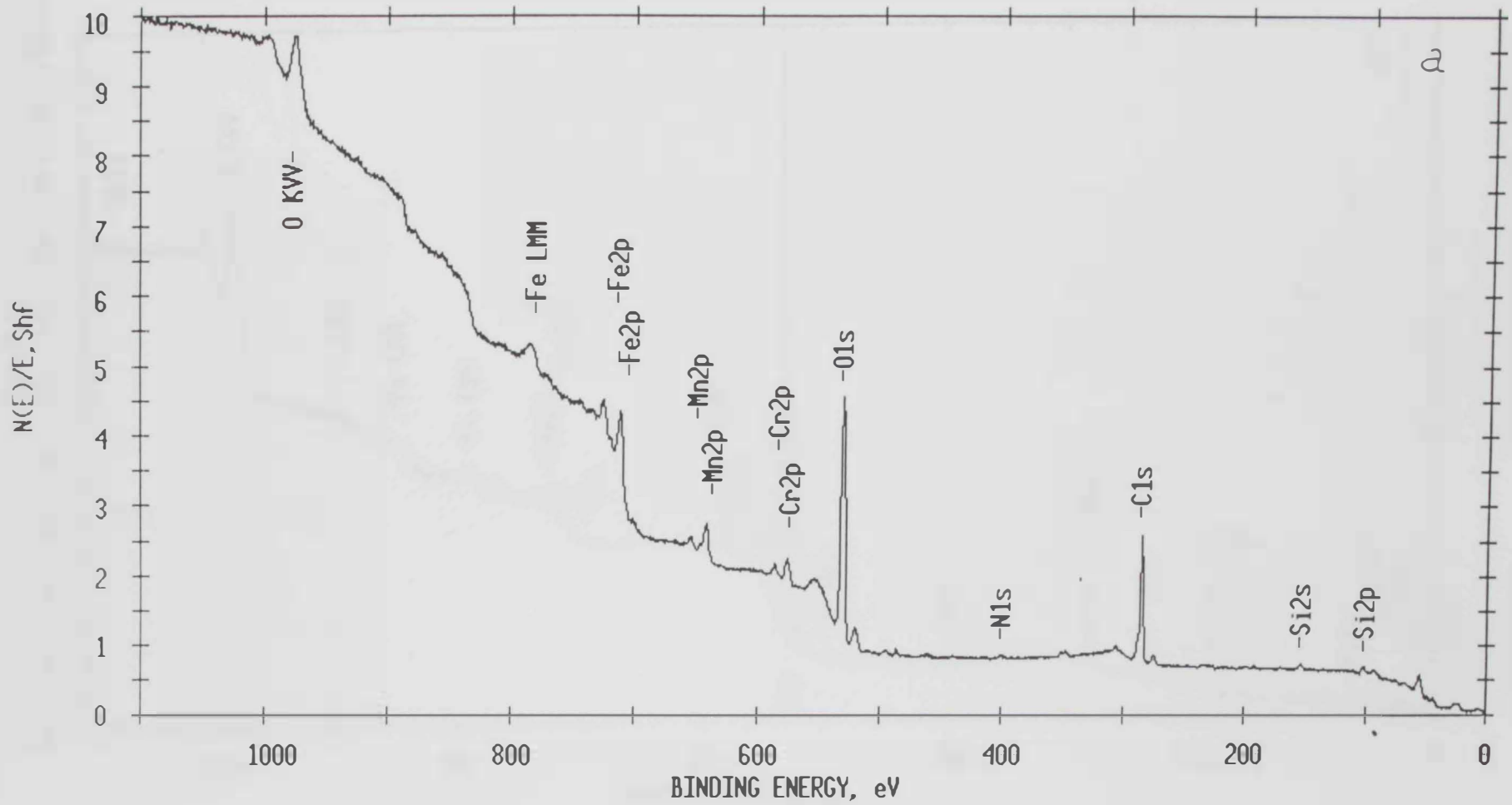

Figure III13a: XPS data for surface-free stainless steel type 316.

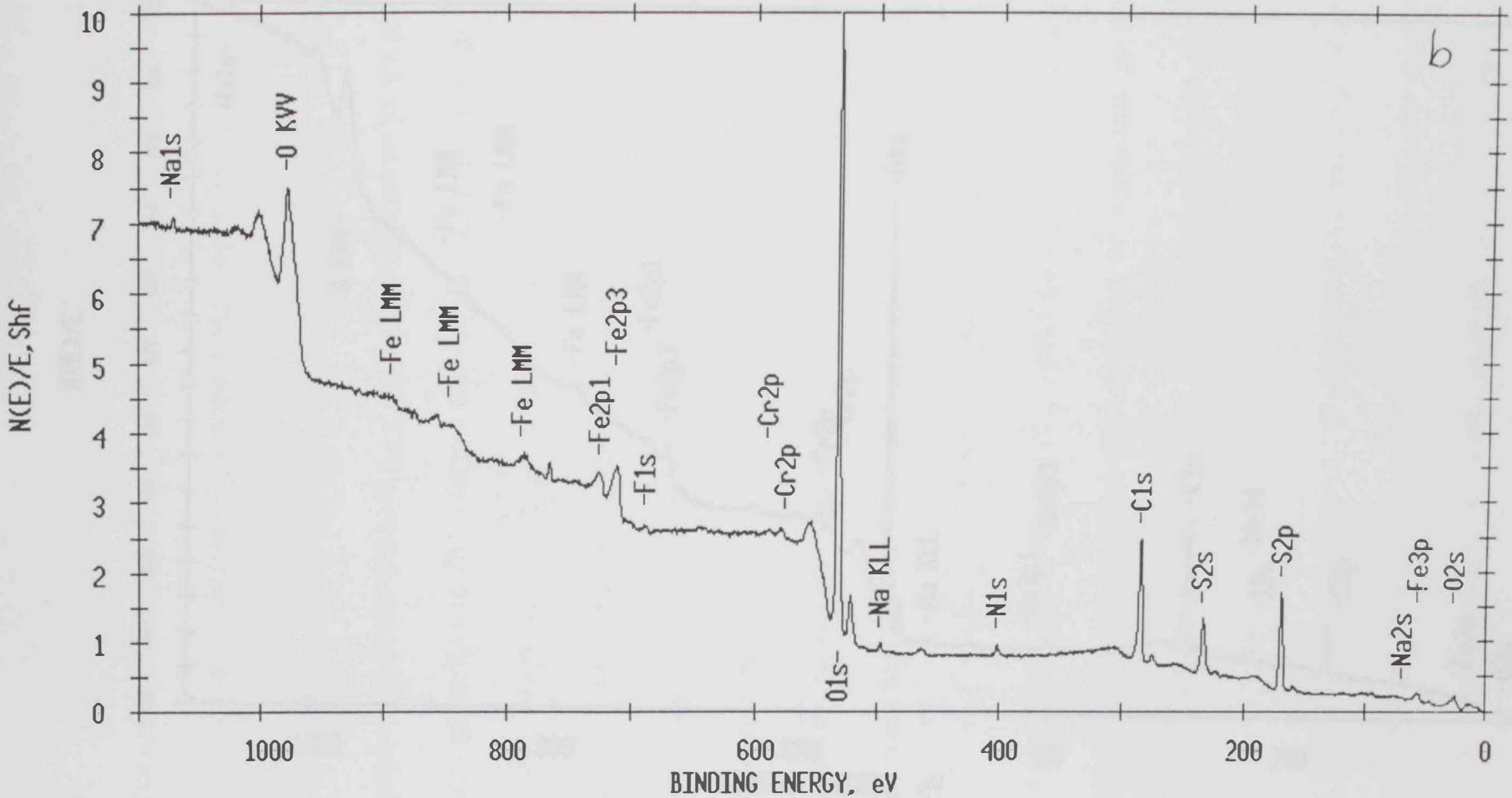

Figure III13b: XPS data for surface-covered oxide stainless steel type 316 formed in 5 M H_2SO_4.

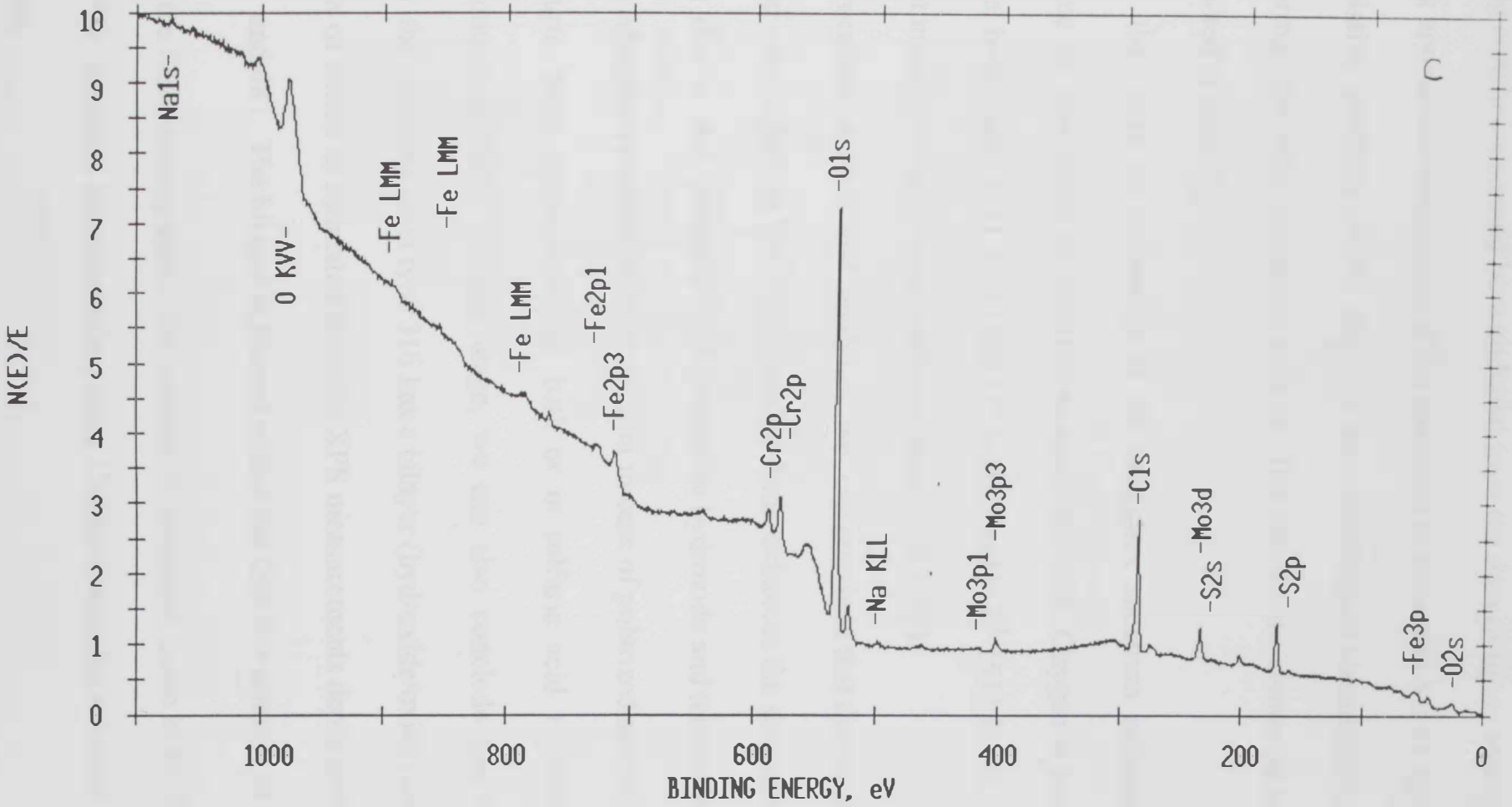

Figure III13c: XPS data for surface-covered oxide stainless steel type 316 formed in 5 M H_2SO_4+ Cr/Mo .

The following conclusions could be withdrawn from the data of figure III13c:

- Ni peak appeared as in the case of the specimen polarized in 5.0 M H_2SO_4.
- The relative amounts of Ni, Mo, Cr and Fe changed considerably when comparing the three specimens studied. The data for the elemental analysis is depicted in table III5.
- Again, the peak of chromium in the multiplex spectrum indicates the presence of chromium as trivalent oxide (576.7 eV). Oxygen is present as OH^- in hydroxide (531.6 eV) and O^{2-} in H_2O and SO_4^{2-} (532.2 eV). Iron is present mainly in the trivalent oxidation state (710.3 eV).

From the preceding section and analyses, we can conclude that the presence of chromate and molybdate in the film-forming bath enhances the structure of the passive film due to the presence of chromium as hydroxide and molybdenum as the oxide. Also, the presence of Ni in the film in case of polarized sample, either in the sulfuric acid only-containing bath or in sulfuric acid + chromate + molybdate-containing bath. At this stage, we can also conclude that the film deposited at the stainless steel type 316 has a bilayer (hydroxide/oxide) structure, the thickness of which as estimated from the XPS measurements depth profiling is between 45 and 48 Å. The bilayer is formed within the first few minutes as will be revealed by the SEM micrographs. The content of chromium oxide in the film and at the alloy/film interface increases when using Cr/Mo-containing solutions during film formation.

Table III5a. XPS Data for blank SS 316 surface

Element peak	Area	Sensitivity facor	Concentration %
C1s	187837	0.250	43.90
O1s	486809	0.660	43.09
Cr2p	86550	2.300	2.20
Fe2p	381927	3.000	7.44
Mn2p	141616	2.600	3.18
S2p	1796	0.540	0.19
Ni2p	0	4.500	0.00

Table III5b. XPS data for SS 316 surface-covered Oxide (formed in 5 M H_2SO_4)

Element	Area	Sensitivity Factor	Concentration %
C1s	145771	0.250	30.99
O1s	660509	0.660	53.19
Cr2p	31265	2.300	0.72
Fe2p	198291	3.000	3.51
Mn2p	11507	2.600	0.24
S2p	98933	0.540	9.74
Ni2p	13602	4.500	0.16
Mo3d	74752	2.750	1.44

Table III5c. XPS data for SS 316 covered-surface oxide (formed in 5 M H2SO4 plus mixture of chromate and molebdate)

Element peak	Area	Sensitivity Facor	Concentration %
C1s	159966	0.250	38.91
O1s	513373	0.660	47.30
Cr2p	96269	2.300	2.58
Fe2p	101395	3.000	2.06
Mn2p	23409	2.600	0.55
S2p	57079	0.540	6.43
Ni2p	8899	4.500	0.12
Mo3d	86783	2.750	2.03

The combination of a chromium-, nickel- and molybdenum-rich film at the surface of the stainless steel surface was beneficial for pitting resistance of the metal as was indicated previously in section 3 of the experimental results and discussion.

6.2 Scanning Electron Microscopy (SEM) – Energy Dispersive X-Ray Analysis (EDAX):

The scanning electron microscopy studies of the stainless steel type 316 surface have shown that the surface morphology is characterized by different structural elements. Isolated micronuclei, this could be the components of the natural oxide film. As could be noticed from the micrograph depicted in figure III14a describes the surface of a non-treated surface of SS type 316. On the other hand, the micrograph of figure III14b describes the surface of stainless steel type 316 after polarization in 5.0 M H_2SO_4 using program # 2 for 400 s. The important feature for the micrograph of figure III14b is the presence of visible differently oriented lamellas of the surface macro-aggregates that have sizes of several tens of microns. The sizes of the nuclei range from 10 – 30 nm. The detailed structure and separation between the lamellas is depicted in the micrograph of figure III14c. The steel surface is relatively smooth, however, some negligible roughness could steel be identified at high resolutions for the untreated surface. The important result of the SEM experiments is the identification of the systematic growth of the oxide layer that consists of oval,

pentagonal and pyramidal aggregates with a high micro-roughness. Thus, figures III15a, III15b, and III15c show the SEM micrographs of oxide film formed using program # 2 and with the Ea_{pp2} potential applied for 100 s, 200 s, and 300 s, respectively. The results indicate that the nucleation of the oxide layer starts (as the time of deposition was limited to 100 s) with islands formation that are well defined with specific orientation as shown in figure III15a and with the general overview with figure III16. As the nucleation has completed, the oxide film starts thickening and mature as shown in figure III15b. The growth of the oxide plates is being completed as the time of film deposition progresses. The important feature difference between the data shown in figures III15b and III15c is the size of the lamellas or plates. As could be noticed by comparing the two figures, the size of lamellas decreased as the time of film deposition increases (see also figure III14c). The thickening of the film was previously established from the EIS, polarization resistance, and Tafel measurements. The white dots at the surface of the specimens were found to be due to precipitation of sulfate salts. The latter was proved by XPS and EDXA experiments.

Figure III 14a: SEM graph for blank surface of stainless steel type 316.

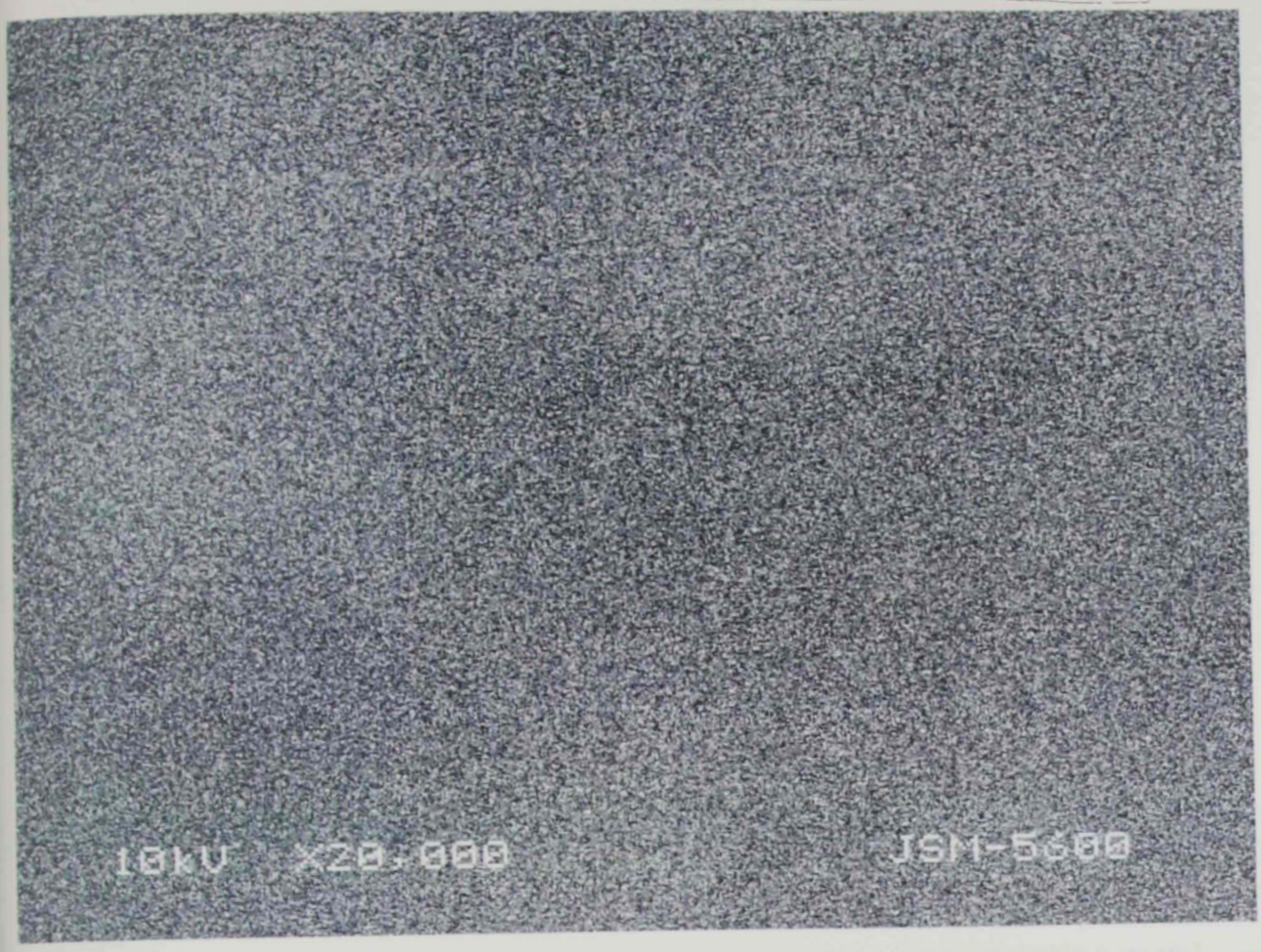

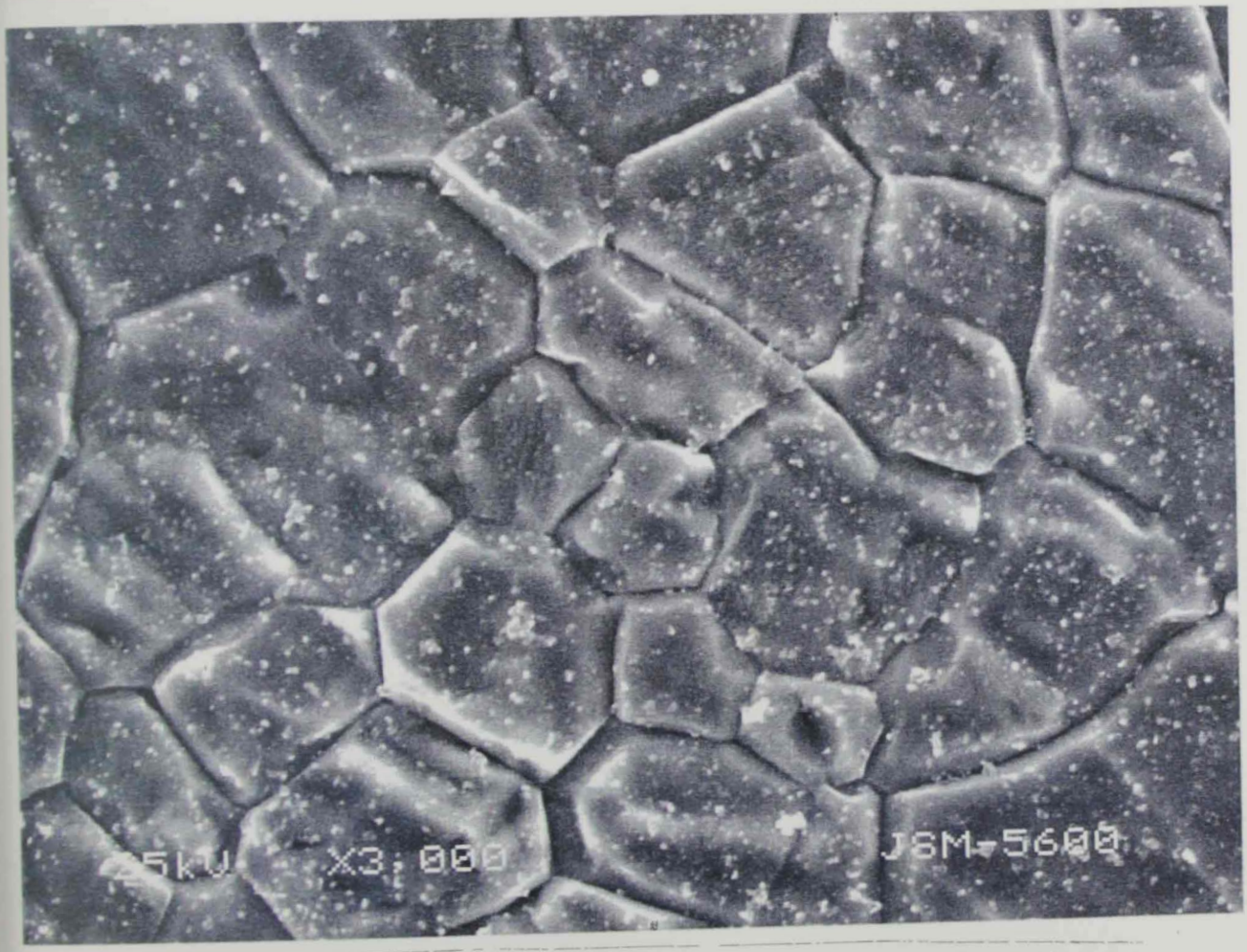

Figure III14b: SEM graph for SS 316 surface after oxide formation in

Figure III14c: SEM graph for SS 316 surface after oxide formation at $E_{app.}$(2), t = 400 s with higher magnification.

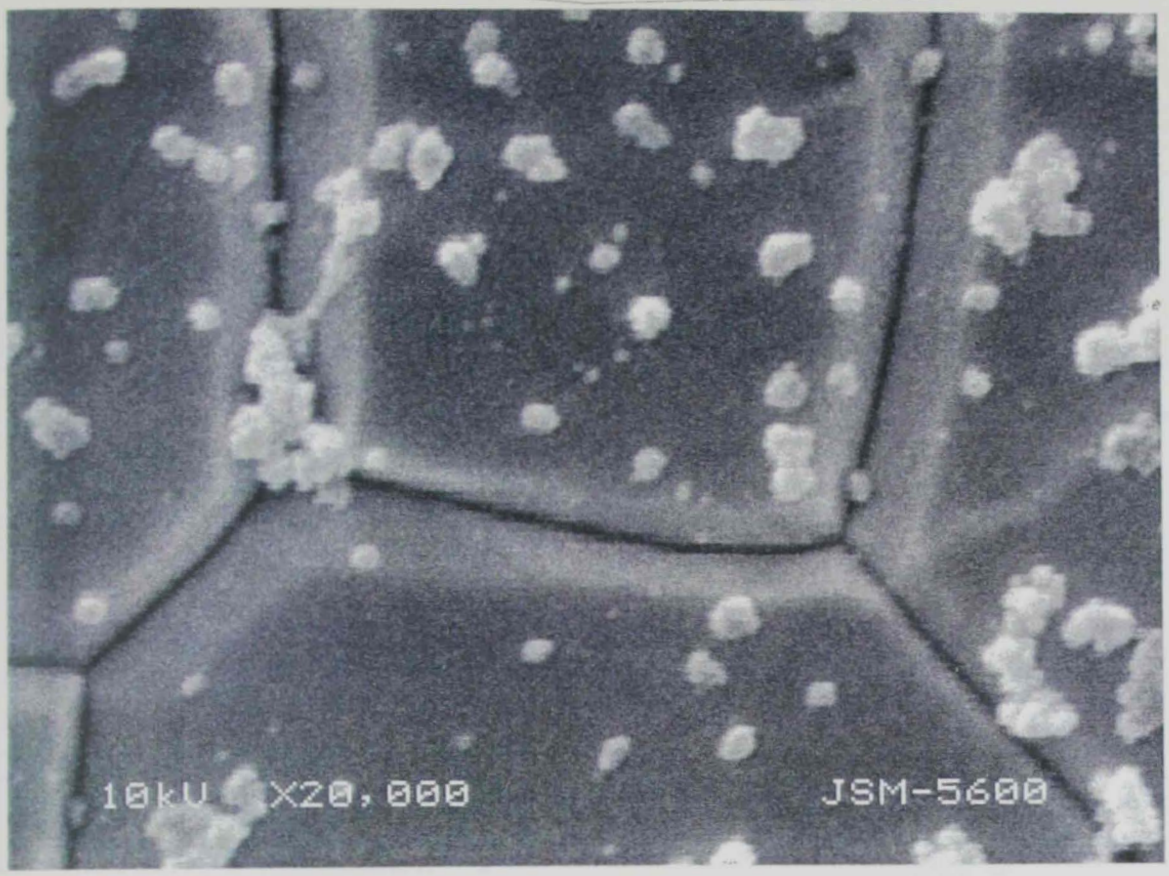

Figure III15a: SEM graph for SS 316 surface after oxide formation at $E_{app.}$(2), t = 100 s .

Figure III15b: SEM graph for SS 316 surface after oxide formation at E_{app}.(2), t = 200 s.

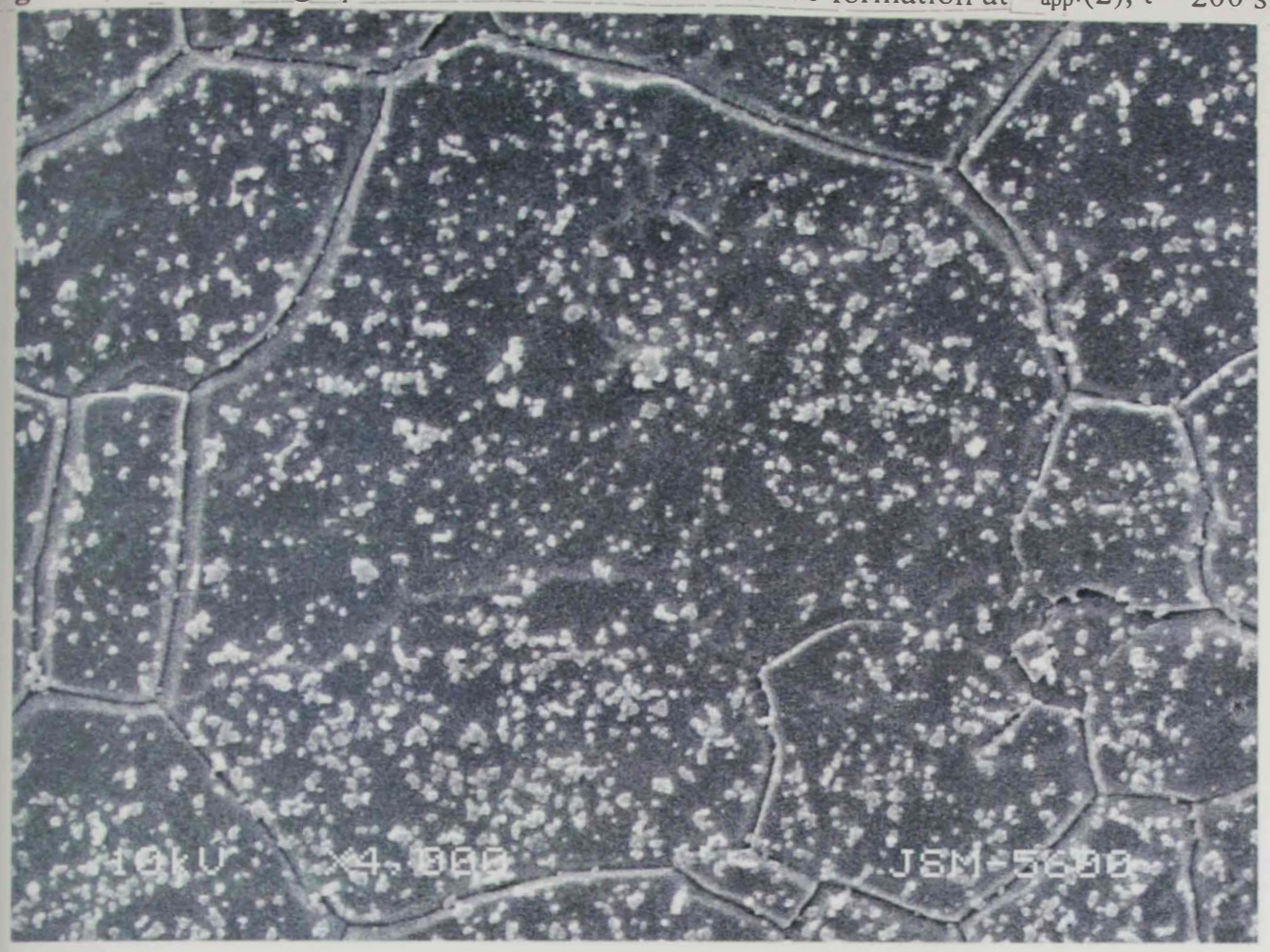

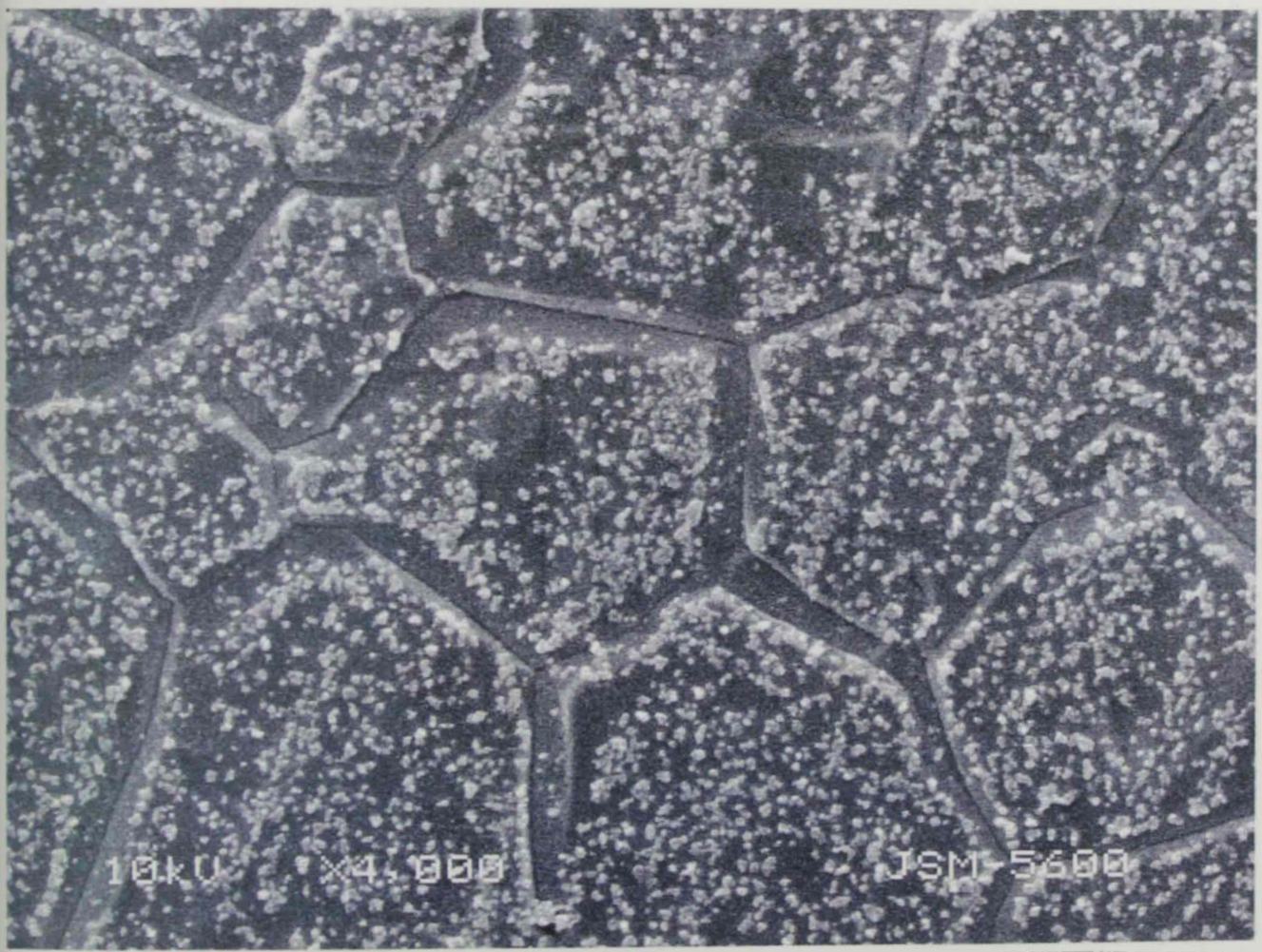

Figure III15c: SEM graph for SS 316 surface after oxide formation at E_{app}.(2), t = 300 s.

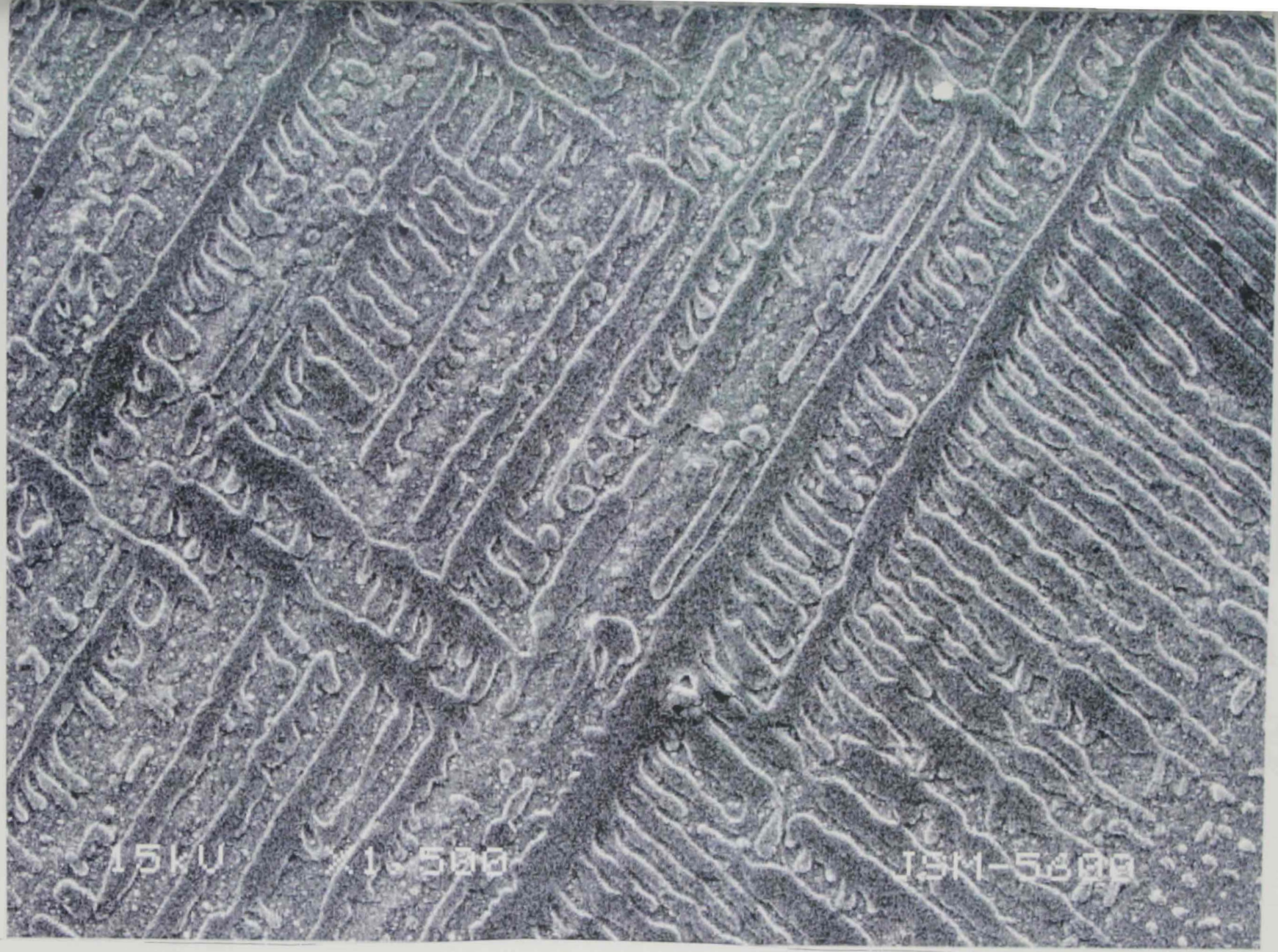

Figure III16: SEM graph for SS 316 surface after oxide formation at E_{app}.(2), t = 100 s, an overview graph.

EDXA of stainless steel specimen type 316 with film formation using program # 2 in 5.0 M H_2SO_4 is given in figure III17a. The data for a sample treated in molybdate bath during film formation is depicted in figure III17b. As seen from the results and when examining the effect of bath composition during the formation of the film, increasing Mo content with Ni increased the passivation behavior of stainless steel type 316. It is also well established that the increase in the amount of Mo increases resistance to pitting. Moreover, from data displayed in figure III17a, Mo content in the oxide film is not markedly different from that in the bulk. However, Mo content increased appreciably for the second sample. The Mo found in the first specimen is from the enrichment of the film during anodic dissolution on the steel. It is also well established that the rate of dissolution of Mo is much lower than that of Fe. The barrier layer suggested earlier from the EIS measurements should contain partially Mo.

6.3 X-ray Diffraction (XRD)

Figure III18 depicts typical XRD patterns for stainless steel type 316. Two peaks can be noticed around $2\theta = 47°$ and $2\theta = 52°$. Curves a, b, c, and d represent the XRD of untreated stainless steel, specimen covered with film formed using program # 2 in 5.0 M H_2SO_4, specimen covered with film formed using program # 1 in 5.0 M H_2SO_4, specimen covered with film formed using

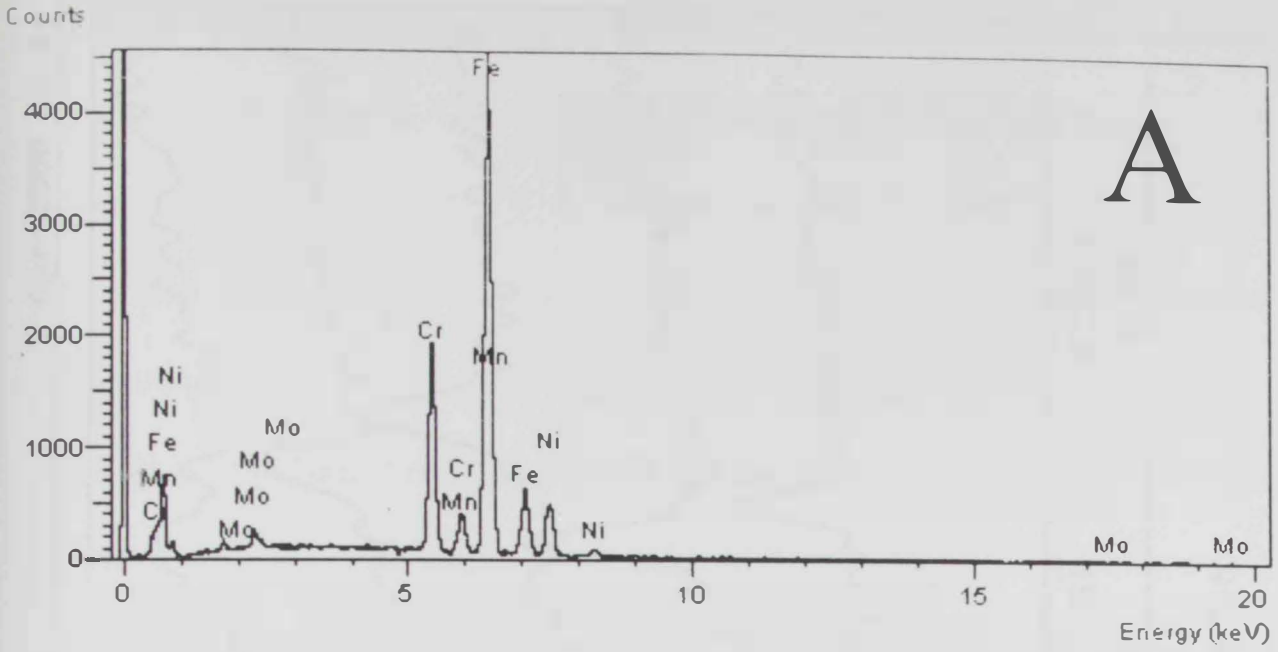

Figure III17a: EDAX analysis for SS 316 covered-surface oxide.

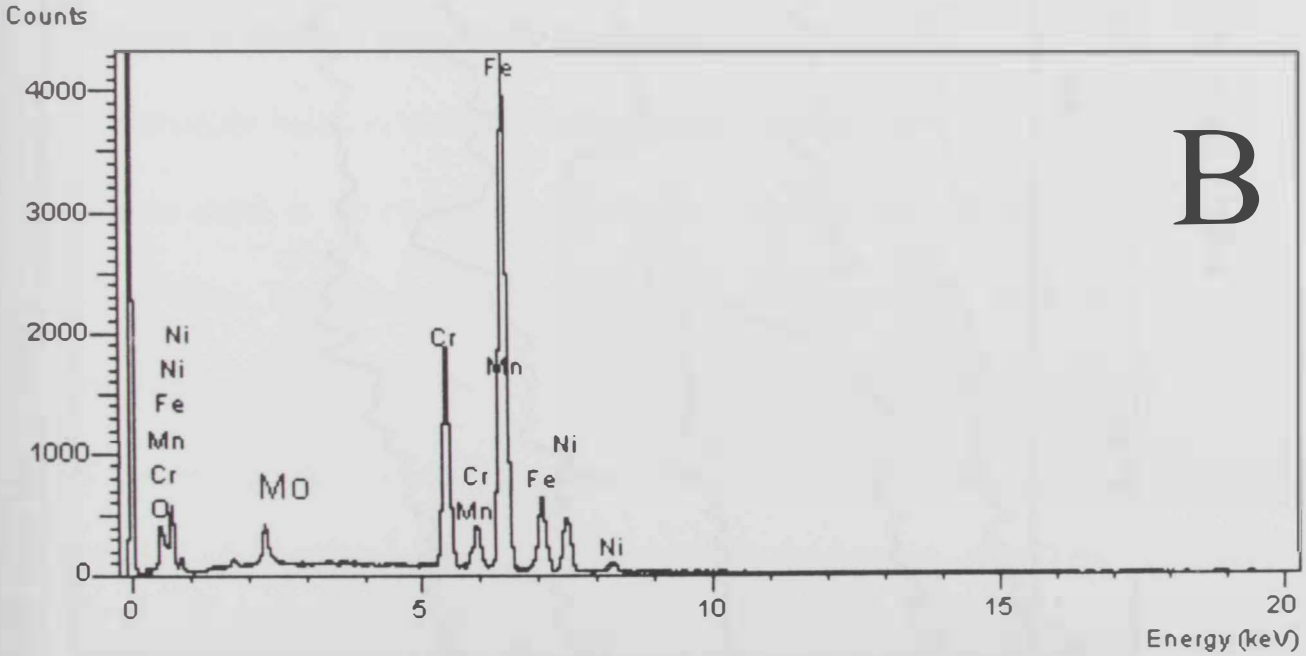

Figure III17b: EDAX analysis for SS 316 surface-covered oxide formed

In 5 M H2SO4 containing Molybdate ions.

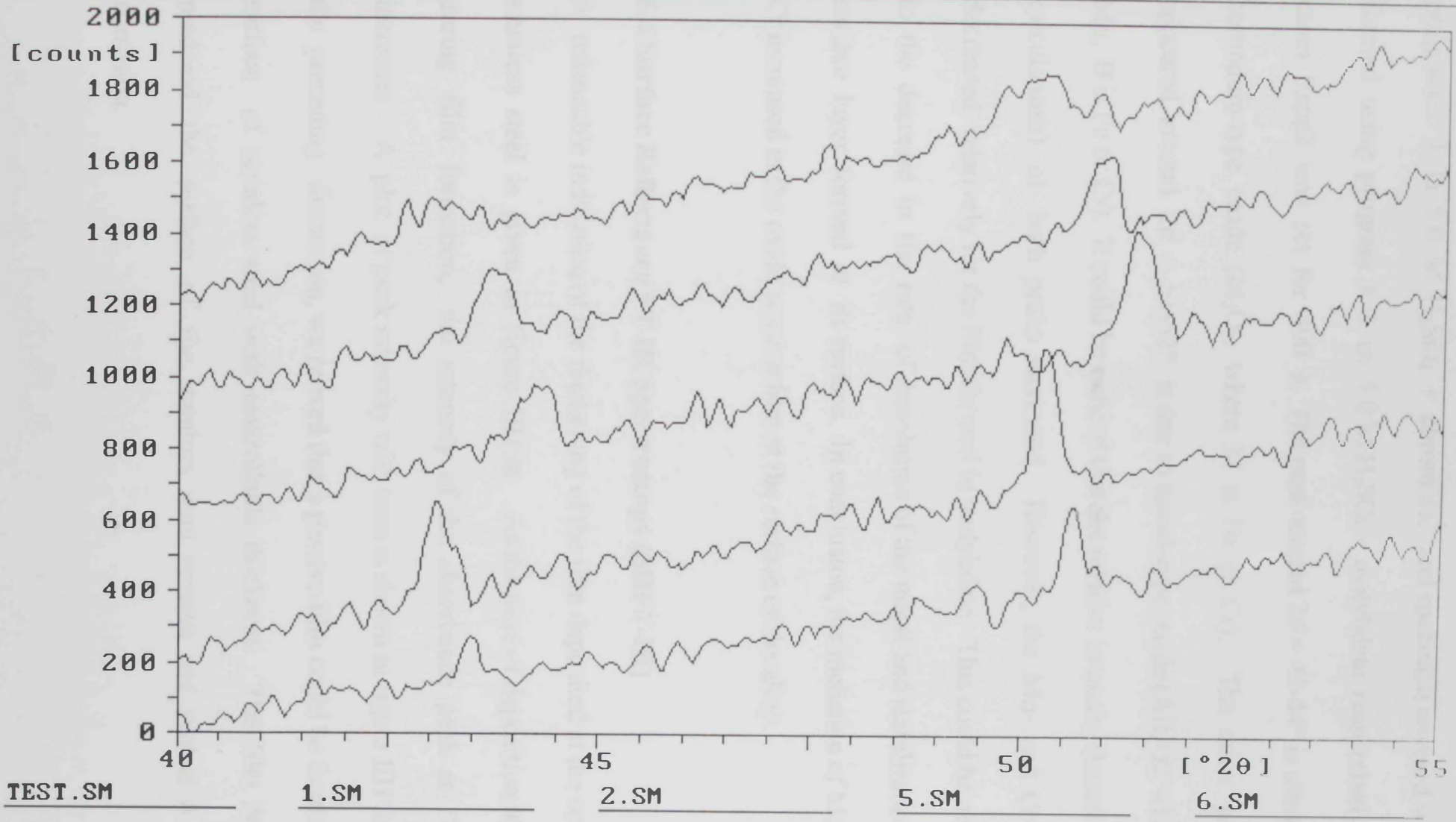

Figure III18: X-ray diffraction results for SS 316.

program # 1 in 5.0 M H_2SO_4 + chromate, and specimen covered with film formed using program # 1 in 5.0 M H_2SO_4 + molybdate, respectively. In all cases Eapp2 was set for 400 s. The peak around 2θ = 43-44° is attributed to corundum-type oxide (M_2O_3, where M is Fe or Cr). The other peak that appeared around 2θ = 51-52° is due to spinel-type oxide (AB_2O_4, where A is Mo, B is Fe or Cr). It could be noticed that the relative intensity (based on area calculations) of both peaks increased. However, the Mo- and Cr- peaks decreased relatively for the film formed in molybdate. This could be attributed to the decrease in the rate of dissolution of the metal and stabilization of the surface layer formed at its surface. In conclusion, the inclusion of Mo and or Cr increased in the oxide passive film at the surface of the alloy.

6.4 Surface Reflectance FT-IR Spectroscopy (SRFT-IR)

A reasonable indication of the thickening of the film deposited at the surface of stainless steel is given in figure III19a. As the time of deposition increases during film formation, the intensity of the absorbance peak at 795 cm^{-1} increases. A plot of peak intensity with time is shown in figure III19b. From the preceding discussion, we proved that a passive film could be formed at the surface of stainless steel with controllable thickness. The film deposited rendered the surface of the stainless steel passive and protect it against corrosion.

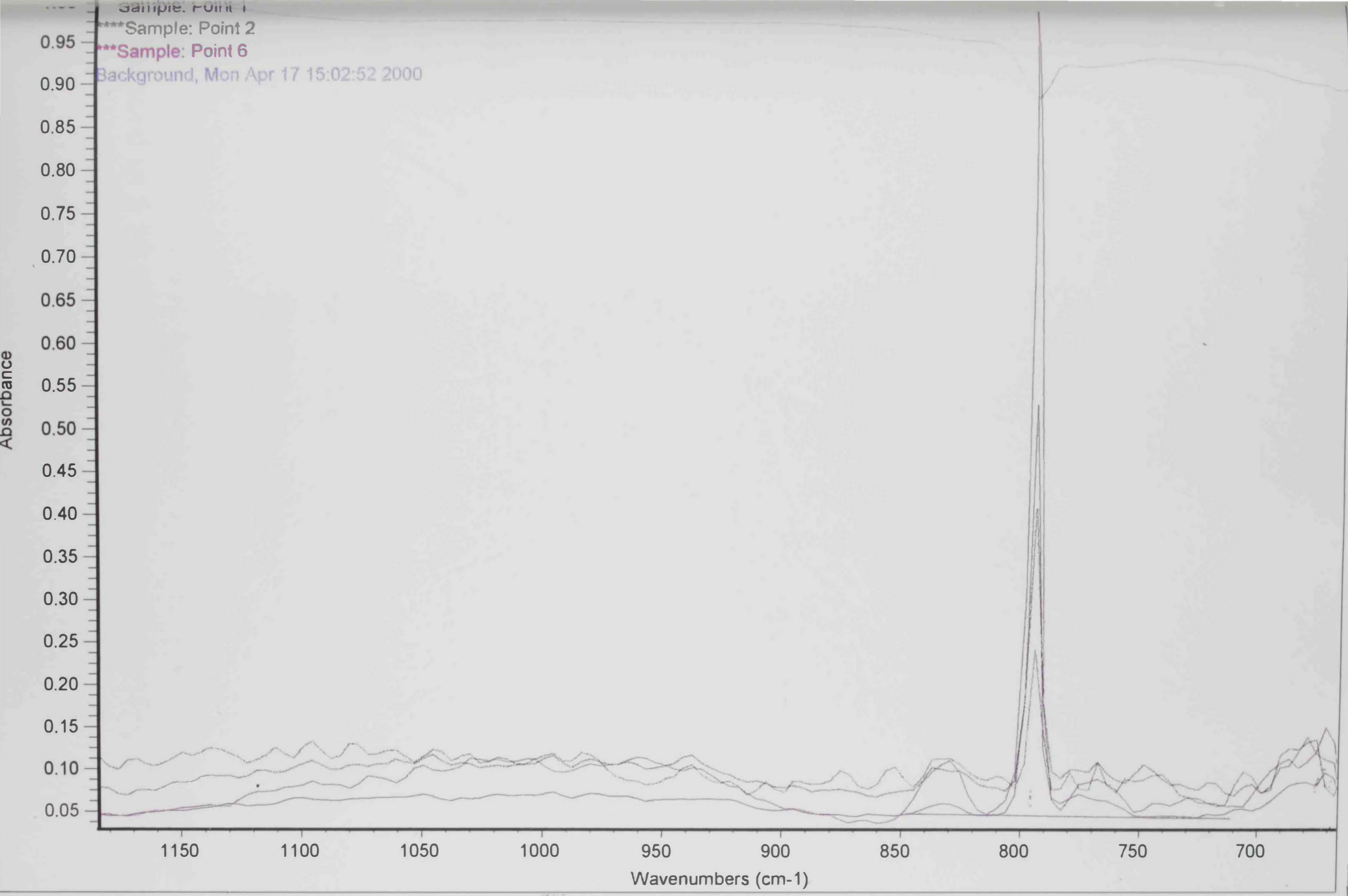

Figure III19a: Surface reflectance FT-IR results for SS 316.

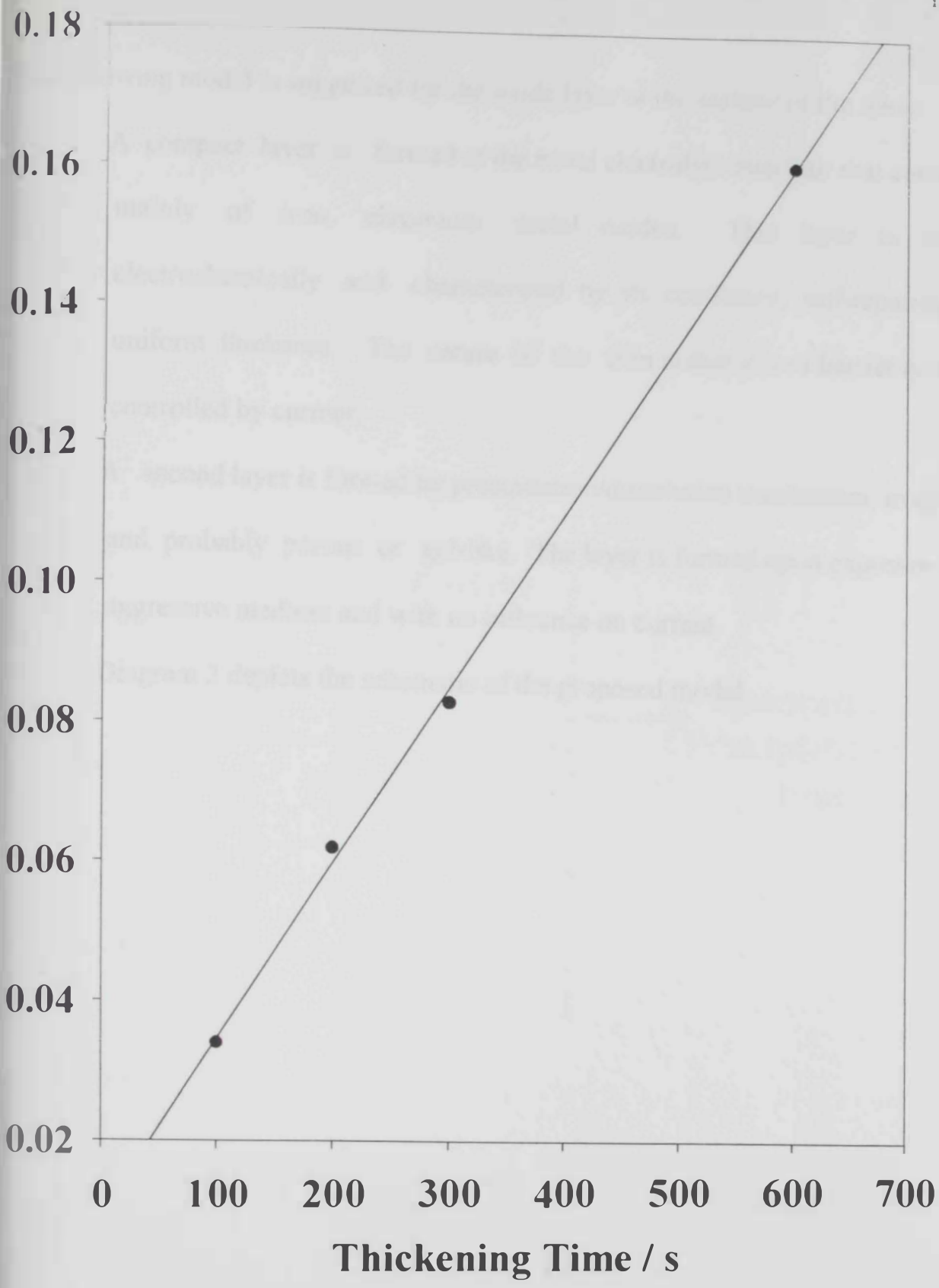

igure III19b. Surface Reflectance FT-IR results for SS 316 formed in 5 M H_2SO_4 with different thickening time

The following model is suggested for the oxide layer at the surface of the alloy:

- A compact layer is formed at the metal electrolyte interface that consisted mainly of iron, chromium metal oxides. This layer is formed electrochemically and characterized by its continuity, self-repairing, of uniform thickness. The nature of the film is that it is of barrier type and controlled by current.
- A second layer is formed by precipitation/dissolution mechanism, irregular, and probably porous or gel-like. The layer is formed upon exposure to an aggressive medium and with no influence on current.
- Diagram 2 depicts the schematic of the proposed model.

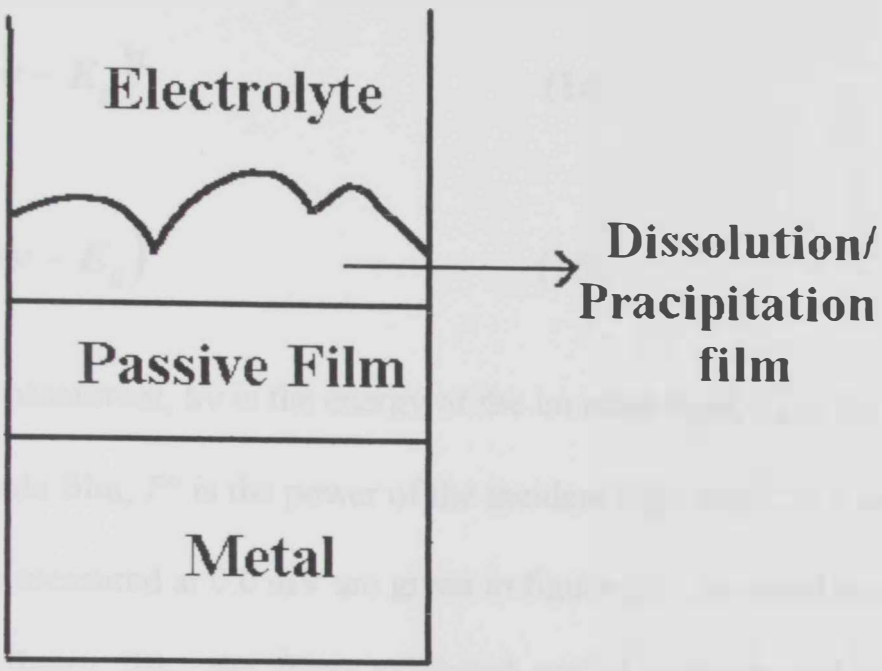
Electrolyte
Dissolution/
Pracipitation
film
Passive Film
Metal

Diagram 2

Photoelectrochemical behavior of oxide films formed at stainlesssteel type 316 surfaces. Oxide films were grown in 5 M H_2SO_4 using potential step programming # 1 as described before. The time used for second applied potential E_{app2} was varied between 100 s and 400 s. A Xe arc lamp with 600 W-power and a monochromator adjusted at 300 nm were used. Measurements were conducted in 0.1 M H_2SO_4 and using a quartz electrochemical one-compartment cell. The photo electrochemical-current can be described by the following relations:

$$\frac{I_{ph}\, h\nu}{P_{\circ}} = const.\left(h\nu - E_g\right)^2 \qquad (14)$$

$$\left(\frac{I_{ph}\, h\nu}{P_{\circ}}\right)^{1/2} = C\left(h\nu - E_g\right) \qquad (15)$$

Where, I_{ph} is the photocurrent, hν is the energy of the incident light, E_g is the optical band gap of the oxide film, $P°$ is the power of the incident light and C is a constant. Photocurrent spectra measured at 0.0 mV are given in figure 20. As could be noticed from the data of figure 20, the films exhibited partial positive and negative photocurrent. This indicates that the film exhibited a mixed n-type and p-type semiconductor properties. The optical band gap, E_g, is 3.81 with about 0.11 electron volt than the expected value of 3.7 eV.

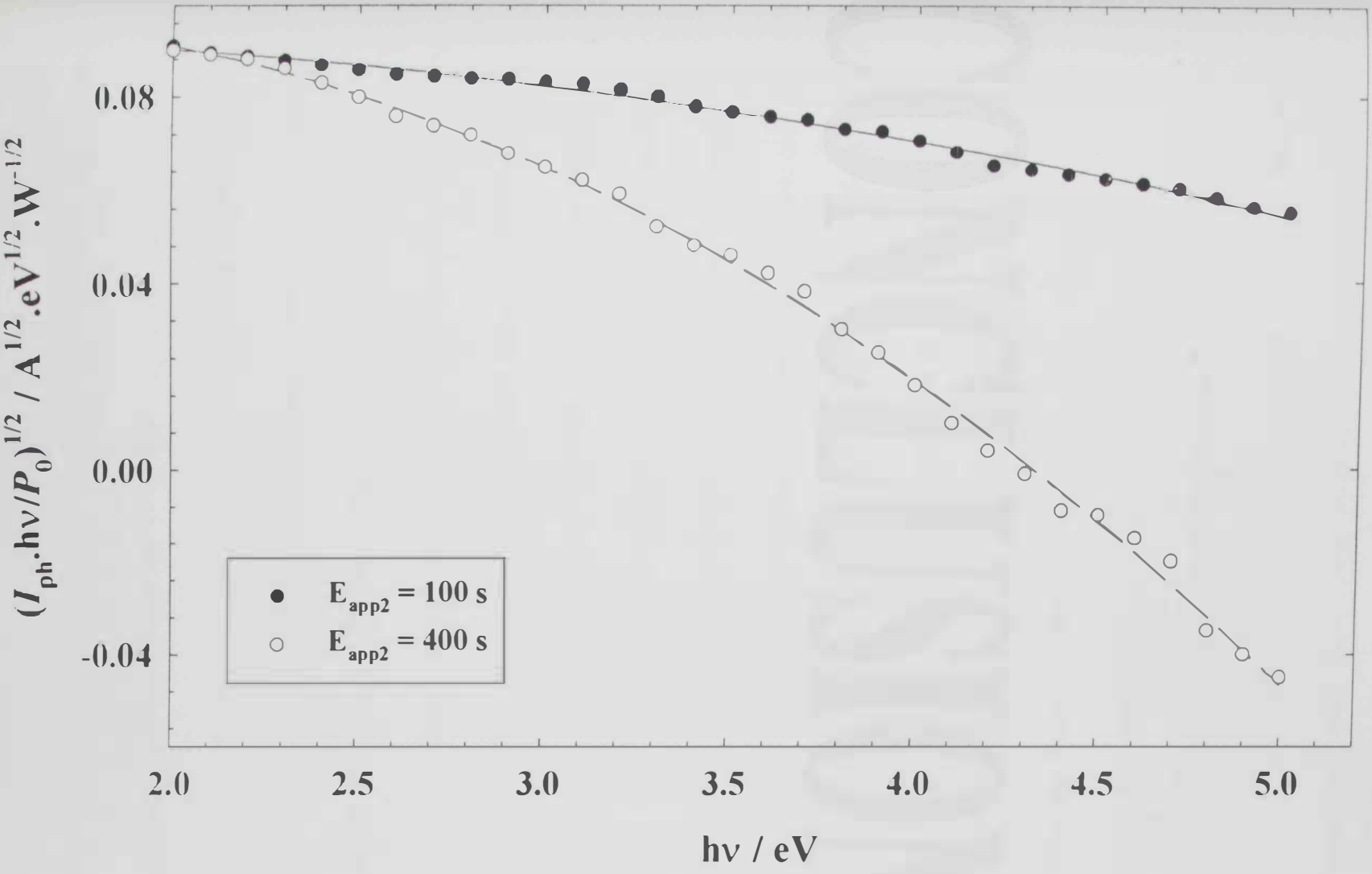

Figure III 20. Photoelectrochemical Spectrum for SS type 316 Films Formed in 5.0 M H_2SO_4 Measured at 25 ^{0}C in 0.1 M H_2SO_4

CONCLUSION

CONCLUSION

It has been shown that the polarization behavior of the different types of stainless steels studied is strongly dependent on the steel structure. The ability of stainless steels type 316 and type 310 to passivate in 5.0 M sulfuric acid is realized and stabilized within a relatively wide range of potential. However, passivating current in the case of stainless steel type 316 is relatively higher than that shown for stainless steel type 310. Oxide film formed over stainless steel type 316 is relatively more stable than that formed over stainless steel type 310 surfaces under similar experimental conditions.

However, overall potentiodynamic experiments conducted for SS 316 proved that the highest corrosion rate in the aggressive medium, 5 M H_2SO_4 + NaCl, was for the oxide-free surface. Moreover, the corrosion current, I_{corr}, showed a gradual decrease in the order of oxide-free surface in 0.1 M H_2SO_4 > oxide-covered surface in 0.1 M H_2SO_4 > oxide-covered surface in 0.1 M H_2SO_4 and 0.1 M NaCl > oxide-covered surface in 0.1 M H_2SO_4 and 0.01M NaCl.

Also it has been concluded that the oxide film formation at the stainless steel surface exhibits an immediate blockage to the surface from corrosion in sulfuric acid. For SS 310, it was found that the oxide film formed at its surface is not stabilized as the time of film deposition increases. The thickness of film deposition at the stainless

steel type 310 could be controlled up to a time of deposition of 400 s. Moreover, no full coverage of the surface of stainless steel that is imparted by the passive oxide film is guaranteed in the case of less time for deposition.

The data of the EIS measurements showed the following conclusions:

- The impedance spectra is simple capacitive in nature as would be expected for a passive film covering the surface of a metal substrate.
- The modulus measured at the low frequency end (ca. below 1 Hz) would indicate the electronic nature of the film. Thus, the film formed using program # 1 exhibited the highest resistance.
- It is possible to control the thickness of oxide/film forming over stainless steel type 316 using program # 1.

In conclusion, in acid media and for the passive layer modified with Mo, the inhibiting role of Mo on the active dissolution current is associated with the insoluble polymer reduced species formed at the potential steps of program # 1. Therefore, Mo has to have a minimum concentration within the passive film to have effect on the protection of the surface. Also, it has been shown that for SS 310; the corrosion currents, i_{corr}, and corrosion rates are relatively higher for the oxides presumably containing Mo or Cr.

we can conclude that the presence of chromate and molybdate in the film-forming bath enhances the structure of the passive film due to the presence of chromium as hydroxide and molybdenum as the oxide. We can also conclude that the film deposited at the stainless steel type 316 has a bilayer (hydroxide/oxide) structure, the thickness of which as estimated from the XPS measurements depth profiling is between 45 and 48 ^{o}A. The bilayer is formed within the first few minutes as revealed by the SEM micrographs. The photoelectrochemical experiment conducted on SS 316 showed that the photocurrent for the film increased by increasing the thickness.

REFERENCES

REFERENCES

1- Alvarez, R. B.; Ruiz, A. A., "Oxidation of vanadium stainless steel", *Universidad, (I) Ciencia Y Technologia [Univ. Cienc. Technol.]*, 2(5), 17-21, **1998.**

2- Strutt, A. J.; Vecchio, K. S.," Imultaneous oxidation and sigma-phase formation in a stainless steel", *Metalurg. Mater. Trans. -A*, 30(2), 355-362, **1999.**

3- Piao, T.; Park, S-M.; "Spectroelectrochemical studies of passivation and transpassive breakdown reactions of stainless steel", *J. Electrochem. Soc.*, 144(10), 3371- 3377, **1997**.

4- Marijan, D.; Vukovic, M.; Pervan, P.; Milun, M., "Surface modification of stainless steel-304 electrode. I. Voltammetric, rotating ring-disc electrode and XPS studies", *Croat. Chemi. Act.* , 72(4), 737-750, **1999.**

5- Saeki, I.; Kouno, H.; Furuichi, R.; Nakamura, T.; Mabuchi, K.; Itoh, M., "Initial oxidation of type 430 stainless steels at 1073-1273 K", *J. Jpn. Inst. Met.*, 61(5), 416-423, **1997.**

6- Ozturk, B.; Matweey, R., "Oxidation of type-304 stainless steels under simulated annealing conditions", *ISIJ Intern.*, 37(2), 169-175, **1997**.

7- Vukovic, M., "The formation and growth of hydrous oxide film on stainless steel in alkaline solution by potential cycling", *Corr. Sci.*, 37(1), 111-120, **1995.**

8- Ohmi, T.; Nakagawa, Y.; Nakamura, M.; Ohki, A.; Koyama, T., "Formation of chromium oxide on 316L austenitic stainless steel", *J. Vacuum Sci. & Technol.*, -A, 14(4), 2505-2510, **1996.**

9- Yen, SK., "A retarding mechanism of thermally grown oxide films on hydrogen embrittlement of AISI 430 stainless steel", *Mater. Chem. & Phys.*, 59(3), 210-219, **1999.**

10- Hubbard, KM.; Espinoza, BF., "Corrosion-resistant erbium oxide coatings by organometallic chemical vapor deposition", *Thin solid films*, 366(1-2), 175-180, **2000.**

11- Perez, FJ.; Cristobal, MJ.; Hierro, MP.; Pedraza, F.; Arnau, G.; Merino, P., "Effects of yttrium and erbium ion implantation on the oxidation behavior of the AISI 304 austenitic steel", *Surface & Coatings Technol.*, 126(2-3), 116-122, **2000.**

12- Marigan, D.; Slavkovic, R.; Vukovic, M., "Surface modification of stainless steel-304 electrode. 2. An experimental comparative study of electrochemically, hydrothermally and chemically modified oxide films", *Croat. Chemi. act.*, 72(4), 751-761, **1999.**

13- Shifler, DA.; Moran, PJ.; Kruger, J., "The passive behavior of 304-stainless-steel in PC-H_2O and DME-H_2O mixtures", *Electrochem. Act.*, 40(7), 897-905, **1995.**

14- Carmezim, MJ.; Carvalho, FG.; Figueiredo, MO., "Improving the passivating efficiency of conversion films on stainless-steel by thermal treatment", *Thin Solid Films*, 258(1-2), 194-197, **1995**.

15- Cho, B.; Chung, S.; Kim, K.; Kang, T.; Park, C.; Kim, B., "Direct observation of oxygen-induced structural changes in stainless steel surfaces", *J. Vacu. Sci. & Technol.-B*, 18(2), 868-872, **2000**.

16- Shieu, FS. ; Deng, MJ. ; Lin, SH., "Microstructure and corrosion resistance of a type 316L stainless steel", *Corr. Sci.*, 40(8), 1267-1279, 1998.

17- Kim, YJ., "Characterization of the oxide film formed on type-316 stainless steel in 288-degrees-C water in cycling normal and hydrogen water chemistries", *Corr.*, 51(11), 849-860, **1995.**

18- Piao, T.; Park, SM., "Specrtochemical studies of passivation and transpassive breakdown reactions", *J. Electrochem. Soc.*, 144(10), 3371-3377, **1997.**

19- Banas, J.; Stypula, B.; Mazurkiewicz, B., "Passivity of metals in anhydrous sulfuric-acid-solutions", *Ach-Models in chem.*, 132(4), 607-618, **1995.**

20- Ishikawa, Y.; Yoshimura, T., "Importance of the surface oxide layer in the reduction of outgassing from stainless steels", *J. Vac. Sci. & Technol. -A*, 13(4), 1847- 1852, **1995**.

21- Reese, E.; Grabke, H. J., "Effects of sodium chloride on the oxidation of high alloy Cr and Cr-Ni steels", *Werkstoffe and Korrosion*, 44(2), 41-47, **1993**.

22- Wenger, F.; Cheriet, S.; Talhi, B.; Galland, J., "Electrochemical impedance of pits – influence of the pit morphology", *Corr. Sci.*, 39(7), 1239-1252, **1997.**

23- Lorang, G.; Belo, MD.; Simoes, AMP.; Ferreira, MGS., "Chemical composition of passive films on AISI 304 stainless steel", *J. Electrochem. Soc.*, 141(12), 3347-3356, **1994.**

24- Mattin, SP.; Burstein, GT., "Detailed resolution of microscopic depassivation events on stainless steel in chloride solution leading to piting", *Philosophical Magazine Letters*, 76(5), 341-347, **1997**.

25- Choe, H-C.; Kim, K-H., "Effects of MoO4 in the acidic electrolytes on the corrosion behavior of sensitized 304 steel in the acidic electrolytes", *J. Corr. Sci. Soc. Of Korea*, 24, 3-13, **1995.**

26- Grover, AK.; Kumar, D.; Goswami, G. L.; Pappachan, AL.; Totlani, MK., "Electrochemical characteristics of high Ni-Mo laser surface alloys produced on stainless steel 304substrates", *Lasers Engineering*, 7(2), 119- 131, **1998**.

27- Montemor, MF.; Ferreira, MMGS.; Hakiki, NE.; Belo, MDC., "Effet of Mo on the composition and electronic properties of the passive films formed on stainless steels at 350 °C", *Electrochem. Methods in Corr. Research*, 289(2), 1139-1150, **1998.**

28- Asteman, H.; Svensson, J-E.; Johansson, L-G.; Norell, M., "Indication of chromium oxide hydroxide evaporation during oxidation of 304L at 873K in the presence of 10% water vapor", *Oxid. Met.*,52(1-2), 95- 111, **1999.**

29- Dowling, NJE.; Kim, YH.; Ahn, SK.; Lee, YD., "Effect of alloying elements and residuals on corrosion resistance of type 444 stainless steel", *Corr.*, 55(2), 187-199, **1999**.

30- Wegrelius, L.; Falkenberg, F.; Olefjord, I., "Passivation of stainless steels in hydrochloric acid", *J. Electrochem. Soc.*, 146(4), 1397-1406, **1999**.

31- Park, JJ.; Pyun, SI.; Lee, WJ.; Kim, HP., "Effects of bicarbonate ion additives on pitting corrosion of type 316L stainless steel in aqueous 0.5 M sodium chloride solution", *Corr.*, 55(4), 380-387, **1999**.

32- Maximovitch, S.; Barral, G.; Lecras, F.; Claudet, F., "The electrochemical Incorporation of molybdenum in the passive layer of a 17-percent Cr Ferritic stainless steel", *Corr. Sci.*, 37(2), 271- 291, **1995.**

33- Hermas, AA.; Ogura, K.; Takagi, S.; Addachi, T., "Effects of alloying additions on corrosion and passivation behaviors of type-304 stainless steel", *Corr.*, 51(1), 3-10, **1995**.

34- Lou, W.; Ogura, K., "Current Oscillations observed on a stainless steel electrode in sulfuric-acid-solutions with and without chromic-acid", *Electrochem. Act.*, 40(6), 667-672, **1995**.

35- Huang, CC.; Tsai, WT.; Lee, JT., "Effects of N and Mo on the electrochemical-behavior of laser-alloyed stainless steels in a 3.5 wt% NaCl solution", *Mat. Chem. & Phys.*, 42(4), 280-284, **1995**.

36- Vanderweijde, DH.; Vanwesting, EPM.; Dewit, DHW, "Electrochemical techniques for delamination studies", *Corr. Sci.*, 36(4), 643-652, **1994.**

37- Vanwesting, EPM.; Ferrari, GM.; Dewit, JHW., "The determination of coating performance with impedance measurements – 2. Water-uptake of coatings", *Corr. Sci.*, 36(6), 957- 977, **1994.**

38- Darowicki, K., "Corrosion rate measurements by nonlinear electrochemical impedance spectroscopy", *Corr. Sci.*, 37(6), 913-925, **1995.**

39- Nishikata, A.; Ichihara, Y.;Tsura, T., "An application of electrochemical impedance spectroscopy to atmospheric corrosion study", *Corr. Sci.*, 37(6), 897-911, **1995**.

40- Mansfeld, F., "The use of electrochemical impedance spectroscopy for the evaluation of the properties of passive filmsand protective coatings", *ACH-Models in Chem.*, 132(4), 619-631, **1995.**

41- Mccafferty, E., "On the determination of distributed double-layer capacitances from Cole-Cole plots", *Corr. Sci.*, 39(2), 243-254, **1997.**

42- Hong, T.; Nagumo, M., "The effect of chloride concentration on early stages of pitting for type-304 stainless steel revealed by the AC-impedance method", *Corr. Sci.*, 39(2), 285-293, **1997.**

43- Bojinov, M.; Betova, I.; Kanazirski, I.; Girginov, A.; Raicheff, R., "Modelling the anodic corrosion of alloys in acid solutions on the basis of AC impedance and photoelectrochemical measurements", *Mater. Sci. Forum*, 289-292(2), 979-988, **1998.**

44- Saario, T.; Laitinen, T.; Makela, K.; Bojinov, M.; Sirkia, P., "A novel teqnique for electrochemical measurements in low conductivity environments", *EUROCORR 98 Book of Abstracts*, 86, **1998**.

45- Jones, PD.; Nisipeanu, E., "Spectral-directional emittance of thermally oxidized 316 stainless steel", *Intern. J. Thermophys.*, 17(4), 967-978, **1996.**

46- Leitao, E.; Silva, RA.; Barbosa, MA., "electrochemical impedance spectroscopy of nitrogen-sputter and carbon-sputter coated 316L stainless steel", *Corr. Sci.*, 39(2), 333-338, **1997.**

47- Mansfeld, F.; Breslin, CB.; Pardo, A.; Perez, FJ., "Surface modification of stainless steel- green technology for corrosion protection", *Surface & Coatings Techno.*, 90(3), 224- 228, **1997.**

48- Lee, WJ.; Pyun, SI.; Yeon, JW.; Chun, KS.; Choi, IK., "A study on pitting corrosion of sensitized 316 stainless steel in aqueous 0.01 M NaCl solution using the abrading electrode technique and AC-impedance specroscopy", *Electrochem. Methods in Corr. Research VI*, 289(2), 915-924, **1998.**

49- Capobianco, G.; Monetta, T.; Bellucci, F., "Electrochemical and corrosion behavior of passive films on stainless steels after gamma-ray irradiation", *Corr. Control for Low-Cost Reliability Conference*, **1993.**

50- Song, G.; Cao, C.; Lin, H., "On the transpassivation-repassivation of type 304 stainless steel in high potential ranges", *J. Chinese Soc. Corr. & Protections*, 14 (3), 208-216, **1994.**

51- Brown, R.; Alias, M. N., "Oxidation of nitride films in aqueous solution : correlation between surface analysis and electrochemical studies", *Corr./qu*, Paper No. 322, **1994**.

52- Slemnik, M.; Petek, A.; Dolecek, V., "Measurements of electrochemical noise on the passive layer of differently heat treated stainless steels", *Mater. & Corr.*, 46(1), 13-17, **1995.**

53- Drogowska, M.; Menard, H.; Lasia, A.; Brossard, L., "Impedance study of the passive film on stainless steel 304 in pH 8 carbonate solution", *J. Appl. Electrochem.*, 26(11), 1169-1177, **1995**.

54- Chou, SL.; Tsai, MJ.; Tsai, WT.; Lee, JT., "Effects of nitrogen on the electrochemical behavior of 301Ln stainless steel in H_2SO_4 solutions", *Mater. Chem. & Phys.*, 51(2), 97-101, **1997**.

55- Bassler, R.; Uhlemann, M.; Mummert, K., "Inhibiting effect of octadecylamine on pitting corrosion behavior of stainless steel type 1.4541 up to 250 °C", *Mater. & Corr.*, 50(3), 146-153, **1999.**

56- Fujimoto, S.; Kawachi, T.; Nishio, T.; Shibata, T., "Impedance and photoelectrochemical properties of porous oxide film on type 304 stainless steel formed by square wave potential pulse polarization", *J. Electrochem. Chem.*, 473(1-2), 265-271, **1999**.

57- Bojinov, M.; Fabricius, G.; Laitinen, T.; Makela, K.; Saario, T.; Sundholm, K., "Conduction mechanism of the anodic film on Fe-Cr alloys in sulfate solutions", *J. Electrochem. Soc.*,146(9), 3238-3247,**1999.**

58- Fujimoto, S.; Shibata, T.; Wada, K.; Tsutae, T., "The electrochemical conditions for colored film formation on type 304 stainless steel with square wave polarization", *Corr. Sci.*, 35(1-4), 147-152, **1993.**

59- Olefjord, I.; Wegrelius, L., "Passivation of high alloyed stainless steels in HCl at 22 °C", *Corr. Control for Low-Cost Reliability Conference*, **1993.**

60- Atrens, A.; Baroux, B.; Mantel, M., "The secondary passive film for type 304 stainless steel in 0.5 M H_2SO_4 ", *J. Electrochem. Soc.*, 144(11), 3697-3704, **1997.**

61- Drogowska, M.; Menard, M.; Brossard, L., "Pitting of AISI 304 stainless steel in bicarbonate and chloride solutions", *J. appl. Electrochem.*, 27(2), 169-177, **1997**.

62- Covino, BS.; Cramer, SD.; Russell, JH.; Simmons, JW., "Corrosion and polarization behavior of sensitized high nitrogen stainless steels", *Corr.*, 53(7), 525-536, **1997.**

63- Breslin, CB.; Chen, C.; Mansfeld, F., "The electrochemical behavior of stainless steels following surface modification in cerium containing solutions", *Corr. Sci.*, 39(6), 1061-1073, **1997.**

64- Rezek, J., "Electrochemical properties of protective coatings on maraging steel", *Corr. Sci.*, 39(2), 385-397, **1997.**

65- Zhang, YS.; Zhu, XM., "electrochemical polarization and passive film analysis of austenitic Fe-Mn-Al steels in aqueous solutions", *Corr. Sci.*, 41(9), 1817-1833, **1999.**

66- Ferreira, M. S. G.; Moura E Silva, M.; Catarino, A.; Pankuch, M.; Melendres, C. A., "Electrochemical and laser Raman spectroscopy studies of stainless steel in 0.15 M NaCl solution", *J. Electrochem. Soc.*, 139(11), 3146-3151, **1992.**

67- Otero, E.; Pardo, A.; Utrilla, MV.; Perez, FJ.; Merino, C., "The corrosion behavior of AISI 304L and 316L stainless steels prepared by powder-metallurgy in the presence of Organic-acids", *Corr. Sci.*, 39(3), 453-463, **1997.**

68- Luo, JL.; Yang, MZ.; Yang, Q.; Qiao, LJ.; Qin, ZQ.; Norton, PR., "Effects of hydrogen on semi-conductivity of passive films and corrosion behavior of 310 stainless steel", *J. Electrochem. Soc.*, 146(6), 2107-2112, **1999.**

69- Du, TB.; Chen, SH.; Yang, MZ.; Chen, L., "Photoelectrochemical study of passive films on sensitized stainless steel", *J. Mater. Sci. & Technol.*, 12(5), 381-384, **1996.**

70- Hakiki, NE.; Da Cinha Belo, M.; Simoes, AMP.; Ferreira, M. G. S., "Semi-conductivity properties of passive films formed on stainless steels", *J. Electrochem. Soc.*, 145(11), 3821-3829, **1998.**

71- Hakiki, NE.; Boudin, S.; Belo, MD., "The electronic structure of passive films formed on stainless steels", *Corr. Sci.*,37(11), 1809- 1822, **1995.**

72- Hakiki, NE.; Belo, MD., "The influence of molybdenum on the electronic structure of ferritic stainless steel passive films", *Comtes Rendus de L acamemie des sciences serie II*, 320(11), 613- 618, **1995.**

73- Breslin, CB.; Macdonald, DD.; Shibata, J.; Sikora, E., "Influence of UV-light on the passive behavior of SS 316 – effect of prior illumination", *Electrochem. Act.*, 42(1), 127-136, **1997.**

74- Fujimoto, S.; Kawachi, S.; Shibata, T., "Modification of passive film on an Fe-18 Cr alloy in sulfuric acid solution by ultra-violet light irradiation", *J. Jpn. Inst. Met.*, 63(3), 375-382, **1999.**

75- Suzuki, S., *J. Iron & Steel Inst. Jpn.*, 82(7), 551-557, **1996.**

76- Tempest, P. A.; Wild, R. K., "Thickness measurements of spinel and chromia layers in stainless steel oxide scales by X-ray diffractometry", *UK Oxid. Met.*, 17(5-6), 345-357, **1982.**

77- Juez-Lorenzo, M.; Kolarik, V.; Eisenreich, N.; Engel, W.; Criado, A. J., "Non-isothermal kinetics of the iron oxides in steels with different carbon

contents studied in situ by a fast X-ray diffraction method", *Progress in the Understanding & Prevention of Corr.*, 2, 1129-1135, **1993.**

78- Saito, M.; Kosaka, T.; Matsubara, E.; Waseda, Y., "Characterization of oxide film grown on stainless steel by anew in-house grazing-incidence X-ray-scattering (GIXS) apparatus", *Mater. Trans. JIM*, 36(1), 1-5 ,**1995.**

79- Ono, S.; Haginuma, M.; Kumagai, M.; Kitamura, M.; Tachibona, K.; Ishigure, K., "Distribution of cobalt in surface oxide film of type 304 stainless steel exposed to high temperature water-quantitative analysis by glow discharge optical emission spectroscopy", *J. nuclear Sci. Technol.*, 32(2), 125-132, **1995.**

80- Saeki, I.; Saito, T.; Furuichi, R.; Konno, H.; Nakamura, T.; Mabuchi, K.; Itoh, M., "Growth process of protective oxides formed on type 304 and 430 stainless steels at 1273K", *Corr. Sci.*, 40(8), 1295-1302, **1998**.

81- Lopez, MF.; Gutierrez, A.; Torres, CL.; Bastidas, MJ., "Soft X-ray absorption spectroscopy study of electrochemically formed passive layers on AISI 304 and 316L stainless steels", *J. Mater. Research*, 14(3), 763-770, **1999**.

82- Choi, B.; Choi, E.; Chung, S., "Oxidation-induced stoichiometric and morphological change of oxide films on stainless steel surfaces", *Appl. Phys. – A*, 69(6), 625-630, **1999**.

83- Stetanov, P.; Stoychev, D.; Stoycheva, M.; Marinova, T., "XPS and SEM studies of chromium oxide films chemically formed on stainless steel 316L", *Mater. Chem. & Phys.*, 65(2), 212-215, **2000**.

84- Tsai, WT.; Huang, KE., "Microstructural aspect and oxidation resistance of an aluminide coating on 310 stainless steel", *Thin Solid Films*, 366(1-2), 164-168, **2000**.

85- Stefanov, P.; Stoychev, D.; Stoycheva, M.; Gonzalez-Elipe, A. R.; Marinova, T., "XPS and TEM characterization of stainless steel 316L surfaces after electrochemical etching and oxidizing", *Surface & Interface Analysis*, 28(1), 106-110, **1999**.

86- Kim, XJ., "Analysis of oxide film formed on type 304 stainless steel in 288 oC water containing oxygen, hydrogen, and hydrogen peroxide", *Corr.*, 55(1), 81-88, **1999**.

87- Nanjo, H.; Newman, RC.; Sanada, N., "Atomic images of 304 SS surface after electrochemical treatments", *Appl. Surface Sci.*, 121, 253-256, **1997**.

88- Shibagaki, S.; Koga, A.; Shirakawa, Y.; Onishi, H.; Yokokawa, H.; Tanaka, J., "Chemical reaction path for thin film oxidation of stainless steel", *Thin Solid Films*, 303(1-2), 101-106, **1997**.

89- Ohkido, S.; Ishikawa, Y.; Yoshimura, T., "POSAP analysis of the oxide alloy interface in stainless steel", *Appl. Surface Sci.*,76(1-4), 261-265, **1994**.

90- Yoshimura, T.; Ishikawa, Y.; Ohkido, S., "Analysis of oxide film on stainless steel via position sensitive atom-probe", *J. Vacu. Sci. & Technol. –A*, 12(4), 2544-2548, **1996.**

91- Yen, SK.; Tsai, YC., "Determination of the critical temperature for forming a chromium-rich oxide on AISI 430 stainless steel and its corrosion resistance", *J. Electrochem. Soc.*, 143(8), 2493-2497, **1996.**

92- SchmidtRieder, E.; Tong, XQ.; Farr, JPG.; Aindow, M., "In situ electrochemical scanning probe microscopy corrosion studies on duplex stainless steel in aqueous NaCl solutions", *British Corr. J.*, 31(2), 139-145, **1996.**

93- Kim, KR.; Lee, KK.; Lee, DJ., "Characteristics of oxide film on 321 stainless steel", *J. Korean Inst. Met. Mater.*, 36(12), 2085-2090, **1998**.

94- Mueller, HJ.; Freeman, D., "FT-Ir spectrometry in materialography", *Mater. Chatacter.*, 35(2), 113-126, **1995**.

95- Mertens, F. P., "Reflectance infrared study of oxidation of stainless steels and component metals", *Corr. (Houston)*, 34(10), 359-365, **1978.**

96- Pecharroman, C.; Gonzalezcarreno, T.; Iglesias, JE., "The infrared dielectric properties of maghemite, gamma-Fe2O3, from reflectance measurement on pressed powders", *Phys. & Chem. Of Minerals*, 22(1), 21-29, **1995**.

97- Wegrelius, L.; Falkenberg, F.; and Olefjord, I., "Passivation of stainless steels in hydrochloric acid," *J. Electrochem. Soc.*, 146 (4), 1397-1406, 1999.

98- Hubschmid, C.; and Landolt, D., "Formation conditions, chloride content, and stability of passive films on an Iron-Chromium alloy" *J. Electrochem. Soc.*, 140, 1898-1901, 1993.

99- Schneider, A.; Kuron, D.; Hofmann, S.; and Kirchheim, R., "AES analysis of pits and passive films formed on Fe-Cr, Fe-Mo and Fe-Cr-Mo alloys" *Corros. Sci.*, 31, 191-196, 1990.

100- Stern, M.; and Geary, A. L.; *J. Electrochem. Soc.*, 104, 56, 1957.

101- Hakiki, N. E.; Boudin, S.; Rondot, B.; and Da Cunha Belo, M., "The Electronic Structure of Passive Films Formed on Stainless Steel," *Corros. Sci.*, 37(11), 1809-1822, 1995.

102- Wallinder, D.; Pan, J.; Leygraf, C.; and Delblanc-Bauer, A., "EIS and XPS Study of Surface Modification of 316LVM Stainless Steel after Passivation," *Corros. Sci.*, 41, 275-289, 1999.

103- Fujimoto, S.; Kawachi, S.; Nishio, T.; and Shibata, T., "Impedance and Photoelectrochemical Properties of Porous Oxide Film on Type 304 Stainless Steel Formed by Square Wave Potential Pulse Polarization," *J. Electroanal. Chem.*, 473, 265-271, 1999.

104- Huang, C.; Tsai, W.; and Lee, J., *Mater. Sci. Eng.*, A190, 199, **1995**.

105- Albella, J. M.; Montero, I. M.; and Martinez-Duart, J. I., *Thin Solid Film*, 125, 57, **1985**.

106- Breiter, M. W., *Electrochim. Acta*, 15, 1145, **1970**.

107- Kerrec, O.; Devilkiers, D.; Groult, H.; and Chelma C., *Electrochim. Acta*, 40, 719, **1995**.

108- Schmuki, P.; and B hni, H., *Electrochim. Acta* , 40, 775, **1995**.

109- Lorang, G.; Da Cunha Belo, M.; and Langeron, J. P., *J. Vac. Sci. Technol.*, A5, 1213, **1987**.

110- Lorang, G.; Bassile, F.; Da Cunha Belo, M.; and Langeron, J. P., "Quantitative Auger Analysis of Passive films formed on Stainless Steels," *Surf. Interface Anal.*, 12, 424-428, **1988**.

111- Simoes, A. M. P.; Ferreira, M. G.; Rondot, B.; and Da Cunha Belo, M., *J. Electrochem. Soc.*, 137, 82, **1990**.

112- Di Paola, A.; Di Quarto, F.; and Sunseri, C.,"A photoelectrochemical Characterization of passive films on stainless steels" *Corros. Sci.*, 26, 935-947, **1986**.

113- Di Paola, A.; Shuka, D.; and Stimming, U., *Electrochim. Acta*, 36, 345,**1991**.

114- Castro, E. B.; and Vilche, J. R., *Electrochim. Acta*, 38, 1567, **1993**.

115- Seal, S.; Nardelli, R.; Kale, A.; and Desai, V., "Role of Surface Chemistry on the Nature of Passive Oxide Film Growth on Fe-Cr (low and high) Steels at High Temperatures," *J. Vac. Sci. Technol.*, A17, 1109-1115, **1999**.

116- Hermas; A. A.; Ogura, K.; Takagi, S.; and Adachi, T., "Effects of Alloying Additions on Corrosion and Passivation Behaviors of Type 304 Stainless Steel," *Corrosion*, 51, 3-10, **1995**.

117- Montemor, M. F.; Simoes, A. M. P.; Ferreira, M. G. S.; and DaCunha Belo, M., "The Role of Mo in the Chemical Composition and Semiconductive Behavior of Oxide Films Formed on Stainless Steels," *Corros. Sci.*, 41, 17-34, **1999**.

118- Marcus, P.; and Grimal, J. M., *Corros. Sci.*, 33, 805, **1992**.

كذلك فإن وجود أيونات الكروم والموليديوم في الوسط الذي يتم فيه تكوين الأكسيد يعزز التركيب الكيميائي لطبقة الأكسيد عن طريق تكوين هيدروكسيد الكروم و أكسيد الموليديوم. و قد وجد أن الأكسيد الذي يتكون على الفولاذ نوع 316 مكون من طبقتين (هيدروكسيد/أكسيد) و هذا ما ظهر واضحاً من خلال الصور التي تم الحصول عليها من المجهر الإلكتروني و التي أعطت فكرة جيدة عن سطح الأكسيد على سطح الفولاذ. و أهم نتيجة لتجارب المجهر الإلكتروني هي توضيح كيفية نمو طبقة الأكسيد و التي تتكون من مجموعة شرائح بيضاوية و هرمية و حماسية الشكل.

الملخص

تلعب سبائك الفولاذ (ستاينلس ستيل) دوراً هاماً و فعالًا في مجال الصناعة، و لأن العديد من هذه الصناعات لابد من أن تعمل في أوساط إتلافية فإن الفولاذ يكون مهددا بالتآكل، مما يؤثر على أدائها ويكلف أصحاب المصانع ملايين الدولارات سنويا ، ولهذا أجريت العديد من المعالجات لحل هذه المشكلة ، وإحداها عن طريق تكوين طبقة أكسيد واقية على سطح الفولاذ لمنع تآكله، وفي هذه الأطروحة ، فإن هذه الطريقة قد طبقت على نوعين مختلفين من الفولاذ هما بالتحديد 310 و 316 وقد تم تكوين طبقة الأكسيد باستخدام برنامج يعطى جهودا تدرجية حيث تم البحث في مدى تأثير تغير سمك الأكسيد وتغير البرامج المستخدمة في تكوين الأكسيد وكذلك المحتوى الكيميائي للوسط الذي تتم فيه عملية الأكسدة باستخدام خليه كهر وكيميائية ثلاثية الأقطاب .وقد تمت دراسة السلوك الكهروكيميائي لطبقة الأكسيد بطرق متعددة هي : استقطاب الجهد الديناميكي، تجارب التافل ومقاومة الاستقطاب وطرق تحليل المعاوقة الكهروكيميائية بعد ذلك تم عمل التحليل السطحي لتعين التركيب الكيميائي وشكل وسمك طبقة الأكسيد باستخدام عدة أجهزه متطورة كالمجهر الإلكتروني وجهاز التحليل الكيميائي السطحي وجهاز انعكاس الأشعة تحت الحمراء السطحي وجهاز حيود الأشعة السينية وقد وجد أن السلوك الاستقطابي لأنواع الفولاذ قيد الدراسة يعتمد بقوة على تركيب الفولاذ نفسه ، لذلك فإن مقدرة الفولاذ نوع 310 ونوع 316 علي التأكسد في 5 مول من حمض الكبريتيك كان واضحا وثابتا لمدى واسع من الجهد، ومع ذلك فإن الأكسيد الذي يتكون علي سطح الفولاذ نوع 316 هو أكثر ثباتا من ذلك الذي يتكون علي سطح الفولاذ نوع 310 تحت نفس الظروف المختبرية . ومن خلال نتائج تحليل المعاوقة الكهروكيميائية فقد وجد أنه بالنسبة للفولاذ نوع 316 فإن مقاومة طبقة الأكسيد لتكوين الفجوات ونقل الشحنات الكهربائية تزداد بزيادة سمك الطبقة. ومن جهة أخرى فإن سعة الأكسيد تقل تدريجيا كلما ازداد سمكه.

أعضاء لجنة الإشراف على الرسالة

أ.د. راشد عبد الرحمن السعيد

أستاذ في الكيمياء الفيزيائية
قسم الكيمياء، كلية العلوم
جامعة الإمارات العربية المتحدة

د. أحمد جلال حلمي

أستاذ مساعد في الكيمياء الفيزيائية و كيمياء المواد
قسم الكيمياء، كلية العلوم
جامعة الإمارات العربية المتحدة

خواص المعاوقة و الكهروكيميائية الضوئية لطبقات الأكسيد المتكونة على الصلب غير القابل للصدأ بطرق الإستقطاب المختلفة

أطروحة مقدمة إلى

عمادة الدراسات العليا

جامعة الإمارات العربية المتحدة

منى سالم صالح سليمان الكعبي

لمتطلبات الحصول على درجة الماجستير

في

علوم وهندسة المواد

2001